eScience 6 (2026) 100506

Contents lists available at ScienceDirect

eScience

journal homepage: www.keaipublishing.com/en/journals/escience

Review

High-entropy alloys for hydrogen storage, separation, and detection: Recent progress and prospects

Jiaxi Liu[a,b,1], Pengru Huang[a,c,1], Yongpeng Xia[a,1], Yanping Liu[d], Yumei Luo[a], Huanzhi Zhang[a], Yongjin Zou[a], Hailiang Chu[a], Sergey P. Verevkin[e], Sergey V. Vostrikov[f], Lixian Sun[a,b,*], Fen Xu[a,*], Zongwen Liu[g,*], Hongge Pan[h,*]

[a] School of Material Science & Engineering, Guangxi Key Laboratory of Information Materials and Guangxi Engineering Research Center of Hydrogen/Heat/Electricity-Related Energy Materials and Sensors, Guilin University of Electronic Technology, Guilin 541004, China
[b] School of Mechanical & Electrical Engineering, Guilin University of Electronic Technology, Guilin 541004, China
[c] Institute for Functional Intelligent Materials, National University of Singapore, 4 Science Drive 2, 117544, Singapore
[d] Institute of Quantum Physics, School of Physics, Central South University, Changsha 410083, China
[e] Department of Physical Chemistry, Kazan Federal University, Kazan 420008, Russia
[f] Chemical-Technological Department, Samara State Technical University, Samara 443100, Russia
[g] School of Chemical and Biomolecular Engineering, The University of Sydney, New South Wales 2006, Australia
[h] Institute of Science and Technology for New Energy, Xi'an Technological University, Xi'an 710021, China

HIGHLIGHTS

- Recent progress in hydrogen storage, separation, and detection using high-entropy alloys is summarized.
- Various design strategies for high-entropy alloys are elucidated.
- Hydrogen absorption and electrochemical/catalytic hydrogen storage properties in HEAs are highlighted.
- Key challenges and perspectives in alloy design and practical application are also discussed.

GRAPHICAL ABSTRACT

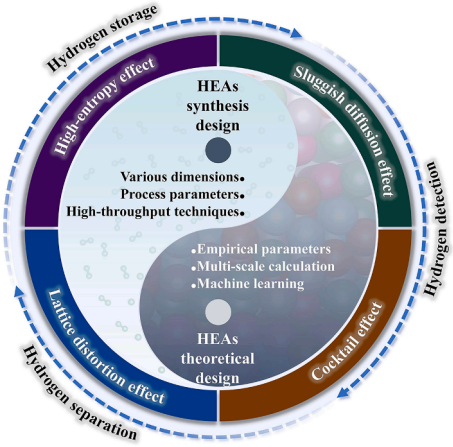

*Corresponding authors.
E-mail addresses: sunlx@guet.edu.cn (L. Sun), xufen@guet.edu.cn (F. Xu), zongwen.liu@sydney.edu.au (Z. Liu), honggepan@zju.edu.cn (H. Pan).
Peer review under the responsibility of Editorial Board of eScience.
[1] These authors contributed equally to this work.

https://doi.org/10.1016/j.esci.2025.100506
Received 12 June 2025; Received in revised form 3 October 2025; Accepted 24 November 2025
Available online 28 November 2025

ARTICLE INFO

Keywords:
High-entropy alloys
Machine learning
Hydrogen storage
Hydrogen separation
Hydrogen detection

ABSTRACT

As a pivotal clean energy carrier with promising efficiency, environmental friendliness, and sustainability, hydrogen stands at the forefront of the global energy technology revolution. However, achieving the efficient storage, easy separation, and trace detection of hydrogen remain critical challenges. High-entropy alloys (HEAs) have garnered attention because of their remarkable attributes, including high stability, single-phase reversibility, and a wide tunable range of composition and electronic structure. Commencing with a succinct background overview, we explore the pivotal role of theoretical methods in designing the phase structure and ensuring the stability of HEAs, focusing especially on diverse element types and contents. We then present a summary of prevalent methods for preparing HEAs, followed by a detailed examination of recent advances in their hydrogen-related properties, encompassing hydrogen storage, separation, and detection. Finally, we look at the existing challenges and offer perspectives on the trajectory of future research and applications in this promising technological domain.

1. Introduction

In response to escalating concerns over the energy crisis and environmental pollution, the demand for clean, renewable energy has experienced a rapid and substantial increase [1–6]. Despite extensive research and development on sources like solar and biomass energy, the uneven temporal and geographical distribution of these options hinders their widespread utilization. As an ideal energy carrier, hydrogen has emerged as a key player for energy transition due to its zero-carbon emissions and high combustion calorific value [7,8]. The comprehensive utilization of hydrogen energy comprises hydrogen production, storage, transport, and application. Achieving a hydrogen economy hinges significantly on having secure, efficient, and economically viable hydrogen storage techniques. However, a multitude of challenges must be overcome to realize these objectives [9–11].

As a versatile energy carrier, hydrogen has garnered significant attention in the transportation sector, guided by specific technical targets outlined by the U.S. Department of Energy (DOE) (Fig. 1) [12,13]. At present, high-pressure compression of hydrogen in tanks stands out as one of the most technically mature and widely adopted storage methods. However, this approach grapples with drawbacks such as low gravimetric capacity and high transport cost [14]. Moreover, safety concerns inevitably arise due to the potential for hydrogen spillage or hydrogen embrittlement as the pressure increases. Storage in the form of liquefied hydrogen needs a specialized tank and faces limitations imposed by the energy required for liquefaction [15]. An alternative approach involves

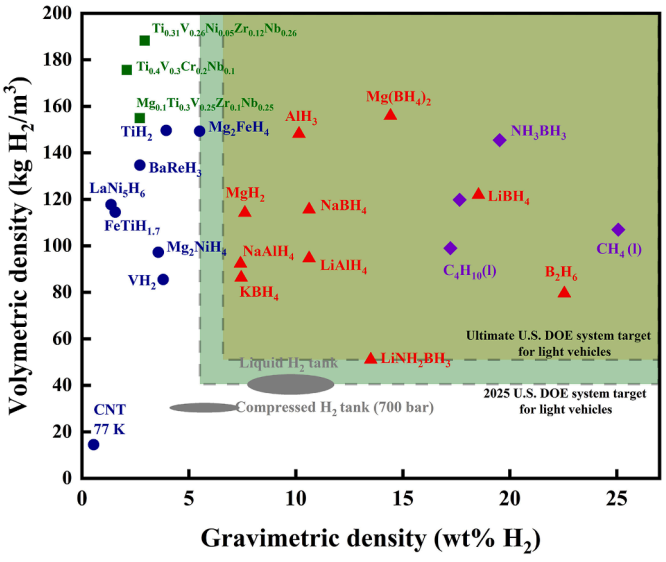

Fig. 1. Comparison of the volumetric and gravimetric densities of various hydrogen storage materials, with U.S. DOE technical targets [12,13].

efficient hydrogen storage utilizing solid-state materials through physisorption or chemisorption. Hydrogen in the form of molecules is physically adsorbed on surfaces, such as inorganic porous materials [16,17], carbon-based hydrogen storage materials [1,18,19], metal–organic framework materials [20–23], and covalent organic framework materials [24]. In contrast, atomic or ionic hydrogen is chemically stored in solid-state materials and exhibits high stability and promising technological potential [25,26]. However, research on such hydrogen storage materials remains in the exploratory, laboratory stage, and the gap between experimental findings and commercial applications of hydrogen energy is substantial.

Metal hydride-based hydrogen storage materials offer a promising avenue to address the recycling challenges inherent in hydrogen storage technology [27–29]. Hydrogen can be stored within metal monomers, alloys, and complex hydrides under specific temperature and pressure. Among the various metal hydrides, MgH_2 has attracted significant attention owing to its remarkable hydrogen capacity, excellent reversibility, and recyclability. Furthermore, the abundance of Mg reserves, coupled with its high structural stability, position it as a promising candidate for hydrogen fuel cells, hydrogen storage systems, and hydrogen purification applications [30]. Mg-based materials display high hydrogen storage density with a theoretical capacity of ~7.6 wt%, but they are limited by high thermodynamics (~573 K at 0.1 MPa) and slow kinetics (~75 kJ · mol^{-1} H_2) [31]. To overcome these obstacles, several strategies have recently been developed, such as particle downsizing to shorten diffusion paths, the addition of transition metal catalysts to reduce activation barriers, and alloying to tailor thermodynamic properties. Recently, Li et al. emphasized that the above various modification strategies serve an essential role in hydrogen capacity, dehydrogenation enthalpy and temperature, and hydriding/dehydriding (H/D) rates in Mg-based hydrogen storage materials [32]. Based on this, the hydrogen storage kinetics of a Mg–Ni–Y alloy prepared by the hot-extrusion method was greatly improved due to the enlarged grain/phase boundaries and the Mg_2Ni and YH_2 particles generated *in situ*, offering critical insights into designing Mg-based hydrogen storage materials [33]. Mao et al. revealed a diffusion-controlled solid-state transformation of In/Ag in MgH_2@MgIn and MgH_2@MgAg composites. This transformation enhances hydrogenation kinetics and thermodynamically destabilizes MgH_2, lowering their desorption peak temperature by 14.5 and 17.8 K, respectively [34]. Extensive research studies have demonstrated the effectiveness of alloys, composites, and nanocrystallization to improve the thermodynamics and kinetics of Mg-based hydrogen storage materials. Nonetheless, the realization of large-scale applications requires the resolution of challenges to achieving reversible hydrogen storage under ambient conditions with long-term cycling stability.

Hydrogen storage alloys, characterized by high volumetric density, low energy loss during storage, and excellent safety features, have found extensive applications in the field of hydrogen energy [35–37]. Typically, a combination of hydride elements (A-type) and non-hydride

elements (B-type) is required for the optimal performance of hydrogen storage alloys [38], based on which various intermetallic hydrides have been explored. Rare-earth-containing alloys stand out for their easy activation, flat hydrogen absorbing/desorbing plateaus, moderate pressure requirements, low hysteresis, robust resistance to impurity gas poisoning, and suitability for room-temperature operation. These alloys find widespread use not only as electrodes in nickel–metal hydride (Ni-MH) secondary batteries but also as key components in safe and efficient hydrogen storage materials for hydrogen–oxygen fuel cells [39]. For example, $LaNi_5$ can absorb hydrogen at room temperature and exhibit reversible hydrogen ab/desorption performance. However, the relatively low gravimetric capacity and limited cycling lifespan hinder its practical application. Moreover, conventional metal hydride-based hydrogen storage materials, designed for reversible hydrogen uptake and release under moderate conditions, still fall short of the DOE's on-board storage targets for light-duty fuel cell vehicles: 5.5 wt% H_2 by 2025 and, ultimately, 6.5 wt%. Recent research interest in light metal complex hydrides is largely driven by their high theoretical hydrogen content, such as $NaAlH_4$ (7.4 wt%), $LiAlH_4$ (10.6 wt%), and NH_3BH_3 (19.6 wt%) [40,41]. Pioneering achievements by Bogdanović et al. demonstrated that $NaAlH_4$ with a small amount of Ti-containing catalyst could achieve reversible de/hydrogenation under mild conditions [42]. However, these complex hydrides, although possessing high theoretical hydrogen capacity, face several practical limitations, such as high desorption temperatures ($>$ 473 K), poor reversibility, and irreversible decomposition or side reactions during cycling [43–46]. In addition, their high sensitivity to air and moisture increases handling complexity. These issues must be well addressed before their large-scale application in hydrogen storage systems.

High-entropy alloys (HEAs) have attracted tremendous attention for their revolutionary design concepts and exceptional physical, chemical, and mechanical properties. HEAs typically consist of five or more elements in equimolar or near-equimolar ratios (i.e., 5–35%), significantly expanding the compositional space and enabling tunable microstructures for superior performance [47–50]. HEAs combine structural stability with wide compositional tunability, enabling the precise control of catalytic properties. They show excellent activity and durability in electrocatalysis (ORR, HER, CO_2RR) and hold promise for sustainable energy technologies [51,52]. Beyond catalysis, HEAs are also attractive for advanced energy storage systems such as Li-, Na-, and K-ion batteries [53]. Their unique multi-elemental composition enables the tailoring of redox activity and ionic transport properties, which are critical for enhancing specific capacity, cycling stability, and rate performance. Unlike conventional alloys, HEAs can leverage their high configurational entropy to achieve superior wear, oxidation and corrosion resistance, as well as high-temperature strength and long-term structural stability. In a word, these attributes underscore the transformative potential of HEAs in next-generation energy conversion and storage systems.

Recent reports have indicated the popularity of HEAs for their ability to store hydrogen [54–57]. Compared to traditional alloys, HEAs exhibit a wider compositional space, allowing for further improvements in hydrogen capacity, reversibility, kinetics, thermodynamics, and cycling stability. In earlier studies, the hydrogen storage properties of HEAs were found to be adjusted by modulation via composition alteration. Kao et al. reported the first HEA for hydrogen storage, CoFeMnTiVZr [58]. $CoFeMnTi_xV_yZr_z$ represents a simple C14 Laves phase, with modified hydrogen storage properties achieved by tuning the amounts of Ti, V, and Zr. The reversible capacity reached 1.8 wt% for $CoFeMnTi_2VZr$ at 298 K. Cheng et al. investigated the hydrogen storage performance of BCC-structured TiVNbCrNi HEAs with varying Ni contents [59]. Their results indicate that Ni addition can effectively shorten the activation period, whereas excessive Ni suppresses the intrinsic hydrogen absorption kinetics. Furthermore, compositional modulation affects the degree of lattice distortion or introduces new alloy phases, both of which are crucial for hydrogen ab/desorption [60,61]. In brief, scientific design and precise control of element ratios in HEAs provide flexibility for optimizing hydrogen storage performance.

Although this compositional tunability is advantageous, it also introduces significant atomic-level complexity. The resulting atomic-scale disorder presents substantial challenges for their synthesis, characterization, mechanistic understanding, and practical application for hydrogen storage. In recent years, numerous design strategies have been developed for HEAs as hydrogen storage materials. Theoretically, there is a range of empirical parametric, multiscale computational simulation, and data-based machine learning methods [49,62,63]. On the synthetic design aspects of HEAs, effective synthesis methods were explored by adjusting process parameters, elemental composition, and morphological structure to optimize hydrogen storage properties [64,65]. Researchers are more concerned with HEAs' hydrogen storage capacity, activation energy, hydrogen uptake and release kinetics, thermodynamics, and cycling properties. However, a unique challenge remains for HEAs as hydrogen storage materials. The hydrogen storage capacity of most HEAs is limited (typically 1–3 wt%), significantly lower than that of complex hydrides or Mg-based systems. Moreover, their compositional complexity retards accurate thermodynamic predictions, complicating experimental validation and data-driven design [66,67]. This complexity not only affects their hydrogen storage behavior but also impacts their potential use in other hydrogen-related applications.

Efficient hydrogen separation and purification are also key steps in developing hydrogen-based clean energy. Since hydrogen produced by conventional methods is often contaminated with impurity gases such as CO, CO_2, and H_2S, achieving high selectivity for hydrogen permeation is critically important [38,68]. The advancement of a new generation of environmentally friendly and efficient separation technologies is of paramount significance for realizing applications in hydrogen energy [69–71]. Among many technologies for hydrogen purification, membrane separation has low energy consumption, continuous operation, low cost, and simple operation. In particular, HEAs have recently garnered attention as a promising class of materials for hydrogen purification membranes. As well, in the field of hydrogen detection, HEAs display great potential based on their cocktail effect created by metal elements with varying hydrogen affinities. HEAs also offer distinct advantages for hydrogen energy applications. The severe lattice distortion and atomic size mismatch in HEAs generate abundant interstitial sites, which facilitate hydrogen adsorption and diffusion. In addition, their multi-principal element design enables tunable thermodynamic properties, allowing for precise control of hydrogen ab/desorption enthalpies and equilibrium pressures. Moreover, their multifunctionality enables HEAs to function as not only hydrogen storage media but also catalysts and sensing materials, thereby enhancing their utility in integrated hydrogen systems. Hence, HEAs demonstrate significant potential in hydrogen technologies, from laboratory to industrial applications. Current research on HEAs is primarily focused on their theoretical and fundamental properties for hydrogen storage, separation, and catalysis. Companies are optimizing alloy compositions and preparation processes to develop high-performance HEAs for solid-state hydrogen storage and related catalysts. HEAs are anticipated to aid in building large-scale hydrogen infrastructures, such as pipelines, storage facilities, and refueling stations.

There are many review articles on HEAs for hydrogen storage. Most of them, however, only focus on hydrogen absorption performance. This review concentrates on a comprehensive design that encompasses both experiment and theory and a broadening of HEA applications. Fig. 2 shows the primary coverage. We commence by elucidating various design methods for HEAs, placing particular emphasis on the contributions of theoretical calculations and machine learning. The synthetic methods for HEAs, such as arc melting and mechanical alloying, are then introduced. Subsequently, their performances for hydrogen storage, separation, and detection are systematically summarized. To conclude, we present a summary and outlook for developing highly efficient and practical hydrogen storage, separation, and detection materials for HEAs.

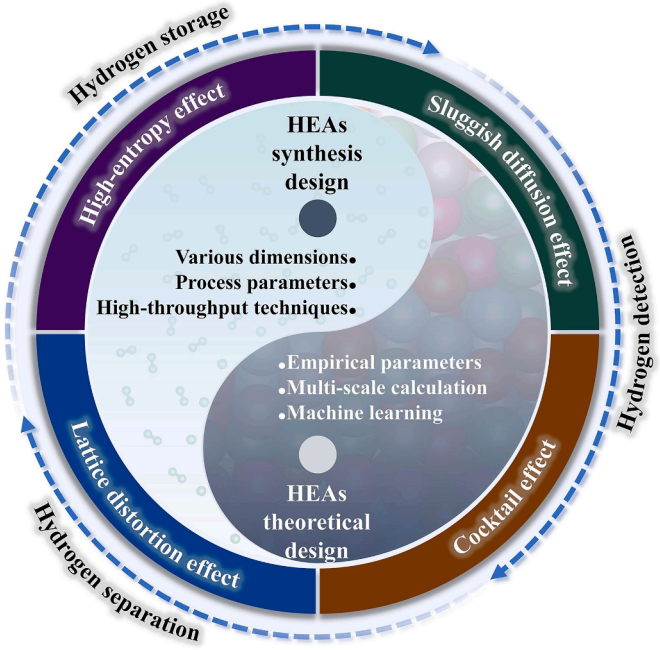

Fig. 2. Primary coverage of this review.

2. Definitions and four core effects of HEAs

HEAs are typically defined from two perspectives, i.e., composition-based and entropy-based. They are a class of multicomponent metallic materials composed of five or more principal elements, each typically accounting for 5–35%. Unlike conventional alloys, HEAs have complex compositions and high configurational entropy. According to the entropy-based definition, an alloy is considered an HEA when its ideal configurational entropy exceeds 1.5R (where R is the gas constant). This high entropy favors the formation of simple solid-solution phases (such as face-centered cubic (FCC), body-centered cubic (BCC), or hexagonal close-packed (HCP)) instead of complex intermetallic compounds. The concept of HEAs was first proposed by Yeh et al. [47]. Importantly, HEAs do not need to be equimolar, and the number of HEAs increases significantly with the addition of minor elements at concentrations below 5% [72]. The term "high entropy" suggests that random solid solutions in these alloys outperform intermetallic compounds. In thermodynamics, entropy serves as a fundamental state function that characterizes the disorder of a system and therefore influences its thermodynamic stability.

An alternative definition of HEAs focuses on mixed entropy values. Total mixed entropy comprises four components: configurational entropy (ΔS_{mix}^{conf}), vibrational entropy (ΔS_{mix}^{vib}), electronic randomness entropy (ΔS_{mix}^{elec}), and magnetic dipole entropy (ΔS_{mix}^{mag}). In an ideal random component, the configurational entropy increases with the number of elements and their concentrations. For equiatomic alloys in liquid or regular solid-solution states, the configurational entropy simplifies accordingly, as described in Eq. (1):

$$\Delta S_{conf} = -R\sum_{i=1}^{n} c_i \ln c_i = R \ln n \tag{1}$$

where R, c_i, and n represent the gas constant, molar percentage of each element, and total number of components, respectively. This equation can be applied to calculate the molar phase transition when the number of elements varies. Note that this equation is derived from the regular solid solution model, where the stochastic state of the alloy is approximated to the regular solute to determine the mixing entropy. HEA formation is driven by the balance between enthalpy and entropy, the mixing Gibbs free energy is:

$$\Delta G_{mix} = \Delta H_{mix} - T\Delta S_{mix} \tag{2}$$

where ΔH_{mix}, ΔS_{mix}, and T represent enthalpy, entropy, and absolute temperature, respectively. In cases where elements of the same kind are continuously miscible in the liquid state, the enthalpy of mixing approaches zero, making changes in enthalpy negligible. Alloys with high entropy exhibit much lower free energy under thermodynamically stable conditions, favoring the formation of solid solutions.

A detailed classification of HEAs based on their entropy values, ΔS_{conf}, falls into three categories [73]: (i) HEAs: $\Delta S_{conf} > 1.5R$ for alloys containing over 5 main elements, (ii) medium-entropy alloys: $1R \leq \Delta S_{conf} \leq 1.5R$ for alloys composed of 2–4 main elements, and (iii) low-entropy alloys: $\Delta S_{conf} < 1R$ for traditional alloys. However, some ternary and quaternary alloys can also exhibit simple disordered solid-solution structures [74–76].

HEAs are well known for exhibiting four core effects: the high-entropy effect in their thermodynamics, significant lattice distortion in their structure, slow diffusion in their kinetics, and the cocktail effect in their performance [77,78].

High-entropy effect: This primary effect indicates that the mixing entropy of alloys gradually increases with the number of principal elements. As the number of metal elements increases, the alloy tends to form a single-phase solid solution. The Gibbs phase rule implies that high mixing entropy can enhance compatibility among primary elements, minimizing the formation of intermetallic compounds or phase separation. Increased entropy reduces the electronegativity difference of the alloy, facilitating better mixing and discouraging compound formation [79]. Consequently, the Gibbs free energy of an alloy system may decrease with increased mixing entropy.

Severe lattice distortion effect: In HEAs, differences in atomic radii among the principal elements cause severe lattice distortions, disrupting the periodic lattice and weakening the diffraction intensity. Such distortions influence key physical properties, including diffusion, electrical/thermal conductivity, and magnetism.

Sluggish diffusion effect: HEAs exhibit slower elemental diffusion than conventional alloys. On the one hand, the heterogeneous local atomic environment complicates migration pathways and impedes atomic jumps into vacancies. On the other hand, the varying diffusion rates of the constituent elements mean that the slowest-diffusing element serves as the rate-limiting step in the overall diffusion process.

Cocktail effect: The presence of multiple principal elements in HEAs can yield unique properties that are not present in individual elements. The cocktail effect suggests a synergistic interaction, where the combined effect may exceed the sum of the individual elements' properties.

The potential application of these four core effects for hydrogen adsorption, diffusion, and storage capacity is illustrated in Fig. 3 [80]. The diverse active surface sites in HEAs facilitate the adsorption and dissociation of hydrogen molecules on their surfaces. Hydrogen retention on the alloy surface is prolonged, thereby enhancing adsorption capacity, selective separation, and sensitivity to low hydrogen concentrations. HEAs possess highly stable solid-solution phases, providing abundant interstitial sites for hydrogen storage. In addition, the numerous defects and irregular grain boundaries in the alloy accelerate hydrogen diffusion. In conclusion, these effects synergistically regulate hydrogen interactions in HEAs, making them promising candidates for hydrogen storage, separation, and detection applications.

3. Theoretical computation and data-driven design

The selection of compositions and synthesis of HEAs involves complex cross-scale physicochemical phenomena. Therefore, relying solely on experimental methods to explore the mechanisms of microstructures

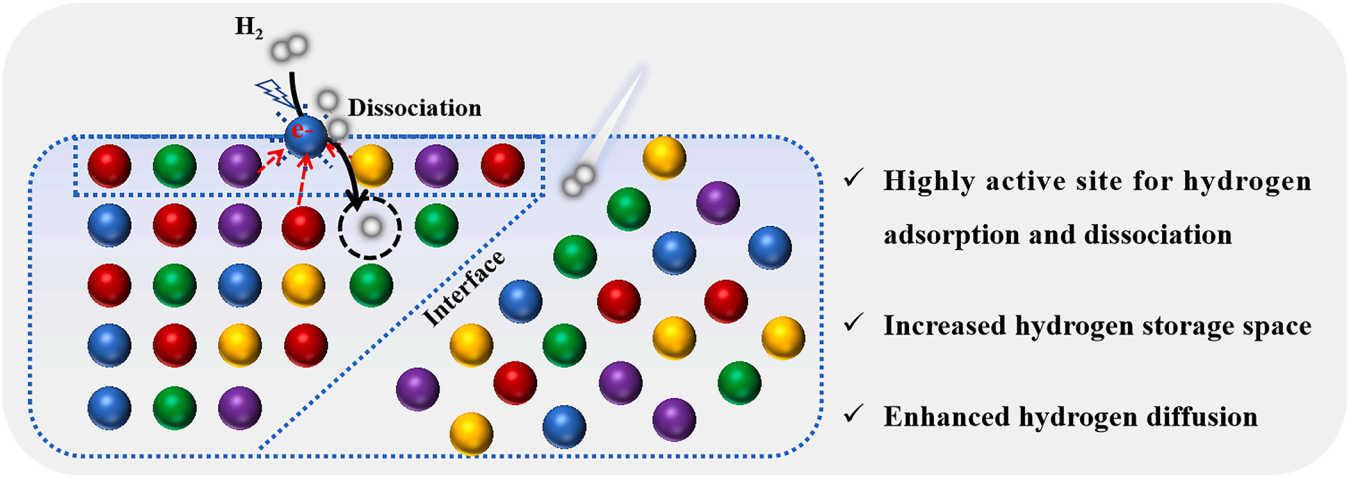

Fig. 3. Potential for HEAs in hydrogen technologies.

and properties is time-consuming. The overall performance of HEAs is influenced by various phases, including intermetallic, nanometric, and amorphous phases [81]. To address these challenges, theoretical computation and machine learning methods have been increasingly integrated into HEA design, thereby providing predictive insights into phase formation, stability, and functional performance.

3.1. Empirical parameters

To date, research on HEAs has primarily focused on multiphase alloys. The formation of single-phase HEAs relies on calculations that incorporate empirical metrics, in line with Hume–Rothery principles [49,82]. Factors such as atomic radius and valence electron concentration (VEC) in alloying elements significantly affect the heat of dissolution for solid solutions in binary alloys. However, further analysis is needed to understand how these factors influence phase stability in HEAs. Key parameters affecting phase stability, including mixing entropy (ΔS_{mix}), mixing enthalpy (ΔH_{mix}), atomic size mismatch (δ), electronegativity difference ($\Delta\chi$), VEC, and thermodynamic origin (Ω), are presented in Fig. 4a [81,83–86]. The equations to calculate these parameters are as follows:

$$\Delta H_{mix} = \sum_{i=1, j\neq i}^{n} 4\Delta H_{ij}^{mix} c_i c_j \tag{3}$$

where ΔH_{ij}^{mix} represents the enthalpy of mixing for binary equiatomic AB alloys;

$$\delta = \sqrt{\sum_{i=1}^{n} c_i \left(1 - \frac{r_i}{\bar{r}}\right)^2} \times 100\% \tag{4}$$

where $\bar{r} = \sum_{i=1}^{n} c_i r_i$ is the average atomic size of the n components in the alloy, c_i is the concentration of component i, and c_j is the atomic radius of component i;

$$\Delta\chi = \sqrt{\sum_{i=1}^{n} c_i(\chi_i - \bar{\chi})^2}, \bar{\chi} = \sum_{i=1}^{n} c_i\chi_i \tag{5}$$

where n is the number of components, c_i is the mole fraction of the i^{th} element, $\bar{\chi}$ is the mean value of electronegativity for the selected alloy, and χ_i is the Pauling electronegativity of component i;

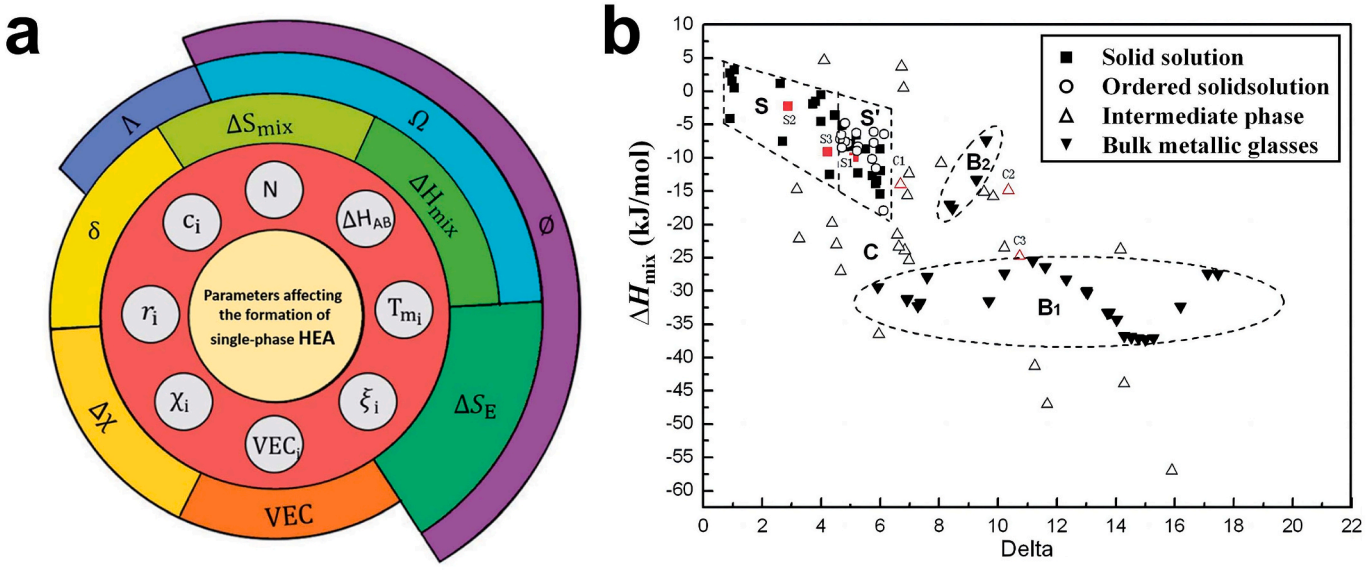

Fig. 4. (a) Parameters affecting the formation of single-phase HEAs. Reproduced with permission [49]. Copyright 2021, Royal Society of Chemistry. (b) Relationship between delta and ΔH_{mix} for HEAs. Reproduced with permission [81]. Copyright 2008, Wiley-VCH.

$$\mathrm{VEC} = \sum_{i=1}^{n} c_i (\mathrm{VEC})_i \tag{6}$$

where n is the number of components, c_i is the mole fraction of the i^{th} element, and $(\mathrm{VEC})_i$ is the valence electron concentration of component i; and

$$\Omega = \frac{T_m \Delta S_{mix}}{|\Delta H_{mix}|} \tag{7}$$

where $T_m = \sum_{i=1}^{n} c_i (T_m)_i$, $(T_m)_i$ is the melting point for the *ith* component of the alloy. Ω is defined as a parameter of the entropy of mixing timing and the average melting temperature of the elements over the enthalpy of mixing.

The findings indicate that HEAs are likely to form solid solution phases when the atomic radius difference (δ) is less than 6.5%, the mixing enthalpy ranges from −15 to −5 kJ · mol^{-1}, and the mixing entropy is confined to values between 12 and 17.5 J · K^{-1}·mol^{-1}, as illustrated in Fig. 4b [81]. Guo et al. introduced the VEC criterion, suggesting that the FCC phase is stable when VEC exceeds 8, while the BCC phase is stable when VEC is below 6.87 [82]. However, VEC alone cannot determine the structure of solid-solution HEAs, indicating a need for further analysis of phase formation laws. Yang et al. formulated the Ω parameter to predict phase formation in HEAs, establishing that solid-solution phases are relatively stable for $\Omega \geq 1.1$ and $\delta \leq 6.6\%$ [83]. To date, there are many phase formation rules and empirical criteria for HEAs, which may not apply to all HEAs. Although empirical methods like calculation of phase diagrams (CALPHAD) for HEA design may lack the sufficient precision of computational approaches, they remain valuable for the rapid screening of candidate alloys and preliminary phase prediction, without the need for complex calculations or extensive experiments.

3.2. Multi-scale calculation

With the aid of multi-scale computational and simulation methods, it is possible to efficiently predict the phase compositions of HEAs and the physicochemical properties they inherently possess. As illustrated in Fig. 5, different modeling techniques operate across distinct temporal and spatial scales. These methods facilitate efficient predictions of phase compositions and physicochemical properties, thus allowing for the facile optimization of alloy compositions to enhance material properties [87,88]. This section highlights the application of representative multiscale simulation methods for HEA design, spanning from the atomic to the macroscopic scale.

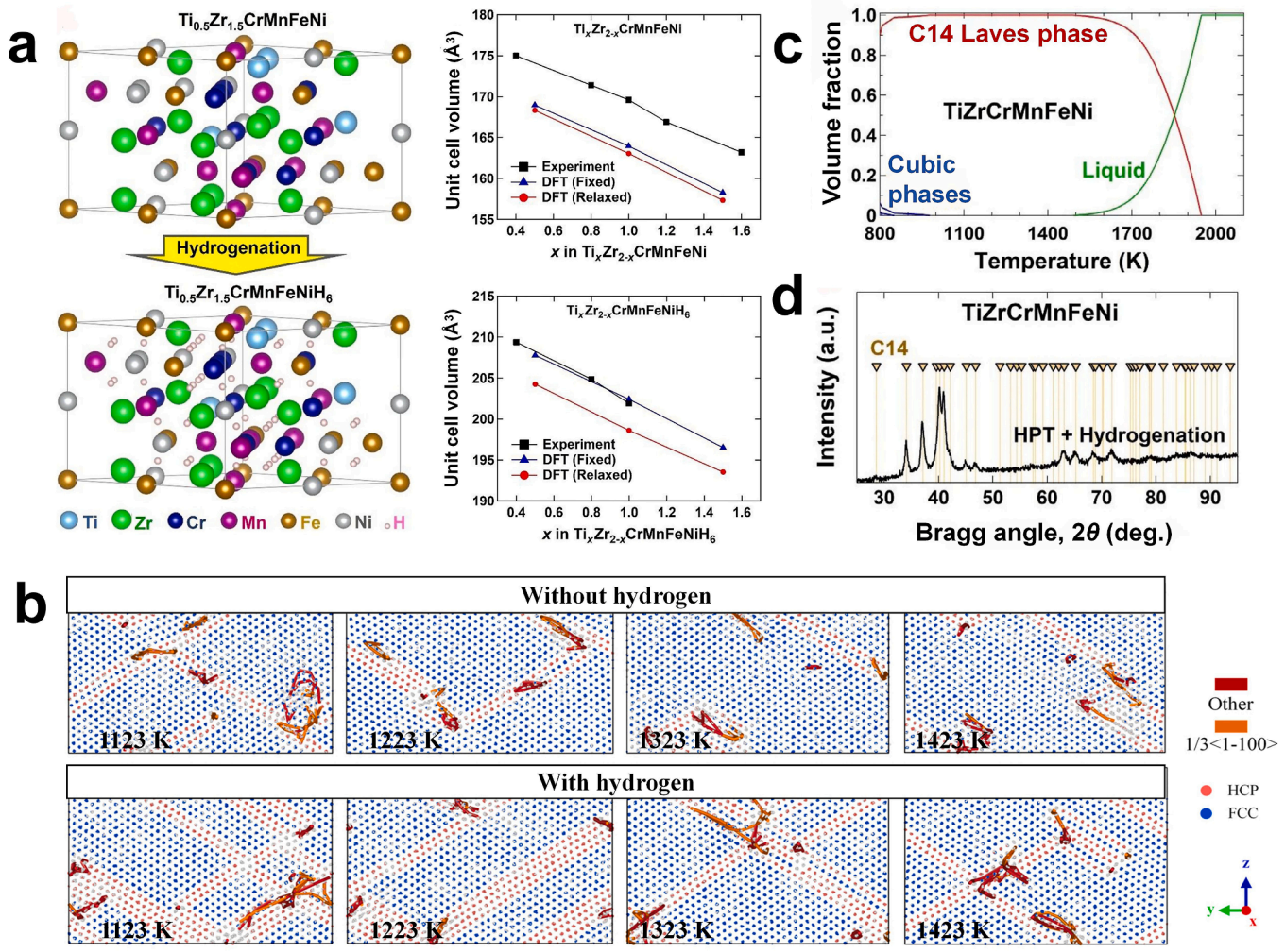

Fig. 5. (a) Crystal lattice and unit cell volume of $Ti_{0.5}Zr_{1.5}CrMnFeNi$ HEA and its corresponding hydride of $Ti_{0.5}Zr_{1.5}CrMnFeNiH_6$. Reproduced with permission [94]. Copyright 2022, Elsevier. (b) Evolution of dislocation behavior in a single crystal under plastic deformation at different temperatures. Reproduced with permission [102]. Copyright 2022, Elsevier. (c) Phase design via CALPHAD and (d) XRD profile after high-pressure torsion (HPT) processing and hydrogenation of TiZrCrMnFeNi. Reproduced with permission [105]. Copyright 2020, Elsevier.

3.2.1. Density functional theory (DFT) calculations

DFT is an effective and typical approach for investigating hydrogen adsorption energies, dissociation pathways, and charge transfer behavior on HEA surfaces and within their crystal lattices. Calculations based on DFT provide atomistic insights into reaction mechanisms and the evolution of electronic structures, playing a crucial role in advancing the understanding and development of HEAs [89,90]. For example, Hu et al. reported that, based on the DFT results, a BCC-structured alloy of TiZrHfScMo can absorb 2.14 wt% hydrogen [62]. Their subsequent studies on the TiZrVMoNb HEA emphasized some of the factors influencing hydride stability, presenting advantages for achieving high reversible hydrogen storage capacity [91,92]. Li et al. demonstrated a 54.1% increase in hydrogen storage capacity due to the regulation of micro-precious metals in $TiZrHfMoNbM_x$ (M = Pt, Pd) [93]. Both the destabilization of hydrides and the significant role of electronic structure were proposed based on their DFT results. The calculated formation energies indicate that Pt and Pd preferentially substitute for Ti and Zr in TiZrHfMoNb HEA. Furthermore, the adjustment of element content had an obvious effect on hydrogen desorption due to the decreased binding energy between hydrogen and HEA hydrides. As shown in Fig. 5a, based on the DFT method, Mohammadi et al. designed AB_2-type C14 Laves phase $Ti_xZr_{2-x}CrMnFeNi$ (x = 0.4 to 1.6) HEAs with a VEC of 6.4 and a low hydrogen absorption strength (close to −0.1 eV, which is beneficial for room-temperature hydrogen storage) [94]. Both experimental and theoretical results exhibit comparable trends, revealing a decrease in unit cell volume as the Ti content increases in both alloys and hydrides. Facilitating the occupation of interstitial sites by hydrogen atoms is a pivotal challenge. Hu et al. identified the primary hurdle of enhancing hydrogen occupancy in interstitial positions to boost their capacities [95]. The findings indicate that the inherent electron delocalization among hydrogen atoms in HEA hydrides significantly differs from that in conventional metal hydrides. In addition, higher occupancy of octahedral sites induces structural disorder, which reduces thermal stability and facilitates dehydrogenation at lower temperatures. The addition of Mg and Al affects the thermodynamics of $Ti_{0.325}V_{0.275}Zr_{0.125}Nb_{0.275}$ hydride, reducing its storage capacity, as demonstrated by analyses of the electronic density of states, crystal orbital Hamilton population, and electron localization function [96]. In fact, significant research progress has been made in elucidating the structural stability, phase formation mechanism, hydride thermodynamics, and hydrogen storage capacity of HEAs via DFT calculations. However, as the number of constituent elements increases, modeling the local chemical environments and atomic-level disorder requires larger supercells. This will significantly raise the computational cost and limit the applicability of DFT across broad compositional spaces.

3.2.2. Molecular dynamics (MD) simulation

MD simulation is also widely used to assess the structural stability of HEAs. It is particularly effective for investigating hydrogen diffusion behavior, including the effects of temperature, lattice defects, and mechanical stress. These simulations can examine the internal microstructural evolution of alloys during deformation. Kao et al. investigated organizational evolution under rapid solidification in equialloys with 2–8 elements and found that an amorphous structure forms with fewer than four principal elements, while a solid-solution structure appears with more than five [97]. Choi et al. pointed out that the stable phase of equiatomic CoCrFeMnNi HEA is a hexagonal close-packed structure at 0 K, and a significant number of stable vacancy sites may cause sluggish diffusion [98]. Furthermore, the hydrogen diffusion effect can be explored through a systematic analysis. Ren et al. investigated the correlation between lattice distortion and hydrogen diffusion [99]. Hydrogen atoms readily become trapped in low-energy zones, significantly retarding long-distance hydrogen migration. In addition, the ab initio molecular dynamics method was employed to investigate the characteristics of icosahedra within $Ni_{32}Nb_{28}Zr_{30}Fe_{10}$ alloy membranes and their effect on hydrogen absorption [100]. Through Voronoi tessellation analysis, icosahedra in the alloy before and after hydrogenation were identified. This revealed the presence of only three complete icosahedra and no Ni-centered ones in the unhydrogenated amorphous structure, which is believed to contribute to its low crystallization activation energy. However, the accuracy and efficiency of molecular dynamics simulations strongly depend on the quality of interatomic potential, making the development of reliable potential functions essential. Cao et al. reported a potential function for GaMnFeNiCu HEA using the machine learning method DeePMD, based on the DFT calculation database [101]. Utilizing machine learning potentials, the cooling process was simulated, revealing that the crystalline structure may be maintained throughout the cooling phase. This finding agrees with *in situ* environmental transmission electron microscopy and *in situ* synchrotron radiation X-ray diffraction results. In a recent work, Li et al. demonstrated via MD simulation that more stacking faults appear in the hydrogen-containing samples, and a high temperature can accelerate hydrogen diffusion (Fig. 5b) [102]. However, MD simulations are limited by their short time scales (typically in the nanosecond range) and the absence of reliable interatomic potentials for complex multicomponent HEAs. These limitations make it difficult to accurately model long-term structural or diffusion behaviors.

3.2.3. Calculation of the phase diagram (CALPHAD) approach

Phase diagrams serve as a roadmap for material design, predicting composition, phase stability, microstructure evolution, and final properties. The CALPHAD approach is a computational framework used to model phase stability and thermodynamic properties in multicomponent alloy systems [103]. At its core, the CALPHAD method describes the Gibbs free energy of each phase in a system as a function of temperature, pressure, and composition. Under constant temperature and pressure, the Gibbs free energy quantifies the stability of a phase. Assessed thermodynamic data from binary and ternary systems are extended to higher-order multicomponent systems through thermodynamically consistent interpolation and extrapolation to predict phase stability and phase diagrams [104]. Edalati et al. developed a single-phase stable TiZrCrMnFeNi alloy that achieved a reversible capacity of 1.7 wt% hydrogen at room temperature, as illustrated in Figs. 5c and d [105]. Floriano et al. used CALPHAD to identify potential compositions for single C14 Laves phase formation, confirming that the existence of the C14 Laves phase is crucial for room temperature applications [106]. Similarly, under the guidance of CALPHAD as well as the TCHEA3 database, a two-phase TiZrNbCrFe HEA with a significant reversible hydrogen capacity was designed by using the amount of equilibrium phases as a function of temperature to predict the formation of both equilibrium and non-equilibrium phases [107]. The experimental results show that TiZrNbCrFe HEA crystallizes primarily as a C15 Laves phase. The CALPHAD method not only can accurately predict hydrogen storage capacity but also allows precise determination of plateau pressure and thermodynamic properties, such as enthalpy change. The applicability of an alloy as a hydrogen storage medium mostly relies on its pressure–composition–temperature (P-C-T) curve. The CALPHAD method, by combining thermodynamic databases, experimental data, and computational techniques, can predict the P-C-T curves by calculating the Gibbs free energies of various phases. For instance, Zeng et al. developed a thermodynamic description of the Mg–Ni–H system based on the thermodynamically assessed constituent binary systems, which can be applied to analyze the hydriding behavior of Mg–Ni alloys [108]. Based on the thermodynamic analysis of the Mg-Ni-Nd-H system, the P-C-T curves and hydrogen storage capacities were precisely predicted, leading to the successful design of two new ternary compounds, $Nd_4Mg_{80}Ni_8$ and $Nd_{16}Mg_{96}Ni_{12}$, as promising hydrogen storage alloys [109]. The above research work suggests that CALPHAD is an effective tool to guide HEA composition design and process optimization, but it is restricted by the absence of a reliable thermodynamic database [110].

3.3. Machine learning

Machine learning has rapidly advanced in the field of hydrogen storage in recent years, showing great potential for material screening, performance prediction, and mechanism understanding [111,112]. High-quality hydrogen storage datasets with informative features are key to achieving accurate predictions using machine learning. Typically, such datasets are compiled from published experimental data, high-throughput computations, and inorganic materials databases. Currently, there are two available hydrogen storage datasets: a HydPARK database maintained by the U.S. DOE and a high-density, composition-rich dataset established by Huang et al. [113,114]. Data cleaning and preprocessing are essential steps for effective machine learning. Initially, Zhou et al. applied machine learning according to the implicit and explicit features of typical metal hydrides, based on a newly constructed proprietary dataset [115]. The most critical factors influencing hydrogen storage capacity, such as mean ionic character and Fe content, were identified through feature importance ranking. Subsequently, by applying composition-property scanning with averaged SVM/GBDT models, followed by targeted parameter screening, a $Ti_{0.9}Zr_{0.12}Mn_{1.2}Cr_{0.55}(VFe)_{0.25}$ HEA was successfully designed. This alloy demonstrated cost-effective and comprehensive performance, achieving 1.9 wt% (127.3 kg $H_2 \cdot m^{-3}$) in saturation. In a word, machine learning-driven composition customization provides a cost-efficient alternative to trial-and-error experiments and offers a promising strategy for developing HEAs as advanced hydrogen storage materials.

Traditional methods for alloy design often rely on experience or limited experimental data, which are inefficient and costly when dealing with the vast compositional space of HEAs. As the research on HEAs progresses, both experimental and computational data are being increasingly utilized to derive insights [116]. Machine learning has become prominent in the compositional design of HEAs through the prediction of phase structure and target properties [117–119]. For instance, Huang et al. used a K-nearest-neighbor algorithm, support vector machines, and neural networks to predict the phase structure of 401 HEAs, achieving a prediction accuracy of 94.3% in classifying solid solutions and compound phases [120]. Similar studies on HEAs with machine learning were conducted and have contributed to this field [121,122]. Qi et al. employed phase parameter information from conventional binary alloys as feature inputs for their machine learning models, achieving over 80% accuracy in predicting more than 600 HEAs' phase structures [123]. Furthermore, the prediction accuracy of phase structure can be improved by a combination of machine learning and traditional thermodynamic simulations. Kaufmann et al. constructed a random forest model based on 13 features using the 1798 DFT calculation results for equiatomic alloy phase structure data [124]. The accuracy of the model in forecasting the phase structure of 134 experimental alloys was 100%, surpassing the outcomes of thermodynamic simulations and DFT calculations. Although the prediction accuracy reported is high, large limitations remain, due to the limitations of training samples and differences in the classification of target phase structure types.

The application of machine learning also extends to predicting the hydrogen storage properties of HEAs; this requires the simple and informative descriptors that are vital to achieve accurate predictions. Features of hydrogen storage alloys generally fall into two main categories: input features (e.g., elemental composition, atomic parameters, structural parameters, and processing conditions) and target features (e.g., hydrogen storage capacity, hydride formation enthalpy, and equilibrium plateau pressure). Witman and co-workers identified the molecular volume of alloys as a significant predictor of hydride properties to accurately predict hydride thermodynamics and hydrogen storage capacity using machine learning [63,125]. It is noteworthy that the molecular volume of alloys serves as the most significant predictor in the realm of thermodynamics, aligning with the empirically derived model established in earlier studies [126]. Strozi et al. employed a compositional machine learning modeling technique to predict the thermodynamics of hydrides and clarify their design principles based on physical insights [127]. The experimentally determined maximum storage capacity (H/M) shows a slight decrease from 2.0 to 1.9 with increasing Cr content up to 30 atom%, and a trend of semi-quantitative prediction in machine learning is consistent. Nevertheless, the HydPAPK database utilized in the earlier research is limited to only 2004, meaning that numerous recent findings have not been included. Zhou et al. predicted the hydrogen solution energies from local HEA chemical environments using machine learning algorithms [128]. Raw data published between 1998 and 2019 were collected and organized by Suwarno and colleagues [129]. According to their results, the three elements Ni, Cr, and Mn play a significant role in influencing the hydrogen properties of AB_2-type alloys. One of the key aspects focused on in this area is the predictable determination of P-C-T curves. To address this important issue, several machine learning techniques were employed [130]. Among the different models, the deep neural network demonstrated superior performance, with an impressive average correlation coefficient (R^2) of 0.9307. BCC metals can often store hydrogen through a two-phase process, first forming a BCC or body-centered tetragonal (BCT) monohydride and then an FCC dihydride. A DFT-informed multi-objective Bayesian optimization strategy was utilized to design BCC HEAs for room-temperature hydrogen storage [131]. In Fig. 6a, a DFT procedure for obtaining hydrogen binding energies gives the descriptor of the thermodynamics for the first and second stages of absorption as bulk modulus and d-band, respectively. Ultimately, the BCC-type VNbCrMoMn HEA was found to meet the target values for ΔE_{mono} and ΔE_{di}, which can theoretically store 2.83 wt% hydrogen at room temperature (Fig. 6b). In a similar study, the enthalpy of hydride formation in HEAs based on 420 datum points was predicted using machine learning [132], with the highest R^2 value of 0.68 (Fig. 6c). Taking TiZrCrMnFeNi HEA as an example (structure shown in Fig. 6d), the prediction of machine learning is consistent with both experimental measurements and DFT calculations, which can be used to design new HEAs with hydride formation enthalpies in the range of −25 to −39 kJ · mol^{-1} (Fig. 6e). These results suggest machine learning is an effective and rapid method for developing high-entropy materials for hydrogen storage. Recently, Radhika et al. accurately predicted the VEC, phase, and hydrogen-to-metal ratio (H/M) by gathering and examining existing HEA data through machine learning techniques [66]. They created a database comprising 741 quaternary alloys and 631 quinary HEAs. Among them, 774 alloys satisfied the set conditions, showing great potential for hydrogen storage applications. Despite significant progress, the complexity of HEAs for extensive ingredients is still the biggest challenge.

Multi-scale calculation methods are gradually being used for design to enhance the hydrogen storage performance of HEAs. These methods are conducive to investigating key factors such as the site preference of hydrogen atoms, phase transformation mechanisms, thermodynamic stability, kinetic behavior, and cyclic stability. This insight provides valuable guidance for designing novel hydrogen storage materials based on HEAs. DFT provides atomic-level insights into hydrogen adsorption, dissociation, and electronic structure in HEAs, while MD captures hydrogen diffusion and the effects of defects, temperature, and stress on transport behavior. In addition, CALPHAD enables phase diagram prediction and thermodynamic analysis for alloy design. Machine learning facilitates rapid property prediction and composition screening based on large-scale data. However, these methods often fail to fully capture the complex behavior of HEAs in practical applications. For instance, theoretical models struggle to accurately predict phase transformation behavior and defect evolution in alloys under high temperatures and stress, which can lead to significant discrepancies compared to experimental observations. Meanwhile, experimental confirmation often lags due to challenges in synthesis reproducibility, phase complexity, and high-throughput testing limitations. To address this gap, future research should aim to establish a closed-loop framework that integrates

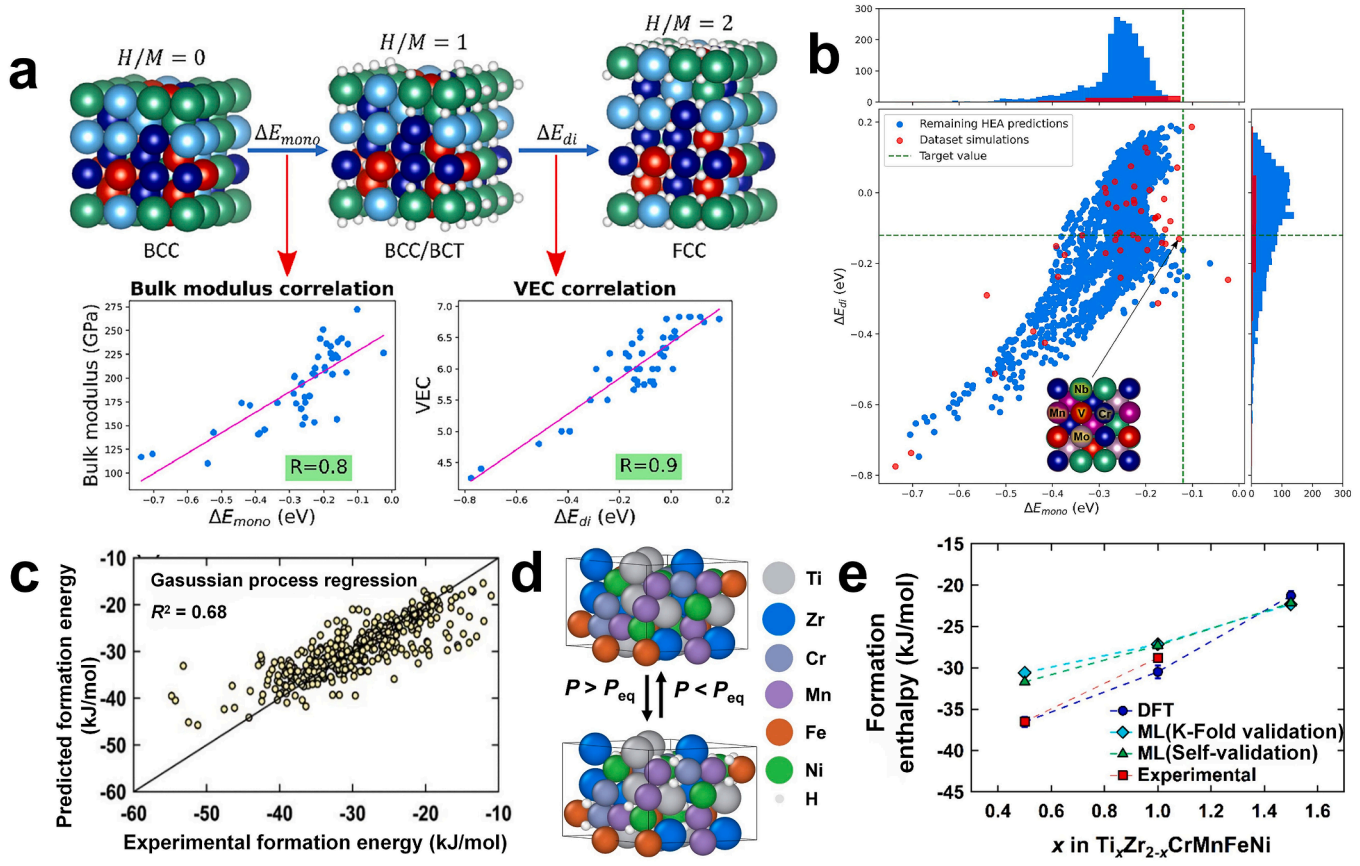

Fig. 6. (a) Illustration of DFT procedure for obtaining hydrogen binding energies, and the thermodynamic descriptor for the first and second stages of absorption. (b) The distribution of predicted and simulated hydrogen binding energies. Reproduced with permission [131]. Copyright 2024, Elsevier. (c) Predicted formation enthalpy versus the measured experimental formation enthalpy, using Gaussian process regression algorithms. (d) Optimized supercells for first-principles DFT calculations of TiZrCrMnFeNi and TiZrCrMnFeNiH$_6$. (e) Comparison of predicted formation enthalpy of hydride for HEAs, using different approaches. Reproduced with permission [132]. Copyright 2024, Elsevier.

theoretical design, experimental validation, and iterative optimization. This process can be accelerated by automated synthesis and artificial intelligence (AI)-assisted testing platforms, enabling efficient coordination between computational and experimental workflows.

4. Synthetic and morphology design

HEAs can be synthesized using conventional alloying methods; Yan and co-workers have systematically summarized the classifications and preparation strategies [133,134]. However, their properties are strongly affected by composition, particle size, and phase structure, all of which are highly dependent on the synthesis methods and experimental conditions employed. It is therefore essential to understand that the interplay among these factors is necessary for optimizing HEA performance in different applications. For hydrogen storage applications, HEAs are often synthesized through arc melting or mechanical alloying, as well as other methods like laser engineered net shaping (LENS), melt spinning, and HPT.

4.1. Synthetic method for bulk HEAs

The most common method for preparing bulk HEAs is melting followed by casting, typically conducted via arc or induction melting. To minimize oxidation, the entire process is generally performed under vacuum or an inert atmosphere. The cooling rate is also critical for the HEA's phase stability and microstructure, as it must be sufficiently rapid to kinetically retain the thermodynamically metastable solid-solution phase. In addition, remelting is often combined with recrystallization to minimize grain boundary formation and enhance crystal quality. This process can ensure compositional homogeneity [86,135–138]. Specific configurations, such as the sequential melting of elements at varying currents, are also employed to avoid oxygen contamination through the use of a Ti getter [139]. For example, Sahlberg et al. developed a TiVZrNbHf HEA with a BCC structure capable of absorbing more hydrogen than the individual element, achieving a H/M ratio of 2.5. However, elements are affected by the molecule's thermal motion and easy volatilization, characteristics of a low melting metal, as these lead to chemical segregation [140]. Kao et al. discussed the hydrogen storage properties of CoFeMnTiVZr HEA produced through vacuum arc melting and found that increased levels of Ti and Zr caused significant segregation, reducing the hydrogen storage capacity [58]. After melting, a solidified HEA can be shaped into disk samples via suction casting [141] or processed into mechanical HEA powders [137,142]. Induction melting is another effective preparation method due to the vacuum environment employed, as that improves the alloy's purity and uniformity [143–145]. Montero et al. prepared a $Ti_{0.325}V_{0.275}Zr_{0.125}Nb_{0.275}$ alloy via high-temperature arc melting and compared its hydrogen storage performance with a rehydrided sample under Ar and the as-cast alloy processed by ball milling under hydrogen [146]. The reversible capacity can be maintained at about 2 wt% in the first cycle.

4.2. Synthetic method for powder HEAs

Mechanical alloying is a nonequilibrium synthesis method that promotes intricate physicochemical processes at the atomic level. Zepon and co-workers prepared an $MgZrTiFe_{0.5}Co_{0.5}Ni_{0.5}$ HEA using high-energy

ball milling to probe the phase transition under different atmospheres [147]. A single BCC phase was formed under argon but transformed to an FCC phase under hydrogen, absorbing 1.2 wt% hydrogen. The effect of milling time on MgTiVCrFe HEA phase formation and hydrogen storage properties was investigated, during which MgTiVCrFe decomposed after hydrogen cycling while MgVCr maintained phase stability, demonstrating a reversible hydrogen capacity of 0.9 wt% at 623 K [148]. Synthesis and processing techniques are crucial in the research and advancement of novel materials such as HEAs. Nonetheless, the existing approach typically demands stringent conditions, such as elevated pressure, high temperatures, and inert atmosphere safeguards. Mechanical alloying always induces severe lattice distortion, high defect density, and nanocrystalline structures through repeated cold welding and fracturing. These microstructural features facilitate hydrogen diffusion and improve storage capacity. In contrast, arc melting yields more homogeneous, coarse-grained solid-solution phases with fewer defects, providing greater thermodynamic stability during hydrogen cycling.

As its dimensions are reduced to the nanoscale, the HEA becomes an ideal platform for various surface reactions due to the increased specific surface area, strong synergistic effects, wide compositional flexibility, and significant lattice distortion. Therefore, HEA nanoparticles (HEA-NPs) show great potential for energy catalysis, but their synthesis is a challenging task [52,149]. This is mainly because they contain diversified elements and require non-equilibrium conditions. The main difficulty results from the different properties of each element, such as atomic size, melting point, and chemical reactivity. These differences can cause phase separation or uneven distribution during synthesis. It is still difficult to control the particle size, shape, and uniform distribution of elements inside HEA-NPs.

Carbon thermal shock (CTS) is a burgeoning method for preparing HEA-NPs [150]. In a typical CTS process, metal precursors are flash-heated and cooled on an oxygenated carbon carrier by adjusting the impact duration and slope. The rapid thermal decomposition of metal precursors at very high temperatures (2000–3000 K) leads to the formation of small droplets containing polymetallic solutions. The subsequent rapid cooling crystallizes these droplets into uniform alloy NPs, preventing issues like element aggregation and phase separation. Careful control of CTS parameters such as substrate, temperature, shock duration, and heating/cooling rate may help uncover novel HEA-NPs with both scientific significance and practical advantages. In addition, sputtering deposition works by bombarding the target surface with high-energy gas ions, resulting in a physical ejection of surface atoms or small clusters [151]. This method is considered a friendly approach for preparing metal NPs because it does not require metal precursors or additional stabilizers. Similarly, the solvothermal method enables the employment of a broad range of metal elements while remaining cost-effective [152,153]. This method also enables the precise regulation of HEA-NP size, morphology, and crystallographic facet exposure. However, achieving atomic-scale precision in nanostructural control remains a formidable task. Recently, Wang et al. synthesized HEA-NPs across various substrates by laser scanning ablation (LSA). This process involves mixing metal chlorides on a carbon substrate, which is then irradiated in hexane with laser pulses at room temperature, achieving uniform mixing of up to nine metal elements (Fig. 7a). Moreover, this technique is highly versatile, allowing HEA-NPs to be synthesized on diverse substrates or as colloidal particles [154].

Gao et al. developed a fast-moving bed pyrolysis (FMBP) technique, wherein the synthetic HEA-NPs can be immobilized upon granuliform supports [155]. At a temperature of 923 K, the distribution of particle sizes for MnCoNiCuRhPdSnIrPtAu HEA-NPs was quite uniform at approximately 2 nm (Fig. 7b). Recently, a liquid metal reaction medium was used to synthesize HEA-NPs under mild conditions [101], where nanoscale dispersed liquid metal served as a reservoir and was mixed with different metal salts as precursors (Fig. 7c). The metal salts then underwent pyrolysis and hydrogen reduction, resulting in the mixing of metal elements with liquid metal to form HEA-NPs at a temperature of 923 K. Furthermore, nanoparticle structures can be precisely produced by tuning the mixing enthalpy. The synthesis of HEA-NPs on various substrates under mild conditions has important implications in the fields of catalysis and energy storage. Identifying HEAs that simultaneously exhibit superior target performance and thermal stability within a vast compositional space is a formidable challenge, as conventional approaches are often time-consuming and inefficient. Therefore, the implementation of high-throughput strategies is urgently needed to accelerate the discovery and development of high-entropy alloys.

4.3. *High-throughput synthetic methods*

The traditional trial-and-error method for HEA research is inefficient, costly, and requires long development cycles. High-throughput synthetic methods can be used for the highly efficient synthesis of both bulk and powder HEAs. High-throughput experiments for HEAs facilitate rapid preparation and characterization, enabling the efficient screening and validation of new compositions and process combinations. Technological development in this area follows two paths: (1) parallel preparation of multiple samples with varying compositions and (2) creation of gradient changes in composition or process parameters on a single sample. As shown in Fig. 8a, *in situ* high-temperature synthesis of $FeCoNiCrCuAl_x$ was performed using a transmission electron microscope (TEM) [156]. The dynamic melting procedure for FeCoNiCrCu combined with Al was documented, and the composition of $FeCoNiCrCuAl_x$ was analyzed using EDS. This method helps solve some problems of traditional arc melting and casting methods, i.e., the element loss that occurs when low-melting-point metals are melted repeatedly. Moorehead et al. employed laser additive manufacturing to control the independent feed rates of nanomaterial powders with different elements (Fig. 8b) [157]. Based on the four-element MoNbTaW refractory alloys, graded samples between a three-component alloy and pure metal elements were compounded. The influence of single element content on alloys' microstructure and microhardness has also been systematically studied. Moreover, Zhu et al. introduced a rapid and high-throughput approach to synthesize bulk HEAs using radio frequency inductively coupled plasma (RF-ICP) (Fig. 8c). Notably, typical HEAs can be synthesized in just 40 s per alloy. Elsewhere, an automated platform designed to simultaneously process 20 samples significantly enhanced the efficiency of HEA synthesis [158]. However, additive manufacturing materials are prone to defects, which can severely degrade performance. High-throughput synthesis helps speed up HEA discovery and improvement, but it still has limits with respect to sample size, accuracy of thermodynamic data, and testing speed. To solve these problems, we need to combine automated production with real-time testing, machine learning, and better process control.

Overall, mechanical alloying facilitates the enhanced solubility of alloying elements in the HEA matrix and enables the formation of metastable phases, but the long-term and intense nature of the milling process may introduce impurities and structural defects. In contrast, arc melting provides a simple and efficient route to obtain bulk HEAs with high purity, although compositional segregation and inhomogeneity may occur, usually during solidification. Although high-throughput synthesis can accelerate the compositional screening of HEAs, it faces a few challenges, such as data overload, sample heterogeneity, and high cost for large-scale implementation. These preparation methods for HEAs have been well developed, and some experimental attempts have been made to validate theoretical predictions. However, the complexity of HEAs presents certain challenges for experimental validation. Variations in alloy compositions, synthesis method, and external conditions inevitably lead to discrepancies in experimental results, making it difficult to achieve full alignment with theoretical predictions. Moreover, the synthesis method employed determines the phase formation and crystallite size, which directly influences hydrogen solubility and hydride stability. Therefore, by adjusting the synthesis parameters, it is possible to control the resulting microstructure, which ultimately

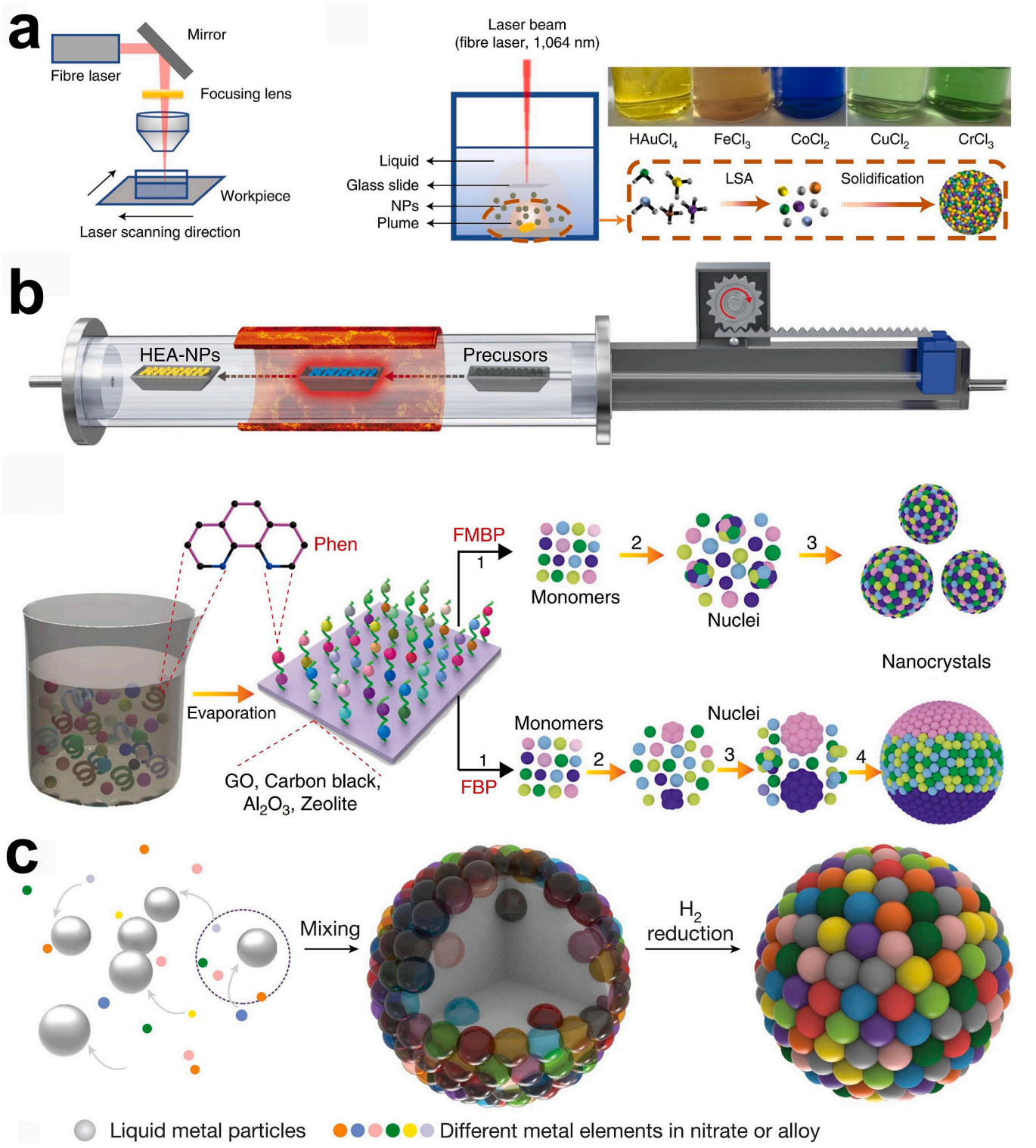

Fig. 7. (a) LSA approach to synthesizing HEA-NPs. Reproduced with permission [154]. Copyright 2022, Springer Nature. (b) FMBP strategy for synthesis of HEA-NPs. Reproduced with permission [155]. Copyright 2020, Springer Nature. (c) Synthesis and characterization of HEA-NPs. Reproduced with permission [101]. Copyright 2023, Springer Nature.

governs key performance indicators such as hydrogen capacity, sorption kinetics, and cyclic durability.

5. HEAs for hydrogen storage

The practical application of hydrogen energy is limited by a major challenge in the form of efficient storage. HEAs offer a promising foundation for advancing solid-state hydrogen storage materials. These materials exhibit objective hydrogen storage capacity, extensive composition space, and excellent catalytic performance, making them effective for both hydrogen storage and catalysis. In this section, we discuss the role of HEAs in hydrogen storage, particularly focusing on absorption, electrochemistry, and catalysis.

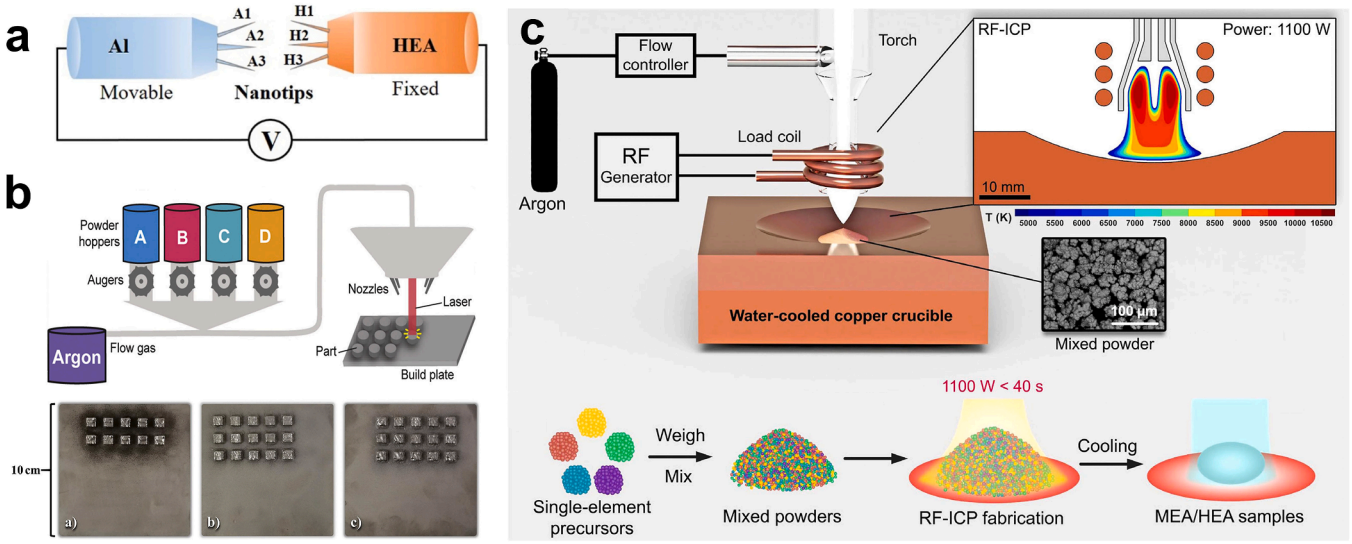

Fig. 8. (a) Schematic illustration of the *in situ* melting process. Reproduced with permission [156]. Copyright 2019, Elsevier. (b) Schematic illustration of the LENS MR-7 system, and pictures of the build plates from each printing iteration. Reproduced with permission [157]. Copyright 2020, Elsevier. (c) Schematics of the experimental setup of the RF-ICP system for alloy synthesis and the RF-ICP synthesis of HEAs using mixed pure metal powders. Reproduced with permission [158]. Copyright 2020, Wiley-VCH.

5.1. Hydrogen absorption

Due to the high-entropy effect, different metal atoms occupy lattice sites in varying ways, influencing hydrogen absorption. As a result, the phase structure of HEAs plays a crucial role in determining their hydrogen storage capacity [159,160]. Current research has primarily focused on HEAs with BCC and the intermetallic C14 Laves phase, these are summarized in Table 1. Here, we explore HEAs in the context of hydrogen absorption.

Among traditional metals and alloys utilized for hydrogen storage, BCC alloys derived from the first 3*d* transition elements (e.g., Ti, V, and Cr) represent the most promising class due to their high hydrogen capacity (H/M of 2). For many BCC-structured HEAs, the H/M ratio can attain a value of 2 or greater. As a successful example, TiVZrNbHf HEA achieves an H/M of 2.5, but that corresponds to only 2.7 wt% owing to the high atomic weight of the elements [140]. In this HEA, both tetrahedral and octahedral interstitial sites are favorable for accommodating hydrogen atoms; this is coupled with large lattice distortions. HEAs designed with hydrogen-absorbing elements in later research did not exhibit a comparable hydrogen storage capacity [161]. However, the practical application of BCC HEAs is limited by the high thermodynamic stability of their hydrides, which hampers the dehydrogenation performance. In addition, the synergistic effect between the main phase and the secondary phase may enhance the hydrogen ab/desorption performance of BCC-type HEAs. On the one hand, the secondary phase can modify lattice parameters and provide favorable interstitial sites, while on the other hand, it influences microstructural stability and hydrogen diffusion pathways. To reduce the hydride stability, Cheng et al. aimed to introduce a new phase in the BCC-type $Ti_4V_3NbCr_2$ alloy by doping with transition metals (Fe, Mn, and Ni) [162]. This successfully resulted in the precipitation of a secondary phase in the BCC matrix, with the largest amount formed in the Ni-containing HEA. Therefore, the lowest endothermic peak was observed at 570 K during differential scanning calorimetry (DSC) characterization of the $Ti_4V_3NbCr_2Ni$ HEA (Fig. 9), corresponding to hydrogen desorption. The presence of the secondary phase obviously creates additional pathways for hydrogen desorption, facilitating hydrogen release from the HEA hydride. Gaspar et al. reveal that Cu substitution in $TiZrHfVNb_{1-x}Cu_x$ alloys induces BCC and C14 Laves dual-phase formation through microstructural segregation, enabling rapid activation and reversible hydrogen storage of ~1.5 wt% in near-ambient conditions, highlighting their promise for practical solid-state hydrogen storage [163]. Similar results were achieved in a Cu-doped ZrTiVFe HEA, in which the doping of Cu reduced the residual hydrogen from 0.37 to 0.084 wt% [164].

Additionally, intermetallic compounds with the C14 Laves phase typically absorb 1 H/M, form hydrides, and maintain the phase unchanged with expanded lattice parameters after absorbing hydrogen [38,105,106]. HEA containing the C14 Laves phase is a promising candidate, as it adsorbs large amounts of hydrogen at room temperature and has a superior reaction rate, a long cycling lifespan, and easy activation. Sleiman et al. synthesized the $Ti_{0.3}V_{0.3}Mn_{0.2}Fe_{0.1}Ni_{0.1}$ HEA with a multiphase structure of BCC and the C14 Laves phase [165]. It can absorb 1.6 wt% hydrogen within an hour at 298 K. Moreover, XRD results demonstrated that both phases can absorb hydrogen while maintaining their crystal structure with increased lattice parameters. Chanchetti et al. designed $Ti_{31}V_{26}Nb_{26}Zr_{12}M_5$ (M = Fe, Co, and Ni) HEAs and investigated their hydrogen storage properties [166]. A multi-step process for hydrogen ab/desorption was confirmed: BCC + C14 alloy ↔ intermediate BCC hydride + C14 hydride ↔ FCC + C14 hydrides. Xiao et al. proposed a dual-phase synergistic effect during the de/hydrogenation process of TiZrCrMnNi(VFe) HEA. It can rapidly reach a saturated capacity of 1.83 wt% H_2 at 273 K without any activation treatment due to its lower energy barrier [167]. These studies suggest that phase engineering is effective for developing pathways to optimize HEA-based hydrogen storage. However, the underlying mechanisms remain only partially understood.

Beyond phase structural design, phase transition and activation behavior are other key factors governing hydrogen storage performance [168]. Typically, HEAs show poor hydrogen uptake during initial exposure, and repeated hydrogenation/dehydrogenation cycles are required to activate the material. For instance, Zhang et al. investigated the activation of TiZrNbTa HEA and proposed a two-step activation mechanism [141]. As illustrated in Figs. 10a and b, activation behavior indicated that the hydrogen absorption temperature dropped significantly, to room temperature (300 K) from 715 K, after the activation process. That is to say, the kinetics of hydrogen absorption was remarkably enhanced for an activated alloy. Upon activation, the majority of oxides on the surface of the TiZrNbTa HEA were transformed into suboxides and subhydroxides, whereas only some of the surface oxides on pure metals were converted, forming suboxides. In addition,

Table 1
Reported absorption hydrogen storage performance of HEAs.

HEA composition (ordered by atomic number)	Synthesis method	Alloy phase	Hydride phase	Hydrogen absorption capacity (wt%)	Hydrogen absorption kinetics	Onset/peak hydride decomposition temperature (K)	Ref.
MgAlTiFeNi	BM[a] (H_2)	BCC[g]	BCC	1.0	1.0 wt% in 3600 s (598 K, 1.5 MPa H_2)	558/598	[184]
MgTiVCrFe	HEBM[b] (H_2)	BCC	BCC	0.3	0.2 wt% in 3600 s (303 K, 2.0 MPa H_2)	483/520	[148]
$Mg_{0.1}Ti_{0.3}V_{0.25}Zr_{0.1}Nb_{0.25}$	BM	BCC	FCC[h]	2.7	2.7 wt% in 60 s (298 K, 2.5 MPa H_2)	523/563	[182]
$Al_{0.1}Ti_{0.3}V_{0.25}Zr_{0.1}Nb_{0.25}$	AM[c]	BCC	BCT[i]	2.6	~2.6 wt% in 300 s (298 K, 2.5 MPa H_2)	383/403	[185]
$Ti_{0.28}V_{0.28}Cr_{0.15}Nb_{0.28}$	AM	BCC	FCC	3.2	3.2 wt% in 60 s (293 K, 2.5–3.0 MPa H_2)	325/-	[186]
$Ti_{0.32}V_{0.32}Co_{0.05}Nb_{0.32}$	AM	BCC	FCC	3.1	3.1 wt% in 60 s (293 K, 2.5–3.0 MPa H_2)	362/-	[186]
$Ti_{0.32}V_{0.32}Ni_{0.04}Nb_{0.32}$	AM	BCC (major)	FCC	3.2	3.2 wt% in 60 s (293 K, 2.5–3.0 MPa H_2)	409/-	[186]
TiVZrNbMo	LENS[d]	BCC (major)	FCC	2.3	2.3 wt% in 1380 s (303 K, 8.5 MPa H_2)	–/–	[187]
TiVZrNbMo	LENS	BCC (major)	BCC	0.6	0.6 wt% in 1380 s (303 K, 8.5 MPa H_2)	–/–	[187]
TiVZrNbHf	AM	BCC	BCT	2.1	1.7 wt% in 300 s (573 K, 2.0 MPa H_2)	623/-	[169]
$Ti_{0.3}V_{0.25}Zr_{0.1}Nb_{0.25}Ta_{0.1}$	AM	BCC	FCC	2.2	~2.4 wt% in 120 s (373 K, 3.3 MPa H_2)	510/-	[188]
TiVNbMo	AM	BCC	FCC	~1.5 H/M	–	473/~593	[86]
TiZrNbHf	AM	BCC	BCT	~2.0 H/M	–	553/-	[86]
TiVNbHf	AM	BCC	FCC	~2.0 H/M	–	553/-	[86]
TiVNbHf	AM	BCC	FCC	2.0 H/M	–	~593/-	[189]
TiVNbTa	AM	BCC	FCC (major) BCT (minor)	1.9 H/M	–	~385/-	[135]
TiCrMnFeNiZr	AM + HPT[e]	C14 Laves (major)	C14 Laves	1.7	1.6 wt% in 60 s (303 K, 3.9 MPa H_2)	303/-	[105]
$Ti_{0.32}Cr_{0.43}Mn_{0.1}Fe_{0.13}Zr_{0.02}$	HFMLM[f]	C14 Laves	C14 Laves	1.6	1.5 wt% in 180 s (293 K, 8.0 MPa H_2)	–/–	[190]
TiZrNbMoHf	AM	BCC	FCC	1.2	–	~540/575	[136]
$Ti_{0.4}V_{0.3}Cr_{0.2}Nb_{0.1}$	AM	BCC	FCC	3.7	3.7 wt% in 150 s (300 K, 5.0 MPa H_2)	602/-	[162]
TiVCrFeCu	AM	C14 Laves (major)	C14 Laves	1.1	1.1 wt% in 1800 s (473 K, 1.0 MPa H_2)	–/–	[164]
TiCrFeNiZrNb	AM	C14 Laves	C14 Laves	1.5	–	–/–	[191]
TiVFeZrNb	AM (vacuum)	C14 Laves (major)	C14 Laves (major) FCC (minor)	1.6	1.6 wt% in 100 s (323 K, 1.0 MPa H_2)	313/448	[142]
$Ti_{0.31}V_{0.26}Fe_{0.05}Zr_{0.12}Nb_{0.26}$	AM	BCC (major) C14 Laves (minor)	FCC (major) C14 Laves (minor)	2.9	2.9 wt% in 36 s (298 K, 4.2–4.3 MPa H_2)	–/–	[166]
$Ti_{0.31}V_{0.26}Co_{0.05}Zr_{0.12}Nb_{0.26}$	AM	BCC (major) C14 Laves (minor)	FCC (major) C14 Laves (minor)	2.9	2.9 wt% in 48 s (298 K, 4.2–4.3 MPa H_2)	–/–	[166]
$Ti_{0.31}V_{0.26}Ni_{0.05}Zr_{0.12}Nb_{0.26}$	AM	BCC (major) C14 Laves (minor)	FCC (major) C14 Laves (minor)	2.9	2.9 wt% in 60 s (298 K, 4.2–4.3 MPa H_2)	–/–	[166]
VMnFeNiLa	LENS	Multiphase	Multiphase	0.1–0.8	0.1–0.8 wt% in 600 s (308 K, 4.5 MPa H_2)	308/-	[192]
$V_{0.5}Cr_{0.5}Mn_{0.5}Fe_{0.5}Zr_1$	AM	C14 Laves	C14 Laves	~1.6	~1.6 wt% in 2400 s (323 K, 4.0 MPa H_2)	–/–	[137]
$Ti_{25}V_{30}Cr_{31}Nb_{10}Mo_4$	AM	BCC	FCC	2.2	3.5 wt% in 70 s (300 K, 9.0 MPa H_2)	323/-	[193]
$Ti_{25}V_{30}Cr_{33}Ni_2Nb_{10}$	AM	BCC	FCC	2.2	2.9 wt% in 140 s (303 K, 1.0 MPa H_2)	303/-	[59]

[a] **BM** ball milling.
[b] **HEBM** high-energy ball milling.
[c] **AM** arc melting.
[d] **LENS** laser-engineered net shaping.
[e] **HPT** high-pressure torsion.
[f] **HFMLM** high-frequency magnetic levitation melting.
[g] **BCC** body-centered cubic.
[h] **FCC** face-centered cubic.
[i] **BCT** body-centered tetragonal.

vacancy clusters caused by the segregation of H atoms were enriched due to sluggish self-diffusion in the TiZrNbTa HEA, and this was responsible for a high nucleation rate after activation (see Fig. 10c). Sleiman et al. performed a systematic study on the activation process for the TiVZrHfNb HEA by controlling particle size, hydrogen pressure, and operating temperature [169]. They found that activation was quick when the particles were less than 0.5 mm in diameter. Moreover, an amorphous phase was formed upon hydrogenation, which may have

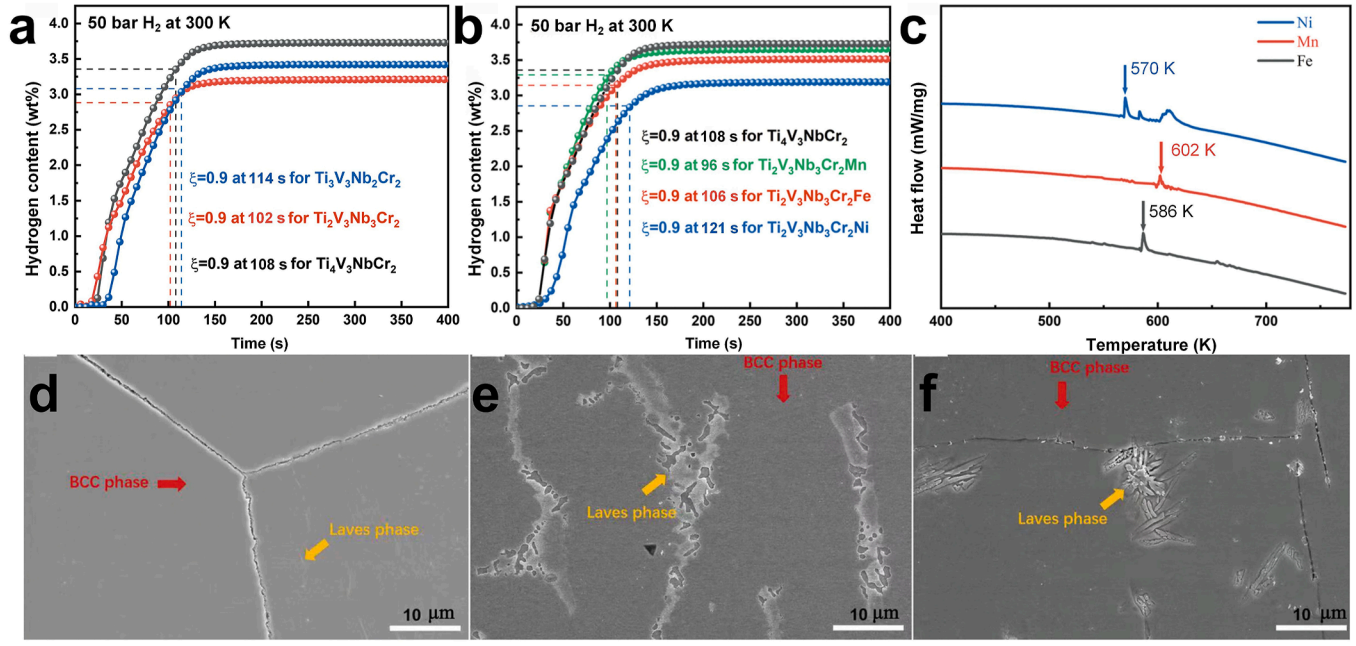

Fig. 9. (a) Hydrogen sorption kinetics of TiVCrNb HEAs in the first cycle under 50 bar H_2 at 300 K. (b) Hydrogen sorption kinetics of $Ti_4V_3NbCr_2M$ (M = Mn, Fe, and Ni) HEAs. (c) DSC curves of hydrogenated alloys at 10 K · min^{-1} heating rate. SEM for (d) $Ti_4V_3NbCr_2Mn$, (e) $Ti_4V_3NbCr_2Fe$, and (f) $Ti_4V_3NbCr_2Ni$. Reproduced with permission [162]. Copyright 2022, Springer.

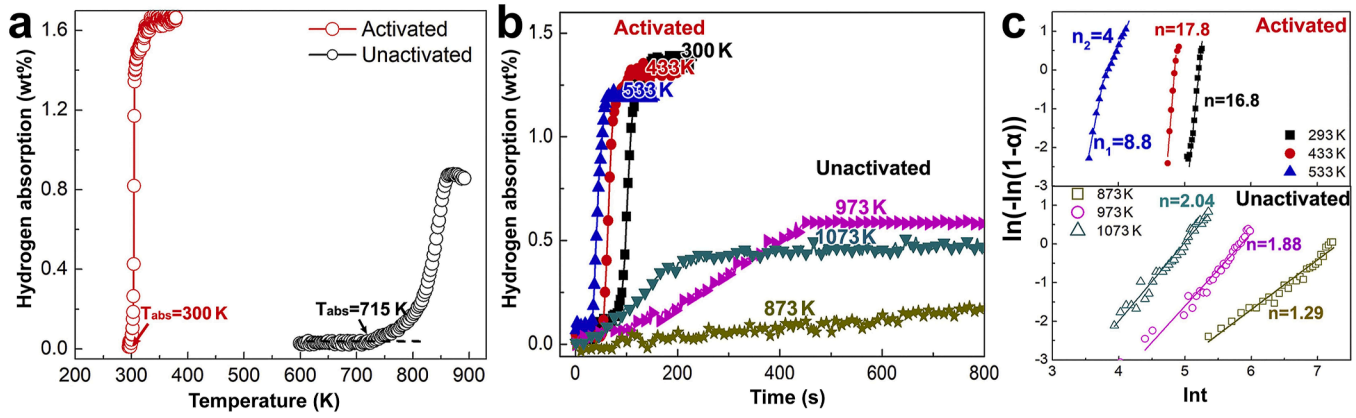

Fig. 10. Activation behavior of TiZrNbTa HEA: (a) hydrogen absorption versus temperature (heat rate 3 K · min^{-1}), (b) hydrogen absorption kinetics (at 2 bar), and (c) hydrogen absorption mechanism before and after activation. Reproduced with permission [141]. Copyright 2019, Elsevier.

been dependent on the hydrogenation temperature and particle size. These findings highlight that activation is a process strongly influenced by microstructural and processing parameters.

Elemental regulation provides another effective strategy to enhance activation behavior and hydrogen storage performance. For example, Wen et al. studied the effect of Zr doping on the hydrogen absorption and desorption of $Ti_{35-x}V_{25}Cr_{15}Nb_{25}Zr_x$ HEAs [170]. The $Ti_{29}V_{25}Cr_{15}Nb_{25}Zr_6$ alloy achieved a hydrogen absorption capacity of 2.21 wt% at 373 K and 3.1 MPa. Zr substitution for Ti induced significant lattice distortion, which enhanced the hydrogen absorption kinetics and improved the overall ab/desorption performance. Higher Zr content also encouraged the formation of C14 Laves phases along the BCC matrix, providing hydrogen diffusion channels and accommodating more H atoms. However, excessive C14 Laves phases decreased the proportion of the primary BCC hydrogen-absorbing phase, reducing the hydrogen capacity at elevated temperatures. On the other hand, DFT calculations for the TiZrHfMoNb HEA revealed that increased H–H bond disorder and reduced lattice distortion destabilized the BCC phase, leading to a BCC → FCC transition [171]. This unique behavior, unlike that of conventional alloys, arises from the severe lattice distortion present before hydrogenation. Ma and coworkers studied the effect of lattice distortion on the activation behavior of $(ZrTiVFe)_xAl_y$ HEA. Results show that $(ZrTiVFe)_{0.8}Al_{0.2}$ HEA, with a high Al content, is easier to activate due to the refined microstructure [172]. Recently, Cheng et al. designed a series of HEAs through Cr substitution for Ti in $V_{30}Nb_{10}(Ti_xCr_{1-x})_{60}$ [173]. The addition of rare earth (RE) elements is particularly important for enhancing the hydrogen storage performance of alloys [174–176]. For example, Pr, Sm, and Nd were introduced to reduce the incubation time of $Ti_{1.1-x}Fe_{0.8}Mn_{0.2}$ alloy [177]. Doping Ho, Ce, and La into $Ti_{1.02}Cr_{1.1}Mn_{0.3}Fe_{0.6}$ alloy can improve activation and hydrogen storage capacity [178]. Zhou and co-workers ingeniously designed Ce-doped TiZeCrMn alloys to influence activation [179]. The foregoing studies provide a feasible way to develop efficient hydrogen storage alloys.

Despite these advances, HEAs often have limited gravimetric capacity due to the heavy elements employed. To address this issue, magnesium (Mg), a low-cost metal with high hydrogen affinity and low

atomic weight, can be incorporated to both enhance hydrogen storage capacity and reduce material cost [180]. However, most reported Mg-based high-entropy alloys can only absorb hydrogen at elevated temperatures, and the resulting hydrides are too stable to be dehydrogenated at room temperature (298–373 K). For example, Zepon et al. experimentally synthesized a single-phase BCC $MgZrTiFe_{0.5}Co_{0.5}Ni_{0.5}$ HEA, which required a high temperature of 623 K to absorb hydrogen. The alloy exhibited sluggish hydrogen absorption kinetics, reaching its maximum hydrogen storage capacity of H/M = 0.67 (corresponding to 1.2 wt%) only after 1.5 h [147]. Marques et al. synthesized $MgTiNbCr_{0.5}Mn_{0.5}Ni_{0.5}$, which exhibited good hydrogen absorption capacity at elevated temperatures of 603–723 K, reaching an H/M ratio of about 0.8 (corresponding to 1.6 wt%). However, complete dehydrogenation could only be achieved at higher temperatures of 623–723 K [181]. Furthermore, due to the low melting point of metallic Mg, conventional arc melting leads to non-negligible evaporation, making accurate control of the elemental composition challenging. Based on this, Mg-containing HEAs are primarily synthesized via ball milling in an Ar atmosphere. A typical $Mg_{0.1}Ti_{0.3}V_{0.25}Zr_{0.1}Nb_{0.25}$ HEA was prepared through this approach by using 10 at% Mg atoms to replace 2.5 at% of each refractory metal in $Ti_{0.325}V_{0.275}Zr_{0.125}Nb_{0.275}$. The Mg-containing HEA exhibited much higher reversible capacity than the corresponding quaternary alloy, especially from the second cyclic test [182]. Theoretically, a BCC $Mg_6Ti_{24}V_{18}Cr_{12}$ was designed based on DFT calculations, and a gravimetric hydrogen storage capacity of 4.091 wt% was predicted [183]. Even with recent advances, though, the gravimetric hydrogen storage capacities of HEAs require further enhancement to make practical applications feasible.

In summary, phase structural design and transition behavior are pivotal in optimizing the hydrogen storage performance of HEAs. Elemental doping and microstructural refinement further expand the directions for design. Continued efforts to unravel the atomic-scale mechanisms governing these processes will be essential for advancing HEAs toward the requirements for practical hydrogen storage applications.

5.2. Electrochemical hydrogen storage

Electrochemical hydrogen storage offers a promising approach in the context of metal–hydrogen batteries. Ni-MH batteries are widely used due to their high power capacity, tolerance to overcharging and discharging, environmental compatibility, and safety. These attributes make them suitable for portable power tools and hybrid electric vehicles, although they exhibit a relatively low energy density [194–198]. Pan et al. focused on the effect of Co substitution for Ni on the cycling stability of Ti–V–Fe-based HEAs. Their optimized $Ti_{0.8}Zr_{0.2}V_{2.7}Mn_{0.5}Cr_{0.6}Ni_{1.15}Co_{0.1}Fe_{0.2}$ HEA demonstrated a cycling stability of 79.8% after 200 cycles [199]. As Ni content increases, both the maximum discharge capacity (C_{max}) and the high-rate discharge ability (HRD) gradually decrease. Building on this result, Young et al. explored how the addition of elements like La, Nd, and Cu influenced the structural, hydrogen storage, and electrochemical characteristics [200–202]. Sarac and co-workers synthesized CoFeMnTiVZr HEA with a single C14 Laves phase through rapid solidification [203]. Electrochemical analyses revealed a maximum reversible hydrogen storage capacity of approximately ~1.9 wt% at room temperature. Meanwhile, gas–solid reaction experiments conducted at 298 K and 5 MPa H_2 pressure yielded a hydrogen uptake of 1.7 wt%, consistent with the electrochemical results. Fukagawa et al. specifically developed a novel ZrTiNiCrMn HEA for Ni-MH batteries [204]. It exhibited enhanced discharge capacity and cycling performance that were correlated with an increase in Ni content. Liu and co-workers designed a non-noble CuNiMoWCo HEA [205]. As a catalyst, this HEA markedly improved the activity of the HER/HOR by refining the electronic structure of active sites. Their assembled Ni–H_2 battery, with CuNiMoWCo grown on Cu foam as the anode, demonstrated significantly improved rate capability. This innovative design not only enhanced the battery's performance during rapid charge and discharge cycles but also exhibited remarkable cycling stability. Notably, the battery maintained its exceptional performance for 1800 h without experiencing any decline in capacity. This work offers a strategy for developing efficient metal-based bifunctional non-noble HEA catalysts for hydrogen batteries in large-scale energy storage systems.

The robust stability of HEAs during reversible hydrogen absorption and desorption makes them highly suitable for electrochemical storage applications. Edalati et al. used $Ti_xZr_{2-x}CrMnFeNi$ HEA with different Ti/Zr ratios for Ni-MH batteries, as shown in Fig. 11 [206]. These alloys were able to hydrate and dehydrate at room temperature, demonstrating high storage capacity and rapid activation. Table 2 summarizes the electrochemical properties of several HEA electrodes. Superior electrical conductivity is crucial for electrochemical reactions, especially during battery charging and discharging. In addition to hydrogen storage capacity and cycling stability, several additional parameters need to be considered for HEAs as electrodes, such as equilibrium pressure, conductivity, corrosion/oxidation resistance, crush resistance, and electrochemical activity. In Ni-MH batteries, the hydrogen storage alloy is crucial in determining the physical and chemical properties. Therefore, comprehensive research on advanced, high-performance, and cost-effective hydrogen storage alloy electrodes is essential to enhance these batteries' overall efficiency and functionality.

5.3. HEA-catalyzed hydrogen storage

HEAs possess multielement and multivalent structural characteristics, making them promising catalysts for hydrogen storage applications, particularly in thermocatalysis and electrocatalysis [218–220]. High-capacity hydrogen storage materials, such as magnesium hybrids (MgH_2), alanates ($[AlH_4]^-$), and borohydrides ($[BH_4]^-$), exhibit significant hydrogen densities surpassing those of compressed hydrogen [221–227]. However, their practical application is hindered by high thermodynamic stability and kinetic barriers for hydrogen absorption and desorption. Therefore, effective catalysts for hydrogen storage materials are essential. In 2018, Meena et al. first studied the catalytic effect of $NiMn_{9.3}Al_{4.0}Co_{14.1}Fe_{3.6}$ HEA on MgH_2. As the HEA proportion increases, hydrogen desorption temperature and dehydrogenation activation energy decrease, but hydrogen storage capacity is significantly reduced [228]. This active attempt presents a new way to develop solid-state hydrogen storage materials with high capacity and friendly reaction conditions. Recently, more and more HEAs are being used as catalysts to promote the hydrogen storage performance of MgH_2, as presented in Table 3. These composite materials, consisting of a HEA and MgH_2, display low dehydrogenation temperatures and activation energies, rapid kinetics, and extraordinary cycling performance.

Table 3 also indicates that the composition and amount of HEAs are the key factors affecting their catalytic performance. Until now, the equiatomic HEAs have been focused on for catalytic MgH_2, with the most common elements being Mn, Fe, Co, and Ni. A TiVNb-based HEA with the C14 Laves phase was designed, and the influence of included elements on catalytic performance was systematically studied [229]. The catalytic effect follows the sequence: TiVNb–ZrFe > TiVNb–ZrNi > TiVNb–CrNi. Therefore, the Mg–Cr system is considered unsuitable for hydrogen storage unless a more stable hydride is added. Adding Zr results in a more effective catalytic effect than Cr. In comparison, Fe is considered destabilizing for MgH_2 due to iron's moderate electron-withdrawing ability. Similarly, Mn added to CrFeCoNi alloy significantly improves the catalytic effect, which is attributed to the similar atomic size promoting HEA stability and enhancing the cocktail effect [230]. Currently, HEA catalysts for MgH_2 are usually synthesized by arc melting. To ensure uniform mixing with MgH_2, pre-ball milling of as-prepared HEA is regarded as an effective strategy [79,231,232]. Additionally, the amount of HEA catalyst introduced plays a crucial role in influencing its catalytic performance. For instance, Zhong et al. performed the dehydrogenation of MgH_2-x wt% FeCoNiCrMo (x = 6, 9, 12)

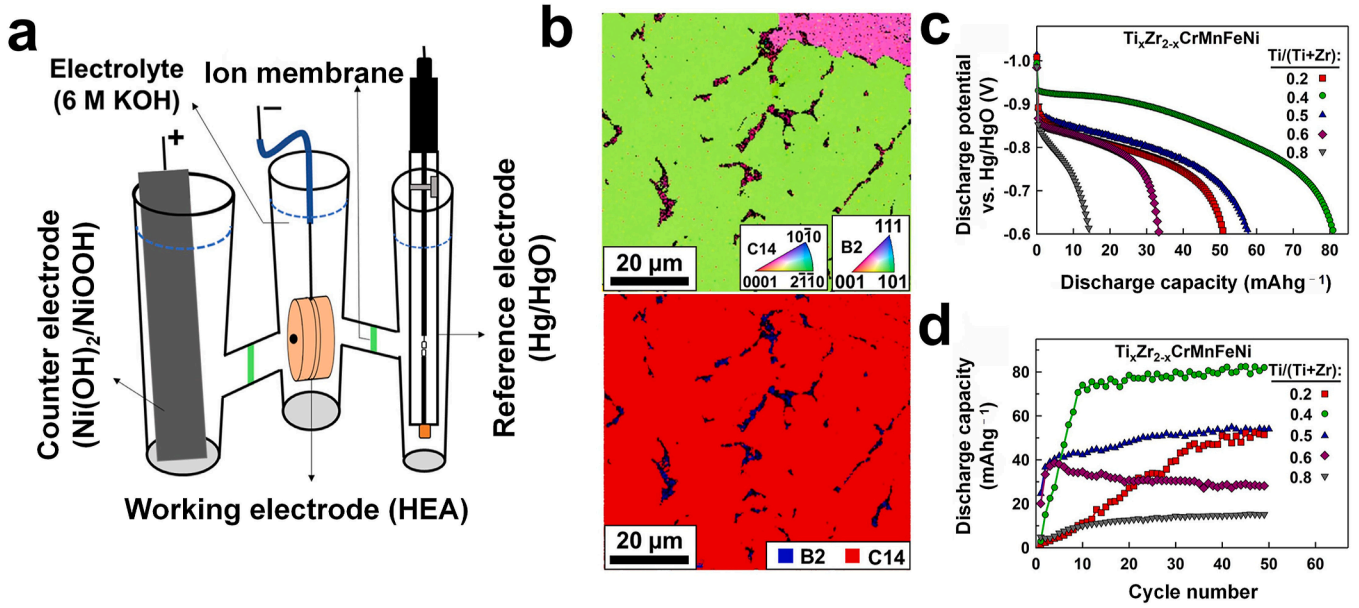

Fig. 11. (a) Schematic illustration of a three-electrode electrochemical cell for Ni-MH battery, (b) microstructure of a HEA, (c, d) electrochemical performance of HEAs as anode materials of a Ni-MH battery. Reproduced with permission [206]. Copyright 2022, Elsevier.

Table 2
Electrochemical properties of some HEA electrodes.

HEA composition	Maximum discharge capacity ($mAh \cdot g^{-1}$)	High-rate discharge ability	Capacity retention	Ref.
$Zr_{0.2}Ti_{0.2}Ni_{0.275}Cr_{0.2}Mn_{0.2}$	368.0	–	–	[204]
$Ti_{0.8}Zr_{0.2}V_{2.7}Mn_{0.5}Cr_{0.6}Ni_{1.15}Co_{0.1}Fe_{0.2}$	333.4	$HRD_{600} = 62.5\%$	$S_{200} = 79.8\%$	[199]
$Ti_{0.7}Y_{0.1}Zr_{0.2}V_{2.7}Mn_{0.5}Cr_{0.6}Ni_{1.25}Fe_{0.2}$	360.2	$HRD_{600} = 67.9\%$	$S_{200} = 69.8\%$	[207]
$Ti_{0.17}Zr_{0.08}V_{0.35}Cr_{0.1}Ni_{0.3}B_{0.01}$	329.0	$HRD_{800} = 72.5\%$	$S_{200} = 89.4\%$	[208]
$La_{0.7}Mg_{0.3}Ni_{2.9}(Al_{0.5}Mo_{0.5})_{0.6}$	397.6	$HRD_{1200} = 70.5\%$	$S_{70} = 70.8\%$	[209]
$La_{0.4}Nd_{0.4}Mg_{0.2}Ni_{3.2}Co_{0.2}Al_{0.2}$	372.0	$HRD_{1200} = 39.2\%$	$S_{100} = 82.3\%$	[210]
$La_{0.6}Pr_{0.1}Mg_{0.3}Ni_{2.45}Co_{0.75}Mn_{0.1}$	372.7	$HRD_{1000} = 70.1\%$	$S_{200} = 78.4\%$	[211]
$La_{1.8}Ti_{0.2}MgNi_{8.7}Al_{0.3}$	339.6	$HRD_{1400} = 61.1\%$	$S_{205} = 60.0\%$	[212]
$La_{0.4}Pr_{0.4}Mg_{0.2}Ni_{3.15}Co_{0.2}Al_{0.1}Si_{0.05}$	377.5	–	$S_{100} = 95.7\%$	[213]
$La_{0.6}Gd_{0.2}Mg_{0.2}Ni_{3.05}Co_{0.25}Al_{0.1}Mn_{0.1}$	391.2	$HRD_{900} = 75.3\%$	$S_{200} = 89.8\%$	[214]
$La_{0.75}Mg_{0.25}Ni_{3.05}Co_{0.2}Al_{0.1}Mo_{0.15}$	372.0	$HRD_{1500} = 60.1\%$	$S_{100} = 80.9\%$	[215]
$LaY_2Ni_{9.7}Mn_{0.5}Al_{0.3}$	385.7	–	$S_{300} = 76.6\%$	[216]
$La_{0.6}Sm_{0.2}Mg_{0.2}Ni_{3.5}Al_{0.2}$	349.0	$HRD_{1800} = 41.3\%$	$S_{100} = 84.4\%$	[217]

in a non-isothermal setup, finding that this significantly improved the dehydrogenation efficiency of MgH_2 [232]. While increasing the HEA content improves the dehydrogenation efficiency, it may reduce the hydrogen storage capacity, making it essential to balance the catalyst amounts.

HEA catalysts primarily enhance hydrogen storage through three mechanisms: "hydrogen pump", phase transitions, and the cocktail effect. The "hydrogen pump" mechanism is driven by the reversible solid-solution phase formed during the first dehydrogenation process, which can simultaneously accelerate the hydrogenation process of Mg and the dehydrogenation rate of MgH_2. In the hydrogenation process, the phase formed *in situ* can more readily capture external hydrogen and quickly dissociate into hydrogen atoms that diffuse to the Mg region, improving the hydrogen absorption kinetics of Mg. On the other hand, the phase formed *in situ* accelerates the cleavage of Mg–H bonds in MgH_2 within the surrounding area, rapidly capturing free hydrogen atoms and immediately releasing H_2 through a reversible phase transition. Wan et al. found that the CrMnFeCoNi HEA particles uniformly dispersed on the MgH_2 matrix provide numerous diffusion channels for the rapid transfer of hydrogen (Fig. 12a). Meanwhile, new reversible phases of Mg_2Co/Mg_2CoH_5 and Mg_2Ni/Mg_2NiH_4 are formed in the first re/dehydrogenation process and then act as "hydrogen pump" to accelerate hydrogen absorption and release. The same catalytic mechanism with phase reversibility appears in the MgH_2–TiCrFeCoNi composite [231]. Obviously, HEAs used in the above two studies have the same elements: Cr, Fe, Co, and Ni. The phase transition behavior in HEAs closely resembles the *in situ* reversible phase mechanism observed during the de/hydrogenation processes of MgH_2. A previous study reported a plausible de/hydrogenation mechanism for MgH_2-$(TiVZrNb)_{83}Cr_{17}$ (Fig. 12b) [79], in which $(TiVZrNb)_{83}Cr_{17}$ HEA has the capability to absorb hydrogen, leading to a transformation of its biphasic structure (FCC + BCC) into a hydrogenated form (FCC). The hydrogenated phase can then revert to the original phase after hydrogen desorption. This mechanism of phase transition enhances the diffusion pathways available for hydrogen and increases the nucleation sites for Mg/MgH_2, thereby considerably lowering the activation energy required for the dehydrogenation and hydrogenation processes of MgH_2.

In the HEA cocktail effect, the elements synergize with each other to cause multielectronic states and higher electronic states in the catalyst, which are beneficial for achieving a better catalytic effect. The arrangement of various elements on the HEA surface is conducive to providing a variety of active sites for hydrogen diffusion, and the multivalent environment helps destabilize the Mg–H bonds in MgH_2, resulting in fast re/dehydrogenation kinetics. This catalytic mechanism can be seen in Figs. 12c and d. In summary, HEAs could be considered as potential

Table 3
Comparison of hydrogen storage properties for MgH_2 catalyzed by various HEAs.

Sample name	Addition amount	Onset dehydrogenation temperature (K)	Hydrogen storage capacity (wt%)	Dehydrogenation activation energy ($kJ \cdot mol^{-1} \cdot H_2$)	Hydrogen release kinetics	Cyclic stability with capacity degradation	Ref.
Ball-milled MgH_2	–	581	6.7	153.0	6.0 wt% (20 min, 573K, 0.002 MPa)	–	[229]
MgH_2–$Al_{4.0}Mn_{9.3}Fe_{3.6}Co_{14.1}Ni$	50 wt%	453	2.0	131.3	–	–	[228]
MgH_2–CrMnFeCoNi	5 wt%	482	6.1	90.2	5.6 wt% (10 min, 553 K, 0.001 MPa)	50 cycles (98.6%)	[233]
MgH_2–CrMnFeCoNi	10 wt%	471	6.5	75.8	6.5 wt% (10 min, 573 K, 0.003 MPa)	20 cycles (97.0%)	[230]
MgH_2–TiVFeZrNb	10 wt%	482	5.8	63.0	5.7 wt% (5 min, 573 K, 0.002 MPa)	100 cycles (106.6%)	[229]
MgH_2–CrFeCoNiMo	9 wt%	473	6.7	84.5	6.3 wt% (10 min, 623 K, 3.2 MPa)	20 cycles (96.2%)	[232]
MgH_2–$Al_{20}Cr_{16}Mn_{16}Fe_{16}Co_{16}Ni_{16}$	7 wt%	611	6.8	121.2	5.4 wt% (40 min, 573 K, 0.1 MPa)	25 cycles (98.9%)	[234]
MgH_2–TiCrFeCoNi	10 wt%	472	6.6	76.1	7.1 wt% (5 min, 563 K, 0.001 MPa)	20 cycles (94.4%)	[231]
MgH_2-$(TiVZrNb)_{83}Cr_{17}$	6 wt%	475	5.3	90.5	4.1 wt% (60 min, 573 K, 0.0001 MPa)	10 cycles (98.5%)	[79]
MgH_2–$Ti_{0.3}V_{0.24}Mn_{1.12}Fe_{0.24}Ni_{2.4}Zr_{1.7}$	10 wt%	513	6.6	94.6	6.5 wt% (9 min, 598 K, 0.0001 MPa)	30 cycles (92.0%)	[235]
MgH_2–AlTiFeNiCu	7 wt%	473	6.2	91.7	5.8 wt% (3.8 min, 573 K, 0.01 MPa)	20 cycles (99.2%)	[236]
MgH_2–AlCrFeNiCu	5 wt%	453	7.3	–	5.0 wt% (5 min, 593 K, 0.01 MPa)	25 cycles (99.0%)	[237]

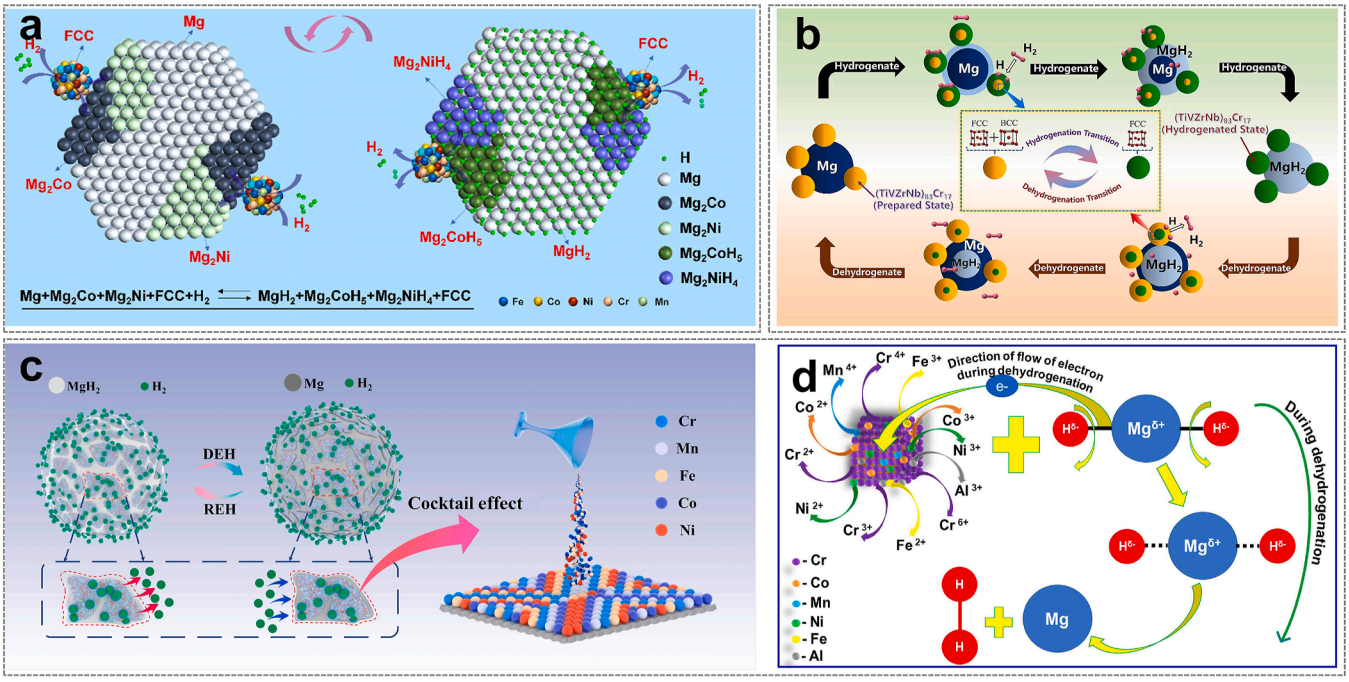

Fig. 12. Schematic catalytic diagram of a HEA on MgH_2: (a) "hydrogen pump" mechanism. Reproduced with permission [233]. Copyright 2023, Elsevier. (b) The phase transition mechanism. Reproduced with permission [79]. Copyright 2023, Elsevier. (c–d) Cocktail effect mechanism. Reproduced with permission [230,234]. Copyright 2023, Elsevier and Copyright 2024, Elsevier, respectively.

catalysts for MgH_2. However, the huge ingredient space poses great challenges for HEA directional design and catalytic mechanism elucidation.

HEA catalysts have also been explored to improve the hydrogen storage capabilities of complex hydrides. Constructing composite systems is an effective way to improve their hydrogen storage performance [238]. In 2018, a combination of metal borohydrides, i.e., $LiBH_4$–$NaBH_4$–KBH_4–$Mg(BH_4)_2$–$Ca(BH_4)_2$, was created utilizing multiple cations in an equimolar ratio, in line with the HEA concept [239]. In general, Co-based catalysts play an important role in sodium borohydride hydrolysis [240]. Recently, an $Fe_{10}Co_{10}Ni_{10}Cr_{10}Mn_{60}$ HEA ribbon

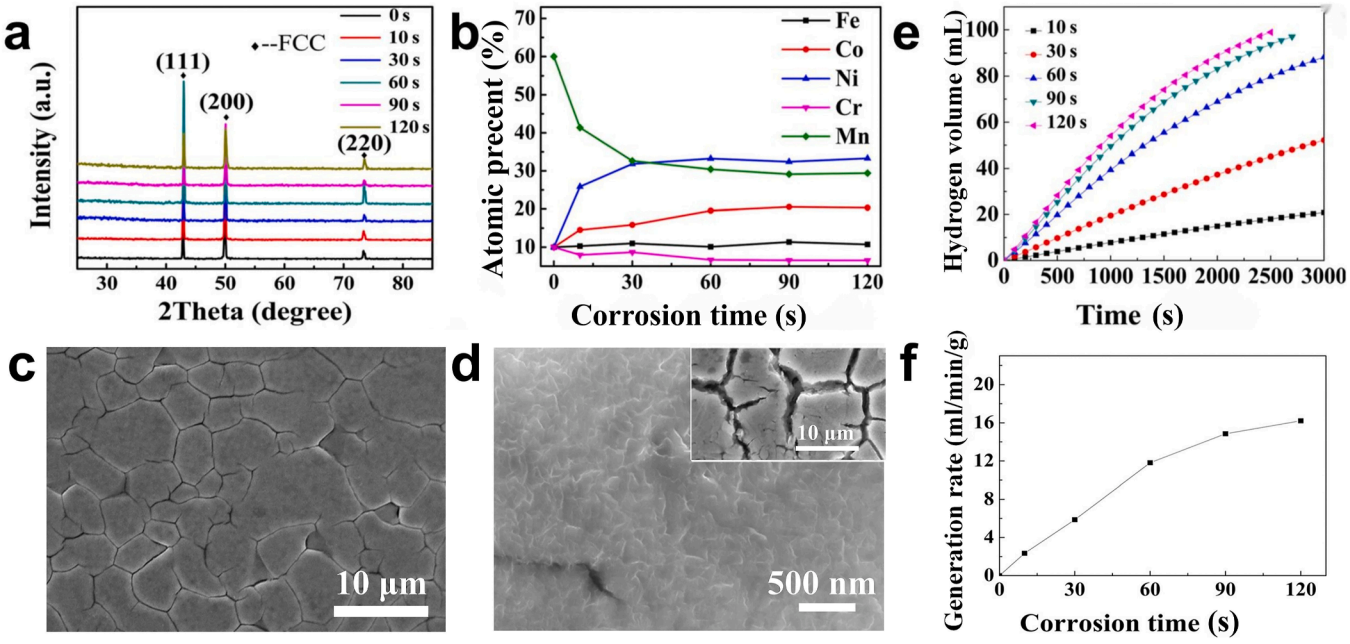

Fig. 13. Structure analysis of $Fe_{10}Co_{10}Ni_{10}Cr_{10}Mn_{60}$ HEA: (a) XRD patterns of as-cast and corroded HEA, (b) components of corroded ribbon, and SEM micrographs of (c) as-cast ribbon and (d) ribbon after corrosion for 120 s. (e and f) Hydrogen production properties of $Fe_{10}Co_{10}Ni_{10}Cr_{10}Mn_{60}$–$NaBH_4$ alkaline solution with various corrosion times. Reproduced with permission [241]. Copyright 2021, AIP Publishing.

was revealed to have dislocation-driven high catalytic performance for HF corrosion treatment in $NaBH_4$ hydrolysis [241]. The change in corrosion time increases the content of Ni and Co but does not change the phase composition, as shown in Figs. 13a and b. After 120 s of corrosion, the depth of the cracks progressively enlarges, evolving into crystalline grains, in contrast to the as-cast sample (Fig. 13c). In addition, the morphology of the HEA ribbon changes into a flocculent microstructure (Fig. 13d), which facilitates the catalytic reaction. The numerous electron-rich Ni and Co catalytic active sites and defect-rich structures are believed to be salient for high catalytic activity. This work provides a highly valuable direction for the development of efficient catalysts for $NaBH_4$ hydrolysis. After 90 s of corrosion, the catalyst exhibits outstanding efficiency for $NaBH_4$ hydrolysis, with a hydrogen production rate of 18.46 $l \cdot m^{-2} \cdot min^{-1}$ (Figs. 13e and f). Furthermore, HEAs have shown remarkable catalytic activity in ammonia borane (AB) hydrolysis. A FeCoNiMnRu HEA with a face-centered cubic structure was synthesized via the polymer fiber nanoreactor method, where Ru incorporation facilitated electron transfer and enhanced synergistic interactions. The $Fe_{23}Co_{27}Ni_{27}Mn_{12}Ru_{11}$ HEA achieved a low apparent activation energy (42.3 $kJ \cdot mol^{-1}$) and a high turnover frequency (55.3 $mol_{H2} \cdot mol_{Ru}^{-1} \cdot min^{-1}$) at 298 K, offering a promising pathway toward cost-effective and efficient catalysts for AB hydrolysis [242]. These studies broaden the potential applications of hydrogen storage in HEAs.

6. HEAs for hydrogen separation

Hydrogen derived from a variety of sources is expected to play a central role in future energy systems. Industrial and by-product hydrogen streams often contain impurities, which can significantly lessen their practical use. Consequently, purification of crude hydrogen is essential to meet application-specific quality requirements, necessitating a focus on both hydrogen permeability (hydrogen permeation coefficient, Φ) and resistance to embrittlement [243]. Membrane-based material separation has emerged as the most promising technology for hydrogen purification. While Pd and its alloy membranes have achieved commercial success, their large-scale application is limited by source scarcity and the high cost of Pd. Consequently, cost-effective alloys with high hydrogen permeability are urgently needed [244,245]. The VB group metals are potential alternatives due to their exceptional hydrogen transport performance. For example, the fabricated $Nb_5Ti_{58}Fe_{35}Cu_2$ alloy shows a high permeability of 4.32×10^{-8} mol $H_2 \cdot m^{-1} \cdot s^{-1} \cdot Pa^{-1/2}$ at 673 K, which is 2.7 times that of pure Pd [246]. Additionally, substantial variations in permeability and hydrogen embrittlement characteristics were discovered based on alloy composition. Nevertheless, more study is required on how trace elements in alloys affect their structure and hydrogen transport behavior. Alloying proves to be an effective method for enhancing hydrogen permeability by modifying lattice constants.

HEAs provide an excellent platform for achieving high hydrogen permeability and brittleness resistance [247]. In an earlier study, Tang et al. explored the effects of additional elements on the ductility, hydrogen permeability, and embrittlement of $Nb_{40}Ti_{18}Zr_{12}Ni_{25}Co_5$, achieving a very high Φ value of 3.82×10^{-8} mol $H_2 \cdot m^{-1} \cdot s^{-1} \cdot Pa^{-1/2}$ at 673 K [248]. Similarly, Marques et al. investigated the concentration of alloy elements' effect on hydrogen diffusivity and trapping for $Fe_{20}Mn_{20}Ni_{20}Co_{20}Cr_{20}$ and $Fe_{22}Mn_{40}Ni_{30}Co_6Cr_2$ HEAs [249]. The H–Cr system exhibits low interaction energy compared with Co, Fe, Ni, and Mn (Fig. 14a). Through comparative studies of various HEAs, the dissolution of hydrogen in nanoscale chemical heterogeneity was further elucidated. It was found that the elastic and chemical contributions to H dissolution energy are closely linked to the capacity of different chemical environments to undergo local volume expansion [250]. Recently, Kashkarov et al. reported the microstructure and hydrogen permeability of NbNiTiZrCo HEAs with equimolar and non-equimolar compositions at 573–773 K [251]. The equimolar HEA shows lower activation energy, higher hydrogen permeability, and higher resistance to hydrogen embrittlement due to its lower hydrogen binding energy and finely dispersed structure. Moreover, hydrogen isotope permeation and retention behavior have been investigated in relation to CoCrFeMnNi [252], AlCrTaTiZr [253], CoCrMnFeNi [254], CoCrMnFeNi [255], and AlCrFeTiNb [256] HEAs. In situations where equipment services are exposed to hydrogen, hydrogen-induced evolution and failure can take place, even in the absence of clear corrosion signs [257]. The penetration of hydrogen is significantly linked to microstructure and nano-scale precipitate phases. As shown in Fig. 14b, Feng et al. investigated the H atom transfer process of $AlCoCrFeNi_{2.1}$ HEA. They found that the growth

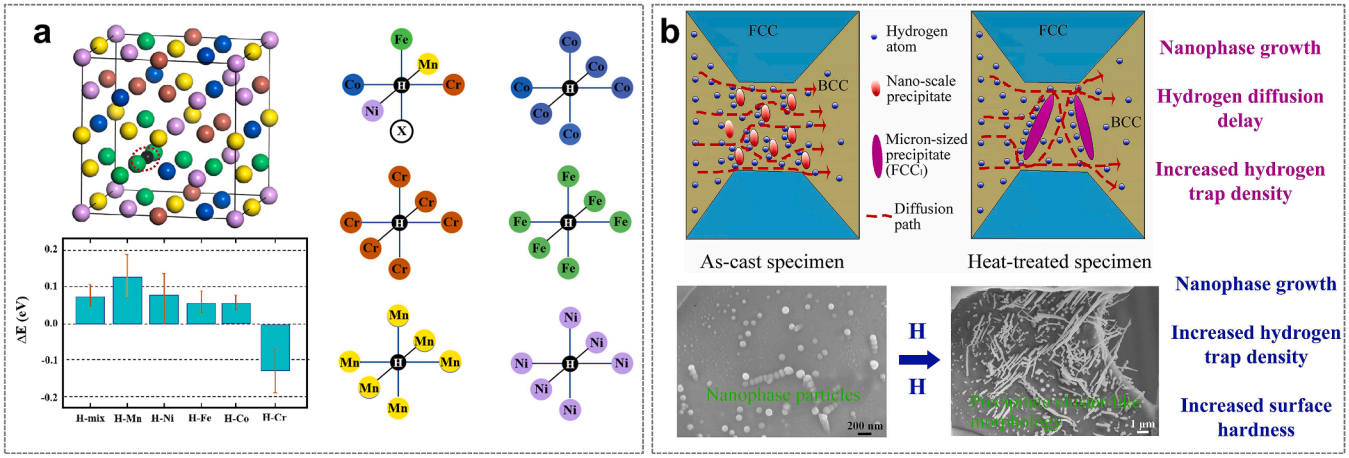

Fig. 14. (a) Hydrogen atomic neighborhood for six investigated systems, showing chemical complexity. Reproduced with permission [249]. Copyright 2021, Elsevier. (b) Schematic and morphologies of nanoscale precipitates, with diagram of hydrogen diffusion path influenced by precipitated phases in BCC. Reproduced with permission [258]. Copyright 2023, Elsevier.

of nanophases shows a stronger blocking effect, caused by hydrogen-induced evolution [258]. Kashkarov et al. synthesized NbNiTiZrCo HEAs using arc melting, focusing on the effects of composition on microstructure, phase composition, lattice constants, hardness, and hydrogen permeability. The prepared $Nb_{20}Ni_{20}Ti_{20}Zr_{20}Co_{20}$ HEA exhibits a high hydrogen permeability of 1.05×10^{-8} mol $H_2 \cdot m^{-1} \cdot s^{-1} \cdot Pa^{-1/2}$ at 673 K and superior resistance to hydrogen embrittlement, making it a promising candidate for hydrogen purification membranes [259]. To elucidate the hydrogen behavior in HEAs, Yang systematically investigated the dissolution, diffusion, and desorption of hydrogen in equiatomic WTaVCr alloy using DFT calculations [260]. The results show that the maximum trapping energy and accommodation number of hydrogen at a mono-vacancy are much lower in WTaVCr than in pure W, which results in weak hydrogen-defect interactions, suppressed hydrogen retention, and hydrogen-induced blistering at high temperatures.

The high thermal stability, complex multi-element structure, and wide compositional flexibility of HEAs make them ideal for hydrogen separation, enhancing their resistance to embrittlement while optimizing both permeability and selectivity for long-term durability. However, an alloy's microstructure needs to be optimized to achieve a balanced relationship between high hydrogen permeability, alloy stability, and resistance to hydrogen embrittlement.

7. HEAs for hydrogen detection

Hydrogen sensing is crucial for applications involving H_2 gas, particularly due to the hazards associated with hydrogen leakage. Various materials have been explored for fabricating hydrogen sensors, including metal oxides, noble metals, and atomically thin materials [261,262]. A commercially viable and highly reliable hydrogen sensor is needed, with features such as portability, miniaturization, real-time monitoring, and rapid response for ensured reliability [263,264].

In particular, lattice strain observed in HEAs makes them promising candidates for hydrogen sensing and detection. The fundamental principle of H_2 sensors is based on changes in the electrical conductivity of materials upon hydrogen absorption. For Pd membranes, which are a crucial option for industrial applications, the mechanism for H_2 sensing involves lattice expansion induced by hydrogen absorption. The alloying method can modify the lattice constants and hydrogen permeability, thereby enhancing the mechanical and chemical stability of Pd-based devices and enabling cost reduction. For example, Sharma et al. designed Pd-based HEAs with adjustable octahedral void sizes in the FCC structure, achieving a 50% cost reduction compared to pure Pd [265]. Zhu et al. examined the mechanical stability and hydrogen permeation behavior of $Nb_{51}W_5Ti_{23}Ni_{16}Pd_5$ HEA under controlled cooling conditions [266]. The incorporation of Pd reduced hydrogen solubility by 14.6% at 673 K and 0.8 MPa while only marginally decreasing the hydrogen diffusion coefficient by 0.5%. Another approach involves functionalizing HEAs onto two-dimensional materials. Biswas et al. used low-temperature grinding and a sonochemical method to synthesize MoS_2 flakes that were exfoliated and decorated with AgAuCuPdPt HEA-NPs [267]. Experimental and DFT results show that this decoration induced a surface-enhanced Raman scattering effect, reduced the work function from 4.9 to 4.75 eV, and formed a Schottky barrier due to surface chemical non-stoichiometry effects. The HEA-MoS_2 junction significantly enhanced hydrogen sensing response, resulting in a tenfold increase in response at 353 K. In the subsequent work, they further investigated the vital role of electronic charge redistribution between HEA and MoS_2 for H_2 adsorption, as shown in Fig. 15 [268]. DFT calculations provide evidence of improved hydrogen adsorption and charge redistribution, highlighting the potential of HEA-NPs as low-cost alternatives to Pd NPs for room-temperature gas sensing applications. This study demonstrates the enhancement of hydrogen sensor sensitivity from 7% to 47% by functionalizing 2D MoS_2 sheets with TiZrVNbHf HEA-NPs. Furthermore, MoS_2 + HEA-NPs exhibit high selectivity for hydrogen (Fig. 15c). These results highlight the potential of HEAs as promising materials for gas-sensing applications. The high compositional flexibility of HEAs allows for the optimization of various parameters, such as sensitivity and selectivity. As research progresses, HEAs can be further developed to improve sensor accuracy, reduce costs, and expand applications in industrial monitoring, environmental sensing, and energy systems.

8. Summary and outlook

In summary, this comprehensive review has explored the multifaceted application of HEAs in hydrogen storage, separation, and detection. Leveraging their tunable phase structure and high surface activities, diverse techniques have been developed for efficient hydrogen storage, including absorption, electrochemical methods, and catalysis. The practical use of HEAs in the field of hydrogen energy demands robust design methods, combining theoretical with experimental approaches. Notably, data-driven methodologies, such as machine learning, are playing an increasingly pivotal role in HEA research, aligning with recent advances in materials and genetic engineering. The composition design of HEAs, guided by structure- and performance-based objectives, promotes innovation while reducing costs and design cycles. However,

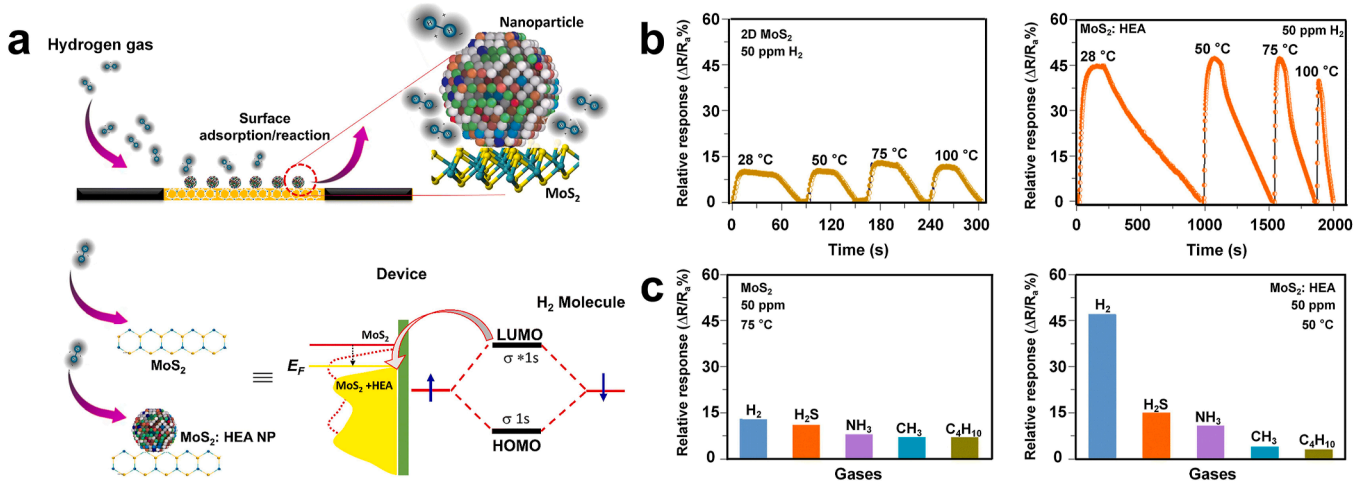

Fig. 15. (a) Schematics of hydrogen adsorption on MoS_2 and MoS_2:HEA. (b) Relative response of MoS_2 and MoS_2 + HEA-NPs. (c) Selectivity of different gases on MoS_2 and MoS_2 + HEA-NPs. Reproduced with permission [268]. Copyright 2023, Royal Society of Chemistry.

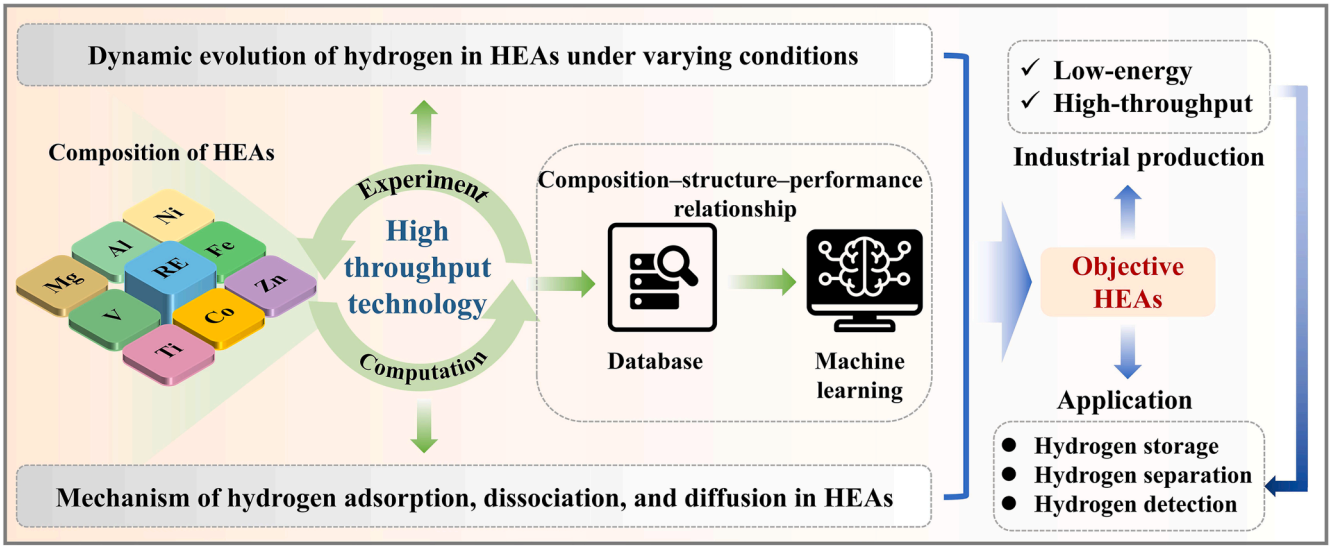

Fig. 16. The development prospects for HEAs in hydrogen energy.

the scarcity of high-quality data sources, including peer-reviewed studies, empirical parameters, multi-scale calculations, and experiments, remains a bottleneck for applying machine learning to HEA-based hydrogen energy. To enhance the efficient application of HEAs in hydrogen energy, the following challenges need to be solved (Fig. 16).

(1) **Optimal Design of Components and Phases:** Cross-validation between theoretical models and experimental results can expedite the discovery of novel materials. By utilizing high-throughput computational and experimental techniques, combining phase diagrams, and applying the CALPHAD approach, performance and cost can be effectively balanced through the introduction of low-cost alternatives and appropriate doping with rare earth elements. Additionally, regulating multi-phase structures and introducing strain and defects can significantly enhance the kinetic properties of hydrogen in HEAs.

(2) **HEA-Hydrogen Dynamic Evolution Mechanisms:** DFT theoretical calculations play a crucial role in guiding the experimental progress of HEA hydrogenation, particularly in terms of site selection, phase transition, and both thermodynamic and kinetic aspects. However, research on the dynamic evolution of hydrogen in HEAs remains underdeveloped. To advance this field, the development of advanced computational methods and *in situ* experimental technologies is essential for accurately investigating hydrogen behavior under varying conditions of temperature, pressure, and strain.

(3) **Clear Composition–Structure–Performance Relationship:** Establishing precise mechanisms for hydrogen adsorption, decomposition, and diffusion through strategies involving chemical composition, atomic arrangement, phase structure, and microstructure is essential for advancing hydrogen storage, separation, and detection. Future research should integrate artificial intelligence techniques to explore HEA–hydrogen interactions by developing machine learning models, while refining the hydrogen storage database to optimize HEA design.

(4) **Scalability and Stability in Real-World Development:** Researchers should focus on the cost-effective HEAs with the BCC phase (such as Ti–V–Fe HEAs), establishing high-throughput and low-energy fabrication methods based on additive manufacturing technology. In addition, integrate high-frequency hydrogen ab/desorption performance under complex environments (such as

temperature fluctuations and the presence of impurity gases) with composition adjustment strategies to enhance the phase stability of HEAs.

Addressing the above challenges will unlock the full potential of HEAs, contributing to the development of efficient and sustainable technologies for hydrogen storage, separation, and detection as hydrogen energy continues to evolve.

CRediT authorship contribution statement

Jiaxi Liu: Writing – original draft, Methodology, Conceptualization. **Pengru Huang:** Writing – original draft, Funding acquisition. **Yongpeng Xia:** Writing – original draft, Conceptualization. **Yanping Liu:** Writing – review & editing. **Yumei Luo:** Writing – review & editing. **Huanzhi Zhang:** Investigation. **Yongjin Zou:** Methodology. **Hailiang Chu:** Writing – review & editing. **Sergey P. Verevkin:** Writing – review & editing. **Sergey V. Vostrikov:** Writing – review & editing. **Lixian Sun:** Writing – review & editing, Funding acquisition, Conceptualization. **Fen Xu:** Writing – review & editing, Funding acquisition. **Zongwen Liu:** Writing – review & editing, Conceptualization. **Hongge Pan:** Writing – review & editing, Conceptualization.

Declaration of interest statement

The authors declare that they have no known competing financial interests or personal relationships that could have appeared to influence the work reported in this paper.

Acknowledgments

The authors are grateful for financial support from National Key Research and Development Program of China (Grant No. 2021YFB3802400), Science and Technology Major Program of Guangxi Province (Grant No. GUIKEAA24206022), National Natural Science Foundation of China (Grant Nos. 52461038, 52461032, 52271205, 52373311, 52371218, and 52161037), Guangxi Bagui Scholar Foundation, Guilin Lijiang Scholar Foundation, Guangxi Engineering Research Center of Hydrogen/Heat/Electricity-Related Energy Materials and Sensors, Graduate Study Abroad Program of Guilin University of Electronic Technology (Grant No. GDYX2025001).

References

[1] M. Sevilla, R. Mokaya, Energy storage applications of activated carbons: supercapacitors and hydrogen storage, Energy Environ. Sci. 7 (2014) 1250–1280.
[2] R. Mohtadi, S.I. Orimo, The renaissance of hydrides as energy materials, Nat. Rev. Mater. 2 (2016) 16091.
[3] G.Z. Guo, C.C. Ji, H.Y. Mi, C. Yang, M.J. Li, C.R. Sun, L.X. Sun, Zincophilic anionic hydrogel electrolyte with interfacial specific adsorption of solvation structures for durable zinc ion hybrid supercapacitors, Adv. Funct. Mater. 34 (2023) 2308405.
[4] C.C. Zhang, H.G. Pan, L.X. Sun, F. Xu, Y.F. Ouyang, F. Rosei, Progress and perspectives of 2D materials as anodes for potassium-ion batteries, Energy Storage Mater. 38 (2021) 354–378.
[5] S. Saifi, X. Xiao, S.M. Cheng, H.T. Guo, J.S. Zhang, P. Muller-Buschbaum, G. M. Zhou, X.M. Xu, H.M. Cheng, An ultraflexible energy harvesting-storage system for wearable applications, Nat. Commun. 15 (2024) 6546.
[6] Y. Zhao, Y. Wang, J. Li, J. Xiong, Q. Li, K.K. Abdalla, Y. Zhao, Z. Cai, X. Sun, Thermodynamic and kinetic insights for manipulating aqueous Zn battery chemistry: towards future grid-scale renewable energy storage systems, eScience 5 (2025) 100331.
[7] Z. Abdin, A. Zafaranloo, A. Rafiee, W. Mérida, W. Lipiński, K.R. Khalilpour, Hydrogen as an energy vector, Renewable Sust. Energy Rev. 120 (2020) 109620.
[8] N. Sazali, Emerging technologies by hydrogen: a review, Int. J. Hydrogen Energy 45 (2020) 18753–18771.
[9] T. Capurso, M. Stefanizzi, M. Torresi, S.M. Camporeale, Perspective of the role of hydrogen in the 21st century energy transition, Energy Convers. Manag. 251 (2022) 114898.
[10] U. Eberle, M. Felderhoff, F. Schüth, Chemical and physical solutions for hydrogen storage, Angew. Chem., Int. Ed. 48 (2009) 6608–6630.
[11] X.Y. Zhang, Y.H. Sun, S.L. Ju, J.K. Ye, X.C. Hu, W. Chen, L. Yao, G.L. Xia, F. Fang, D.L. Sun, X.B. Yu, Solar-driven reversible hydrogen storage, Adv. Mater. 35 (2023) e2206946.
[12] M.D. Allendorf, V. Stavila, J.L. Snider, M. Witman, M.E. Bowden, K. Brooks, B. L. Tran, T. Autrey, Challenges to developing materials for the transport and storage of hydrogen, Nat. Chem. 14 (2022) 1214–1223.
[13] J.X. Zou, J.Q. Zhang, Y.Y. Zhao, X. Lin, W.J. Ding, Progress in the research and application of high-capacity Mg-based hydrogen storage alloy materials, Acta Metall. Sin. 61 (2025) 420–436.
[14] M.R. Usman, Hydrogen storage methods: review and current status, Renewable Sust. Energy Rev. 167 (2022) 112743.
[15] S.Z.S. Al Ghafri, S. Munro, U. Cardella, T. Funke, W. Notardonato, J.P.M. Trusler, J. Leachman, R. Span, S. Kamiya, G. Pearce, A. Swanger, E.D. Rodriguez, P. Bajada, F.Y. Jiao, K. Peng, A. Siahvashi, M.L. Johns, E.F. May, Hydrogen liquefaction: a review of the fundamental physics, engineering practice and future opportunities, Energy Environ. Sci. 15 (2022) 2690–2731.
[16] N. Heinemann, J. Alcalde, J.M. Miocic, S.J.T. Hangx, J. Kallmeyer, C. Ostertag-Henning, A. Hassanpouryouzband, E.M. Thaysen, G.J. Strobel, C. Schmidt-Hattenberger, K. Edlmann, M. Wilkinson, M. Bentham, R. Stuart Haszeldine, R. Carbonell, A. Rudloff, Enabling large-scale hydrogen storage in porous media-the scientific challenges, Energy Environ. Sci. 14 (2021) 853–864.
[17] Z.J. Chen, K.O. Kirlikovali, K.B. Idrees, M.C. Wasson, O.K. Farha, Porous materials for hydrogen storage, Chem 8 (2022) 693–716.
[18] Y.Q. Huang, G.L. Xia, J. Zhang, Z.P. Guo, X.B. Yu, Graphene-tailored molecular bonds for advanced hydrogen and lithium storage performance, Energy Storage Mater. 17 (2019) 178–185.
[19] Y. Gao, Z.L. Li, P. Wang, C. Li, Q.Y. Yue, W.G. Cui, X.W. Wang, Y.X. Yang, F. Gao, M.C. Zhang, J.T. Gan, C.C. Li, Y.X. Liu, X.Q. Wang, F.L. Qi, J. Miao, J. Zhang, X. Han, W.B. Du, C.X. Liu, Y.Y. Wan, Y.C. Yang, Z.H. Xia, H.G. Pan, Solid-state hydrogen storage origin and design principles of carbon-based light metal single-atom materials, Adv. Funct. Mater. 34 (2024) 2316368.
[20] L.F. Song, J. Zhang, L.X. Sun, F. Xu, F. Li, H.Z. Zhang, X.L. Si, C.L. Jiao, Z.B. Li, S. Liu, Y.L. Liu, H.Y. Zhou, D.L. Sun, Y. Du, Z. Cao, Z. Gabelica, Mesoporous metal-organic frameworks: design and applications, Energy Environ. Sci. 5 (2012) 7508.
[21] S.P. Shet, S. Shanmuga Priya, K. Sudhakar, M. Tahir, A review on current trends in potential use of metal-organic framework for hydrogen storage, Int. J. Hydrogen Energy 46 (2021) 11782–11803.
[22] X.L. Si, C.L. Jiao, F. Li, J. Zhang, S. Wang, S. Liu, Z.B. Li, L.X. Sun, F. Xu, Z. Gabelica, C. Schick, High and selective CO_2 uptake, H_2 storage and methanol sensing on the amine-decorated 12-connected MOF CAU-1, Energy Environ. Sci. 4 (2011) 4522.
[23] S. Liu, L.X. Sun, F. Xu, J. Zhang, C.L. Jiao, F. Li, Z.B. Li, S. Wang, Z.Q. Wang, X. Jiang, H.Y. Zhou, L.N. Yang, C. Schick, Nanosized Cu-MOFs induced by graphene oxide and enhanced gas storage capacity, Energy Environ. Sci. 6 (2013) 818.
[24] S. Cao, B. Li, R.M. Zhu, H. Pang, Design and synthesis of covalent organic frameworks towards energy and environment fields, Chem. Eng. J. 355 (2019) 602–623.
[25] X.B. Yu, Z.W. Tang, D.L. Sun, L.Z. Ouyang, M. Zhu, Recent advances and remaining challenges of nanostructured materials for hydrogen storage applications, Prog. Mater. Sci. 88 (2017) 1–48.
[26] J.O. Abe, A.P.I. Popoola, E. Ajenifuja, O.M. Popoola, Hydrogen energy, economy and storage: review and recommendation, Int. J. Hydrogen Energy 44 (2019) 15072–15086.
[27] N.A.A. Rusman, M. Dahari, A review on the current progress of metal hydrides material for solid-state hydrogen storage applications, Int. J. Hydrogen Energy 41 (2016) 12108–12126.
[28] L.Z. Ouyang, K. Chen, J. Jiang, X.S. Yang, M. Zhu, Hydrogen storage in light-metal based systems: a review, J. Alloys Compd. 829 (2020) 154597.
[29] Z.Y. Li, Y.J. Sun, C.C. Zhang, S. Wei, L. Zhao, J.L. Zeng, Z. Cao, Y.J. Zou, H.L. Chu, F. Xu, L.X. Sun, H.G. Pan, Optimizing hydrogen ad/desorption of Mg-based hydrides for energy-storage applications, J. Materi. Sci. Technol. 141 (2023) 221–235.
[30] M.C. Song, L.T. Zhang, F.Y. Wu, H.Y. Zhang, H. Zhao, L.X. Chen, H. Li, Recent advances of magnesium hydride as an energy storage material, J. Materi. Sci. Technol. 149 (2023) 99–111.
[31] Y. Zheng, S.L. Yang, B. Hu, Y.F. Lu, Y. Yang, K. Tang, Q. Luo, B. Liu, Q. Li, F. S. Pan, The enthalpy changes for hydrogenation/dehydrogenation of Mg-based alloys, J. Magnesium Alloys 13 (2025) 2959–2977.
[32] Q. Li, Y.F. Lu, Q. Luo, X.H. Yang, Y. Yang, J. Tan, Z.H. Dong, J. Dang, J.B. Li, Y. Chen, B. Jiang, S.H. Sun, F.S. Pan, Thermodynamics and kinetics of hydriding and dehydriding reactions in Mg-based hydrogen storage materials, J. Magnesium Alloys 9 (2021) 1922–1941.
[33] X. Sun, X.H. Yang, Y.F. Lu, Q. Luo, C.Z. Wu, Y. Zhang, T. Lyu, Q.F. Gu, Q. Li, F. S. Pan, Hot extrusion-induced Mg-Ni-Y alloy with enhanced hydrogen storage kinetics, J. Mater. Sci. Technol. 202 (2024) 119–128.
[34] J.W. Mao, T.P. Huang, S. Panda, J.X. Zou, W.J. Ding, Direct observations of diffusion controlled microstructure transition in Mg-In/Mg-Ag ultrafine particles with enhanced hydrogen storage and hydrolysis properties, Chem. Eng. J. 418 (2021) 129301.
[35] H.J. Lin, Y.S. Lu, L. Zhang, H.Z. Liu, K. Edalati, Á. Révész, Recent advances in metastable alloys for hydrogen storage: a review, Rare Met. 41 (2022) 1797–1817.

[36] Y.R. Wang, X.W. Chen, H.Y. Zhang, G.L. Xia, D.L. Sun, X.B. Yu, Heterostructures built in metal hydrides for advanced hydrogen storage reversibility, Adv. Mater. 32 (2020) e2002647.

[37] Y. Meng, J. Zhang, S.L. Ju, Y.X. Yang, Z.L. Li, F. Fang, D.L. Sun, G.L. Xia, H. G. Pan, X.B. Yu, Understanding and unlocking the role of V in boosting the reversible hydrogen storage performance of MgH_2, J. Mater. Chem. A 11 (2023) 9762–9771.

[38] F. Marques, M. Balcerzak, F. Winkelmann, G. Zepon, M. Felderhoff, Review and outlook on high-entropy alloys for hydrogen storage, Energy Environ. Sci. 14 (2021) 5191–5227.

[39] F. Liang, J. Lin, Y. Cheng, D.M. Yin, Y.M. Wu, L.M. Wang, Gaseous sorption and electrochemical properties of rare-earth hydrogen storage alloys and their representative applications: a review of recent progress, Sci. China Technol. Sci. 61 (2018) 1309–1318.

[40] H.M. Sun, J. Meng, L.F. Jiao, F.Y. Cheng, J. Chen, A review of transition-metal boride/phosphide-based materials for catalytic hydrogen generation from hydrolysis of boron-hydrides, Inorg. Chem. Front. 5 (2018) 760–772.

[41] J. Du, F.Y. Cheng, M. Si, J. Liang, Z.L. Tao, J. Chen, Nanoporous Ni-based catalysts for hydrogen generation from hydrolysis of ammonia borane, Int. J. Hydrogen Energy 38 (2013) 5768–5774.

[42] B. Bogdanović, M. Schwickardi, Ti-doped alkali metal aluminium hydrides as potential novel reversible hydrogen storage materials, J. Alloys Compd. 253–254 (1997) 1–9.

[43] Y.M. Luo, L.X. Sun, F. Xu, Z.W. Liu, Improved hydrogen storage of $LiBH_4$ and NH_3BH_3 by catalysts, J. Mater. Chem. A 6 (2018) 7293–7309.

[44] S.J. Qiu, H.L. Chu, Y.J. Zou, C.L. Xiang, F. Xu, L.X. Sun, Light metal borohydrides/amides combined hydrogen storage systems: composition, structure and properties, J. Mater. Chem. A 5 (2017) 25112–25130.

[45] S.Y. Zheng, F. Fang, G.Y. Zhou, G.R. Chen, L.Z. Ouyang, M. Zhu, D.L. Sun, Hydrogen storage properties of space-confined $NaAlH_4$ nanoparticles in ordered mesoporous silica, Chem. Mater. 20 (2008) 3954–3958.

[46] B. Peng, J. Chen, Ammonia borane as an efficient and lightweight hydrogen storage medium, Energy Environ. Sci. 1 (2008) 479–483.

[47] J.W. Yeh, S.K. Chen, S.J. Lin, J.Y. Gan, T.S. Chin, T.T. Shun, C.H. Tsau, S. Y. Chang, Nanostructured high-entropy alloys with multiple principal elements: novel alloy design concepts and outcomes, Adv. Eng. Mater. 6 (2004) 299–303.

[48] B. Cantor, I.T.H. Chang, P. Knight, A.J.B. Vincent, Microstructural development in equiatomic multicomponent alloys, Mater. Sci. Eng., A 375–377 (2004) 213–218.

[49] A. Amiri, R. Shahbazian-Yassar, Recent progress of high-entropy materials for energy storage and conversion, J. Mater. Chem. A 9 (2021) 782–823.

[50] H. Zhao, Z. Zheng, H.R. Zhou, L. Chang, K. Tsoutas, L.M. Yang, S.K.H. Alavi, Y. P. Liu, B. Akhavan, M.M. Bilek, Z.W. Liu, Cathodic arc deposition of high entropy alloy thin films with controllable microstructure, Surf. Interfaces 37 (2023) 102692.

[51] M.G. Li, F.X. Lin, S.P. Zhang, R. Zhao, L. Tao, L. Li, J.Y. Li, L.Y. Zeng, M.H. Luo, S. J. Guo, High- entropy alloy electrocatalysts go to (sub-)nanoscale, Sci. Adv. 10 (2024) eadn2877.

[52] J.T. Ren, L. Chen, H.Y. Wang, Z.Y. Yuan, High-entropy alloys in electrocatalysis: from fundamentals to applications, Chem. Soc. Rev. 52 (2023) 8319.

[53] Y.S. Zheng, Y.F. Meng, X. Hu, H.Y. Peng, L.L. Feng, Y. Wang, B.H. Li, Synthesis-structure-property of high-entropy layered oxide cathode for Li/Na/K-ion batteries, Adv. Mater. 37 (2025) e2413202.

[54] F.S. Yang, J. Wang, Y. Zhang, Z. Wu, Z.X. Zhang, F.Q. Zhao, J. Huot, J. Grobivć Novaković, N. Novaković, Recent progress on the development of high entropy alloys (HEAs) for solid hydrogen storage: a review, Int. J. Hydrogen Energy 47 (2022) 11236–11249.

[55] L.J. Kong, B. Cheng, D. Wan, Y.F. Xue, A review on BCC-structured high-entropy alloys for hydrogen storage, Front. Mater. 10 (2023) 1135864.

[56] H. Zhao, Z. Zheng, L.X. Sun, H.W. Liu, K. Tsoutas, B. Akhavan, Y.P. Liu, M. M. Bilek, Z.W. Liu, Introducing a new heterogeneous nanocomposite thin film with superior mechanical properties and thermal stability, Mater. Des. 234 (2023) 112333.

[57] N.A. Khan, B. Akhavan, C.F. Zhou, H.R. Zhou, L. Chang, Y. Wang, Y.P. Liu, L. Fu, M.M. Bilek, Z.W. Liu, RF magnetron sputtered $AlCoCrCu_{0.5}FeNi$ high entropy alloy (HEA) thin films with tuned microstructure and chemical composition, J. Alloys Compd. 836 (2020) 155348.

[58] Y.F. Kao, S.K. Chen, J.H. Sheu, J.T. Lin, W.E. Lin, J.W. Yeh, S.J. Lin, T.H. Liou, C. W. Wang, Hydrogen storage properties of multi–principal–component $CoFeMnTi_xV_yZr_z$ alloys, Int. J. Hydrogen Energy 35 (2010) 9046–9059.

[59] B. Cheng, L.J. Kong, H.M. Cai, Y.K. Li, Y.M. Zhao, D. Wan, Y.F. Xue, Exploring microstructure variations and hydrogen storage characteristics in TiVNbCrNi high-entropy alloys with different Ni incorporation, Int. J. Hydrogen Energy 72 (2024) 29–40.

[60] Y.T. Zhai, Y.M. Li, Z.C. Liu, L. Bolzoni, J. Kennedy, F. Yang, Hydrogen ab/desorption behavior of the mechanical alloyed Ti-V-Cr-Mn-Fe HEAs with varying Mn/Cr ratio, Int. J. Hydrogen Energy 109 (2025) 1008–1022.

[61] M.K. Cui, T.M. Zhang, J.M. Ni, W.M. Zhao, S.Y. Li, Q.Y. Liu, S.Y. Zhang, Z.K. Ye, Y.F. Deng, Y.H. Chen, First-principles study on the hydrogen embrittlement resistance of CoCrFeMnNi high-entropy alloys, Int. J. Hydrogen Energy 106 (2025) 1275–1284.

[62] J.T. Hu, H.A. Shen, M. Jiang, H.F. Gong, H.Y. Xiao, Z.J. Liu, G.G. Sun, X.T. Zu, A DFT study of hydrogen storage in high-entropy alloy TiZrHfScMo, Nanomaterials 9 (2019) 461.

[63] M. Witman, G. Ek, S. Ling, J. Chames, S. Agarwal, J. Wong, M.D. Allendorf, M. Sahlberg, V. Stavila, Data-driven discovery and synthesis of high entropy alloy hydrides with targeted thermodynamic stability, Chem. Mater. 33 (2021) 4067–4076.

[64] Y.B. Zhou, X.W. Shen, T. Qian, C.L. Yan, J.M. Lu, A review on the rational design and fabrication of nanosized high-entropy materials, Nano Res. 16 (2023) 7874–7905.

[65] X. Wang, W. Guo, Y.Z. Fu, High-entropy alloys: emerging materials for advanced functional applications, J. Mater. Chem. A 9 (2021) 663–701.

[66] N. Radhika, M.S. Niketh, U.V. Akhil, A.A. Adediran, T.C. Jen, High entropy alloys for hydrogen storage applications: a machine learning-based approach, Results Eng. 23 (2024) 102780.

[67] P. Edalati, G. Andrade, R.B. Strozi, S. Dangwal, K. Edalati, R. Floriano, Room temperature hydrogen storage properties of Ti-Zr-Mn-Fe-Co high-entropy alloys designed by semi-empirical descriptors, thermodynamic calculations and machine learning, J. Alloys Compd. 1022 (2025) 180051.

[68] M. Rethinasabapathy, S.M. Ghoreishian, S.K. Hwang, Y.K. Han, C. Roh, Y.S. Huh, Recent progress in functional nanomaterials towards the storage, separation, and removal of tritium, Adv. Mater. 35 (2023) e2301589.

[69] J.Y. Kim, H. Oh, H.R. Moon, Hydrogen isotope separation in confined nanospaces: carbons, zeolites, metal-organic frameworks, and covalent organic frameworks, Adv. Mater. 31 (2019) e1805293.

[70] E.H. Yan, W. Liu, H. Wang, K.X. Zhang, X.Y. Ge, R.J. Huang, J. Cheng, Y.J. Zou, H.L. Chu, H.Z. Zhang, F. Xu, L.X. Sun, Quaternary Nb-Hf-Co-Fe alloy with superior hydrogen permeation properties over a wide temperature range, J. Alloys Compd. 912 (2022) 165232.

[71] E. Magnone, M.C. Shin, J.I. Lee, J.H. Park, Relationship between hydrogen permeability and the physical-chemical characteristics of metal alloy membranes, J. Membr. Sci. 674 (2023) 121513.

[72] J.W. Yeh, Recent progress in high-entropy alloys, Ann. Chim. Sci. Mat. 31 (2006) 633–648.

[73] J.W. Yeh, Alloy design strategies and future trends in high-entropy alloys, JOM 65 (2013) 1759–1771.

[74] W. Guo, W. Dmowski, J.Y. Noh, P. Rack, P.K. Liaw, T. Egami, Local atomic structure of a high-entropy alloy: an X-ray and neutron scattering study, Metall. Mater. Trans. A 44 (2012) 1994–1997.

[75] Y.W. Zhang, G.M. Stocks, K. Jin, C.Y. Lu, H.B. Bei, B.C. Sales, L.M. Wang, L. K. Beland, R.E. Stoller, G.D. Samolyuk, M. Caro, A. Caro, W.J. Weber, Influence of chemical disorder on energy dissipation and defect evolution in concentrated solid solution alloys, Nat. Commun. 6 (2015) 8736.

[76] T.T. Zuo, M.C. Gao, L.Z. Ouyang, X. Yang, Y.Q. Cheng, R. Feng, S.Y. Chen, P. K. Liaw, J.A. Hawk, Y. Zhang, Tailoring magnetic behavior of $CoFeMnNi_X$ (X = Al, Cr, Ga, and Sn) high entropy alloys by metal doping, Acta Mater. 130 (2017) 10–18.

[77] W.D. Li, D. Xie, D.Y. Li, Y. Zhang, Y.F. Gao, P.K. Liaw, Mechanical behavior of high-entropy alloys, Prog. Mater. Sci. 118 (2021) 100777.

[78] J. Chen, X.Y. Zhou, W.L. Wang, B. Liu, Y.K. Lv, W. Yang, D.P. Xu, Y. Liu, A review on fundamental of high entropy alloys with promising high-temperature properties, J. Alloys Compd. 760 (2018) 15–30.

[79] M.X. Wei, Y.J. Liu, X.F. Xing, Z. Zhang, T. Liu, $(TiVZrNb)_{83}Cr_{17}$ high-entropy alloy as catalyst for hydrogen storage in MgH_2, Chem. Eng. J. 476 (2023) 146639.

[80] R.R. Shahi, A.K. Gupta, P. Kumari, Perspectives of high entropy alloys as hydrogen storage materials, Int. J. Hydrogen Energy 48 (2022) 21412–21428.

[81] Y. Zhang, Y.J. Zhou, J.P. Lin, G.L. Chen, P.K. Liaw, Solid-solution phase formation rules for multi-component alloys, Adv. Eng. Mater. 10 (2008) 534–538.

[82] S. Guo, C.T. Liu, Phase stability in high entropy alloys: formation of solid-solution phase or amorphous phase, Prog. Nat. Sci. Mater. Int. 21 (2011) 433–446.

[83] X. Yang, Y. Zhang, Prediction of high-entropy stabilized solid-solution in multi-component alloys, Mater. Chem. Phys. 132 (2012) 233–238.

[84] S.S. Fang, X.S. Xiao, L. Xia, W.H. Li, Y.D. Dong, Relationship between the widths of supercooled liquid regions and bond parameters of Mg-based bulk metallic glasses, J. Non-Cryst. Solids 321 (2003) 120–125.

[85] X. Yang, S.Y. Chen, J.D. Cotton, Y. Zhang, Phase stability of low-density, multiprincipal component alloys containing aluminum, magnesium, and lithium, JOM 66 (2014) 2009–2020.

[86] M.M. Nygård, G. Ek, D. Karlsson, M.H. Sørby, M. Sahlberg, B.C. Hauback, Counting electrons - a new approach to tailor the hydrogen sorption properties of high-entropy alloys, Acta Mater. 175 (2019) 121–129.

[87] I. Toda-Caraballo, J.S. Wróbel, D. Nguyen-Manh, P. Pérez, P.E.J. Rivera-Díaz-Del-Castillo, Simulation and modeling in high entropy alloys, JOM 69 (2017) 2137–2149.

[88] J. Li, Q.H. Fang, P.K. Liaw, Microstructures and properties of high-entropy materials: modeling, simulation, and experiments, Adv. Eng. Mater. 23 (2020) 2001044.

[89] Y.H. Deng, J.T. Hu, S.Q. Zhao, W.D. Wang, L. Xie, G.A. Sun, H.H. Shen, X.T. Zu, H.Y. Xiao, Hydrogen storage properties of $Mg_{0.10}Ti_{0.30}V_{0.25}Zr_{0.10}Nb_{0.25}$ lightweight high entropy alloy: a theoretical study, Int. J. Hydrogen Energy 50 (2024) 314–323.

[90] J.J. Gong, Y. Li, X.Q. Song, Y.X. Wang, Z. Chen, Hydrogen storage of high entropy alloy NbTiVZr and its effect on mechanical properties: a first-principles study, Vacuum 219 (2024) 112754.

[91] J.T. Hu, J.J. Zhang, H.Y. Xiao, L. Xie, G.A. Sun, H.H. Shen, P.C. Li, J.W. Zhang, X. T. Zu, A first-principles study of hydrogen storage of high entropy alloy TiZrVMoNb, Int. J. Hydrogen Energy 46 (2021) 21050–21058.

[92] J.J. Zhang, J.T. Hu, H.Y. Xiao, H.H. Shen, L. Xie, G.A. Sun, X.T. Zu, A first-principles study of hydrogen desorption from high entropy alloy TiZrVMoNb hydride surface, Metals 11 (2021) 553.

[93] P.C. Li, J.T. Hu, G. Huang, J.W. Zhang, W.D. Wang, C.X. Tian, H.Y. Xiao, X. S. Zhou, H.H. Shen, X.G. Long, S.M. Peng, X.T. Zu, Electronic structure regulation toward the improvement of the hydrogenation properties of TiZrHfMoNb high-entropy alloy, J. Alloys Compd. 905 (2022) 164150.

[94] A. Mohammadi, Y. Ikeda, P. Edalati, M. Mito, B. Grabowski, H.W. Li, K. Edalati, High-entropy hydrides for fast and reversible hydrogen storage at room temperature: Binding-energy engineering via first-principles calculations and experiments, Acta Mater. 236 (2022) 118117.

[95] J.T. Hu, J.J. Zhang, M.L. Li, S. Zhang, H.Y. Xiao, L. Xie, G.A. Sun, H.H. Shen, X. S. Zhou, X.Q. Li, P.C. Li, J.W. Zhang, L. Vitos, X.T. Zu, The origin of anomalous hydrogen occupation in high entropy alloys, J. Mater. Chem. A 10 (2022) 7228–7237.

[96] J.T. Hu, X.Q. Li, L. Vitos, S. Schönecker, Effects of Mg and Al doping on the desorption energetics and electronic structure of a Ti-V-Zr-Nb alloy hydride, Acta Mater. 277 (2024) 120198.

[97] S.W. Kao, J.W. Yeh, T.S. Chin, Rapidly solidified structure of alloys with up to eight equal-molar elements—a simulation by molecular dynamics, J. Phys. Condens. Matter 20 (2008) 145214.

[98] W.M. Choi, Y.H. Jo, S.S. Sohn, S. Lee, B.J. Lee, Understanding the physical metallurgy of the CoCrFeMnNi high-entropy alloy: an atomistic simulation study, npj Comput. Mater. 4 (2018) 1.

[99] X.L. Ren, P.H. Shi, W.W. Zhang, X.Y. Wu, Q. Xu, Y.X. Wang, Swamps of hydrogen in equiatomic FeCuCrMnMo alloys: First-principles calculations, Acta Mater. 180 (2019) 189–198.

[100] F. Trequattrini, S. Brutti, O. Palumbo, M. Hulyalkar, L.T. Mushongera, W. Ye, M. R. Khan, M. Dolan, D. Chandra, A. Paolone, Crystallization and hydrogen absorption in a $Ni_{32}Nb_{28}Zr_{30}Fe_{10}$ melt spun alloy and correlation with icosahedral clusters, Int. J. Hydrogen Energy 47 (2022) 10298–10307.

[101] G.H. Cao, J.J. Liang, Z.L. Guo, K.N. Yang, G. Wang, H.L. Wang, X.H. Wan, Z.Y. Li, Y.J. Bai, Y. Zhang, J.L. Liu, Y.P. Feng, Z.Y. Zheng, C. Lu, G.Z. He, Z.Y. Xiong, Z. Liu, S.L. Chen, Y.Z. Guo, M.Q. Zeng, J.H. Lin, L. Fu, Liquid metal for high-entropy alloy nanoparticles synthesis, Nature 619 (2023) 73–77.

[102] L.X. Li, Q.Y. Du, Y.H. Wang, K. Xu, M.H. Sun, J.N. Sun, F.S. Du, Hydrogen behavior during high-temperature plastic deformation in low-alloy steels, J. Mater. Process. Technol. 302 (2022) 117487.

[103] F. Zhang, C. Zhang, S.L. Chen, J. Zhu, W.S. Cao, U.R. Kattner, An understanding of high entropy alloys from phase diagram calculations, Calphad 45 (2014) 1–10.

[104] Q. Luo, Y. Guo, B. Liu, Y. Feng, J. Zhang, Q. Li, K. Chou, Thermodynamics and kinetics of phase transformation in rare earth–magnesium alloys: a critical review, J. Mater. Sci. Technol. 44 (2020) 171–190.

[105] P. Edalati, R. Floriano, A. Mohammadi, Y. Li, G. Zepon, H.W. Li, K. Edalati, Reversible room temperature hydrogen storage in high-entropy alloy TiZrCrMnFeNi, Scripta Mater. 178 (2020) 387–390.

[106] R. Floriano, G. Zepon, K. Edalati, G.L.B.G. Fontana, A. Mohammadi, Z. Ma, H.W. Li, R.J. Contieri, Hydrogen storage in TiZrNbFeNi high entropy alloys, designed by thermodynamic calculations, Int. J. Hydrogen Energy 45 (2020) 33759–33770.

[107] R. Floriano, G. Zepon, K. Edalati, G.L.B.G. Fontana, A. Mohammadi, Z. Ma, H. W. Li, R.J. Contieri, Hydrogen storage properties of new A_3B_2-type TiZrNbCrFe high-entropy alloy, Int. J. Hydrogen Energy 46 (2021) 23757–23766.

[108] K. Zeng, T. Klassen, W. Oelerich, R. Bormann, Thermodynamic analysis of the hydriding process of Mg-Ni alloys, J. Alloys Compd. 283 (1999) 213–224.

[109] Q. Li, Q. Luo, Q.F. Gu, Insights into the composition exploration of novel hydrogen storage alloys: evaluation of the Mg-Ni-Nd-H phase diagram, J. Mater. Chem. A 5 (2017) 3848–3864.

[110] R.B. Strozi, D.R. Leiva, J. Huot, W.J. Botta, G. Zepon, Synthesis and hydrogen storage behavior of Mg-V-Al-Cr-Ni high entropy alloys, Int. J. Hydrogen Energy 46 (2021) 2351–2361.

[111] P.P. Zhou, Q.W. Zhou, X.Z. Xiao, X.L. Fan, Y.J. Zou, L.X. Sun, J.H. Jiang, D. Song, L.X. Chen, Machine learning in solid-state hydrogen storage materials: challenges and perspectives, Adv. Mater. 37 (2025) e2413430.

[112] G. Wang, Z. Luo, H.G. Desta, M. Chen, Y. Dong, B. Lin, AI-driven development of high-performance solid-state hydrogen storage, Energy Rev. 4 (2025) 100106.

[113] US DOE Hydrogen Storage Database, 2025. https://datahub.hymarc.org/dataset/hydrogen-storage-materials-db. (Accessed 4 May 2025).

[114] P.R. Huang, D. Cai, H.Z. Lin, J.X. Liu, Z.Y. Li, B. Li, Y.J. Zou, H.L. Chu, L.X. Sun, F. Xu, Materials genome engineering-based hydrogen storage materialsdatabase and its applications, Sci. Sin. Chim. 52 (2022) 1863–1870.

[115] P.P. Zhou, X.Z. Xiao, X.Y. Zhu, Y.P. Chen, W.M. Lu, M.Y. Piao, Z.M. Cao, M. Lu, F. Fang, Z.N. Li, L.J. Jiang, L.X. Chen, Machine learning enabled customization of performance-oriented hydrogen storage materials for fuel cell systems, Energy Storage Mater. 63 (2023) 102964.

[116] K.X. Cui, J.W. Qiao, P.K. Liaw, Y. Zhang, Data driving design of high-entropy alloys for lightweight and dynamic applications, Sci. China Phys. Mech. 67 (2024) 227101.

[117] G.L.W. Hart, T. Mueller, C. Toher, S. Curtarolo, Machine learning for alloys, Nat. Rev. Mater. 6 (2021) 730–755.

[118] R. Feng, C. Zhang, M.C. Gao, Z. Pei, F. Zhang, Y. Chen, D. Ma, K. An, J. D. Poplawsky, L. Ouyang, Y. Ren, J.A. Hawk, M. Widom, P.K. Liaw, High-throughput design of high-performance lightweight high-entropy alloys, Nat. Commun. 12 (2021) 4329.

[119] C.L. You, W.J. Fan, X.S. Xiong, H.Y. Yang, L.J. Fu, T. Wang, F.X. Wang, Z. Zhu, J. R. He, Y.P. Wu, Design strategies for anti-freeze electrolytes in aqueous energy storage devices at low temperatures, Adv. Funct. Mater. 34 (2024) 2403616.

[120] W.J. Huang, P. Martin, H.L. Zhuang, Machine-learning phase prediction of high-entropy alloys, Acta Mater. 169 (2019) 225–236.

[121] D.B. Dai, T. Xu, X. Wei, G.T. Ding, Y. Xu, J.C. Zhang, H.R. Zhang, Using machine learning and feature engineering to characterize limited material datasets of high-entropy alloys, Comput. Mater. Sci. 175 (2020) 109618.

[122] S. Risal, W.H. Zhu, P. Guillen, L. Sun, Improving phase prediction accuracy for high entropy alloys with machine learning, Comput. Mater. Sci. 192 (2021) 110389.

[123] J. Qi, A.M. Cheung, S.J. Poon, High entropy alloys mined from binary phase diagrams, Sci. Rep. 9 (2019) 15501.

[124] K. Kaufmann, K.S. Vecchio, Searching for high entropy alloys: a machine learning approach, Acta Mater. 198 (2020) 178–222.

[125] M.D. Witman, S. Ling, M. Wadge, A. Bouzidi, N. Pineda-Romero, R. Clulow, G. Ek, J.M. Chames, E.J. Allendorf, S. Agarwal, M.D. Allendorf, G.S. Walker, D.M. Grant, M. Sahlberg, C. Zlotea, V. Stavila, Towards Pareto optimal high entropy hydrides via data-driven materials discovery, J. Mater. Chem. A 11 (2023) 15878–15888.

[126] J.J. Reilly, G.D. Adzic, J.R. Johnson, T. Vogt, The correlation between composition and electrochemical properties of metal hydride electrodes, J. Alloys Compd. 293–295 (1999) 569–582.

[127] R.B. Strozi, M. Witman, V. Stavila, J. Cizek, K. Sakaki, H. Kim, O. Melikhova, L. PerrièRe, A. Machida, Y. Nakahira, G. Zepon, W.J. Botta, C. Zlotea, Elucidating primary degradation mechanisms in high–cycling–capacity, compositionally tunable high-entropy hydrides, ACS Appl. Mater. Interfaces 15 (2023) 38412–38422.

[128] X.Y. Zhou, J.H. Zhu, Y. Wu, X.S. Yang, T. Lookman, H.H. Wu, Machine learning assisted design of FeCoNiCrMn high-entropy alloys with ultra-low hydrogen diffusion coefficients, Acta Mater. 224 (2022) 117535.

[129] S. Suwarno, G. Dicky, A. Suyuthi, M. Effendi, W. Witantyo, L. Noerochim, M. Ismail, Machine learning analysis of alloying element effects on hydrogen storage properties of AB_2 metal hydrides, Int. J. Hydrogen Energy 47 (2022) 11938–11947.

[130] J.M. Kim, T. Ha, J. Lee, Y.S. Lee, J.H. Shim, Prediction of pressure–composition–temperature curves of AB_2-type hydrogen storage alloys by machine learning, Met. Mater. Int. 29 (2022) 861–869.

[131] E. Halpren, X. Yao, Z.W. Chen, C.V. Singh, Machine learning assisted design of BCC high entropy alloys for room temperature hydrogen storage, Acta Mater. 270 (2024) 119841.

[132] S. Dangwal, Y. Ikeda, B. Grabowski, K. Edalati, Machine learning to explore high-entropy alloys with desired enthalpy for room-temperature hydrogen storage: prediction of density functional theory and experimental data, Chem. Eng. J. 493 (2024) 152606.

[133] W.Q. Wan, K.M. Liang, P.Y. Zhu, P. He, S.Y. Zhang, Recent advances in the synthesis and fabrication methods of high-entropy alloy nanoparticles, J. Mater. Sci. Technol. 178 (2024) 226–246.

[134] X.H. Yan, Y. Zou, Y. Zhang, Properties and processing technologies of high-entropy alloys, Mater, Futures 1 (2022) 022002.

[135] M.M. Nygård, G. Ek, D. Karlsson, M. Sahlberg, M.H. Sørby, B.C. Hauback, Hydrogen storage in high-entropy alloys with varying degree of local lattice strain, Int. J. Hydrogen Energy 44 (2019) 29140–29149.

[136] H.H. Shen, J.W. Zhang, J.T. Hu, J.C. Zhang, Y.W. Mao, H.Y. Xiao, X.S. Zhou, X. T. Zu, A novel TiZrHfMoNb high-entropy alloy for solar thermal energy storage, Nanomaterials 9 (2019) 248.

[137] H.M. Zhao, P.F. Yao, Y.F. Zhao, Z.Q. Zeng, C.Q. Xia, T. Yang, Microstructure and hydrogen storage properties of Zr-based AB_2-type high entropy alloys, J. Alloys Compd. 960 (2023) 170665.

[138] L. Serrano, M. Moussa, J.Y. Yao, G. Silva, J.L. Bobet, S.F. Santos, K.R. Cardoso, Development of Ti-V-Nb-Cr-Mn high entropy alloys for hydrogen storage, J. Alloys Compd. 945 (2023) 169289.

[139] H.H. Shen, J.T. Hu, P.C. Li, G. Huang, J.W. Zhang, J.C. Zhang, Y.W. Mao, H. Y. Xiao, X.S. Zhou, X.T. Zu, X.G. Long, S.M. Peng, Compositional dependence of hydrogenation performance of Ti-Zr-Hf-Mo-Nb high-entropy alloys for hydrogen/tritium storage, J. Mater. Sci. Technol. 55 (2020) 116–125.

[140] M. Sahlberg, D. Karlsson, C. Zlotea, U. Jansson, Superior hydrogen storage in high entropy alloys, Sci. Rep. 6 (2016) 36770.

[141] C. Zhang, Y. Wu, L. You, X.Z. Cao, Z.P. Lu, X.P. Song, Investigation on the activation mechanism of hydrogen absorption in TiZrNbTa high entropy alloy, J. Alloys Compd. 781 (2019) 613–620.

[142] X.F. Ma, X. Ding, R.R. Chen, X.G. Chen, Q. Song, H.Z. Cui, Study on microstructure and the hydrogen storage behavior of a TiVZrNbFe high-entropy alloy, Intermetallics 157 (2023) 107885.

[143] T.Z. Huang, J.T. Han, Y.H. Zhang, J.M. Yu, G.X. Sun, H. Ren, X.X. Yuan, Study on the structure and hydrogen absorption–desorption characteristics of as-cast and annealed $La_{0.78}Mg_{0.22}Ni_{3.48}Co_{0.22}Cu_{0.12}$ alloys, J. Power Sources 196 (2011) 9585–9589.

[144] K. Young, B. Chao, B. Huang, J. Nei, Studies on the hydrogen storage characteristic of $La_{1-x}Ce_x(NiCoMnAlCuSiZr)_{5.7}$ with a B2 secondary phase, J. Alloys Compd. 585 (2014) 760–770.

[145] L.X. Liu, L.X. Chen, X.Z. Xiao, C.C. Xu, J. Sun, S.Q. Li, H.W. Ge, L.J. Jiang, Influence of annealing treatment on the microstructure and hydrogen storage performance of $Ti_{1.02}Cr_{1.1}Mn_{0.3}Fe_{0.6}$ alloy for hybrid hydrogen storage application, J. Alloys Compd. 636 (2015) 117–123.

[146] J. Montero, C. Zlotea, G. Ek, J.C. Crivello, L. Laversenne, M. Sahlberg, TiVZrNb multi-principal-element alloy: synthesis optimization, structural, and hydrogen sorption properties, Molecules 24 (2019) 2799.

[147] G. Zepon, D.R. Leiva, R.B. Strozi, A. Bedoch, S.J.A. Figueroa, T.T. Ishikawa, W. J. Botta, Hydrogen-induced phase transition of $MgZrTiFe_{0.5}Co_{0.5}Ni_{0.5}$ high entropy alloy, Int. J. Hydrogen Energy 43 (2018) 1702–1708.

[148] M.O. De Marco, Y. Li, H.W. Li, K. Edalati, R. Floriano, Mechanical synthesis and hydrogen storage characterization of MgVCr and MgVTiCrFe high-entropy alloy, Adv. Eng. Mater. 22 (2019) 1901079.

[149] Y. Wang, W.H. Luo, S. Gong, L.X. Luo, Y.X. Li, Y.Y. Zhao, Z. Li, Synthesis of high-entropy alloy nanoparticles by a step-alloying strategy as a superior multifunctional electrocatalyst, Adv. Mater. 35 (2023) 2302499.

[150] Y.G. Yao, Z.N. Huang, P.F. Xie, S.D. Lacey, R.J. Jacob, H. Xie, F.J. Chen, A.M. Nie, T.C. Pu, M. Rehwoldt, D.W. Yu, M.R. Zachariah, C. Wang, R. Shahbazian-Yassar, J. Li, L.B. Hu, Carbothermal shock synthesis of high-entropy-alloy nanoparticles, Science 359 (2018) 1489–1494.

[151] Y. Chida, T. Tomimori, T. Ebata, N. Taguchi, T. Ioroi, K. Hayashi, N. Todoroki, T. Wadayama, Experimental study platform for electrocatalysis of atomic-level controlled high-entropy alloy surfaces, Nat. Commun. 14 (2023) 4492.

[152] Z.K. Jing, Y.K. Guo, Q. Wang, X.R. Yan, G.Z. Yue, Z.D. Li, H.W. Liu, R.X. Qin, C. Y. Zhong, M.Z. Li, D.G. Xu, Y.X. Yao, Y.G. Yao, M.B. Shuai, Ambient hydrogenation of solid aromatics enabled by a high entropy alloy nanocatalyst, Nat. Commun. 15 (2024) 5806.

[153] D.Y. Feng, Y.B. Dong, P. Nie, L. Zhang, Z.A. Qiao, CoNiCuMgZn high entropy alloy nanoparticles embedded onto graphene sheets via anchoring and alloying strategy as efficient electrocatalysts for hydrogen evolution reaction, Chem. Eng. J. 430 (2022) 132883.

[154] B. Wang, C. Wang, X.W. Yu, Y. Cao, L.F. Gao, C.P. Wu, Y.F. Yao, Z.Q. Lin, Z. G. Zou, General synthesis of high-entropy alloy and ceramic nanoparticles in nanoseconds, Nat. Synth. 1 (2022) 138–146.

[155] S.J. Gao, S.Y. Hao, Z.N. Huang, Y.F. Yuan, S. Han, L.C. Lei, X.W. Zhang, R. Shahbazian-Yassar, J. Lu, Synthesis of high-entropy alloy nanoparticles on supports by the fast moving bed pyrolysis, Nat. Commun. 11 (2020) 2016.

[156] Y.Q. Xu, Y.Q. Bu, J.B. Liu, H.T. Wang, In-situ high throughput synthesis of high-entropy alloys, Scripta Mater. 160 (2019) 44–47.

[157] M. Moorehead, K. Bertsch, M. Niezgoda, C. Parkin, M. Elbakhshwan, K. Sridharan, C. Zhang, D. Thoma, A. Couet, High-throughput synthesis of Mo-Nb-Ta-W high-entropy alloys via additive manufacturing, Mater. Des. 187 (2020) 108358.

[158] B. Zhu, S. Alavi, C.J. Cheng, H.K. Sun, H.W. Zhao, K.S. Kim, J. Mostaghimi, Y. Zou, Fast and high-throughput synthesis of medium- and high-entropy alloys using radio frequency inductively coupled plasma, Adv. Eng. Mater. 23 (2020) 2001116.

[159] J.T. Chen, H.X. Huang, T.T. Xu, Y.J. Lv, B.G. Liu, B. Zhang, J.G. Yuan, Y. Wu, Enhancement of vanadium addition on hydrogen storage properties of high entropy alloys $TiZrFeMnCrV_x$, Int. J. Hydrogen Energy 50 (2024) 1223–1233.

[160] G. Andrade, B.H. Silva, G. Zepon, R. Floriano, Hydrogen storage properties of Zr-based multicomponent alloys with C14-Laves phase structure derived from the Zr-Cr-Mn-Fe-Ni system, Int. J. Hydrogen Energy 51 (2024) 246–254.

[161] C. Zlotea, M.A. Sow, G. Ek, J.P. Couzinié, L. Perrière, I. Guillot, J. Bourgon, K. T. Møller, T.R. Jensen, E. Akiba, M. Sahlberg, Hydrogen sorption in TiZrNbHfTa high entropy alloy, J. Alloys Compd. 775 (2019) 667–674.

[162] B. Cheng, Y.K. Li, X.X. Li, H.B. Ke, L. Wang, T.Q. Cao, D. Wan, B.P. Wang, Y. F. Xue, Solid-state hydrogen storage properties of Ti-V-Nb-Cr high-entropy alloys and the associated effects of transitional metals (M = Mn, Fe, Ni), Acta Metall. Sin. 36 (2022) 1113–1122.

[163] G. Andrade, J. Huot, R. Floriano, Microstructural evolution and hydrogen storage performance of $TiZrHfVNb_{1-x}Cu_x$ (for X = 0, 0.6, 0.8 and 1) high-entropy alloys, Mater. Chem. Phys. 343 (2025) 131069.

[164] X. Ma, X. Ding, R. Chen, J. Zhang, Q. Song, H. Cui, Microstructural features and improved reversible hydrogen storage properties of ZrTiVFe high-entropy alloy via Cu alloying, Int. J. Hydrogen Energy 48 (2023) 2718–2730.

[165] S. Sleiman, M. Moussa, J. Huot, Microstructure and hydrogen storage properties of the multiphase $Ti_{0.3}V_{0.3}Mn_{0.2}Fe_{0.1}Ni_{0.1}$ alloy, Reactions 2 (2021) 287–300.

[166] L.F. Chanchetti, B. Hessel Silva, J. Montero, C. Zlotea, Y. Champion, W.J. Botta, G. Zepon, Structural characterization and hydrogen storage properties of the $Ti_{31}V_{26}Nb_{26}Zr_{12}M_5$ (M = Fe, Co, or Ni) multi-phase multicomponent alloys, Int. J. Hydrogen Energy 48 (2023) 2247–2255.

[167] J.X. Wang, P.P. Zhou, Y.X. Jia, J. Feng, J.C. Qi, F. Chu, L.X. Chen, X.Z. Xiao, Binding energy crossover mechanism enables low-temperature hydrogen storage performance of dual-phase TiZrCrMnNi(VFe) high-entropy alloy, Chem. Eng. J. 502 (2024) 157871.

[168] S. Dangwal, K. Edalati, Significance of interphase boundaries on activation of high-entropy alloys for room-temperature hydrogen storage, Int. J. Hydrogen Energy 50 (2024) 626–636.

[169] S. Sleiman, J. Huot, Effect of particle size, pressure and temperature on the activation process of hydrogen absorption in TiVZrHfNb high entropy alloy, J. Alloys Compd. 861 (2021) 158615.

[170] Z. Wen, G. Li, S. Wang, Y. Li, T. Zhang, X. Ding, Y. Qu, Effect of Zr content on hydrogen absorption and desorption properties of $Ti_{35-x}V_{25}Cr_{15}Nb_{25}Zr_x$ (x = 0, 2, 4, 6, 8) high entropy alloys, Int. J. Hydrogen Energy 175 (2025) 151468.

[171] J. Hu, J. Zhang, H. Xiao, L. Xie, H. Shen, P. Li, J. Zhang, H. Gong, X. Zu, A density functional theory study of the hydrogen absorption in high entropy alloy TiZrHfMoNb, Inorg. Chem. 59 (2020) 9774–9782.

[172] X.F. Ma, X. Ding, R.R. Chen, W.C. Cao, Q. Song, Study on hydrogen storage property of (ZrTiVFe) Al high-entropy alloys by modifying Al content, Int. J. Hydrogen Energy 47 (2022) 8409–8418.

[173] B. Cheng, L.J. Kong, Y.K. Li, Hydrogen desorption kinetics of $V_{30}Nb_{10}(Ti_xCr_{1-x})_{60}$ high-entropy alloys, Metals 13 (2023) 230.

[174] H. Fu, Y. Jiang, M.Z. Zhang, Z.Y. Zhong, Z. Liang, S.Y. Wang, Y.P. Du, C.H. Yan, High-entropy rare Earth materials: synthesis, application and outlook, Chem. Soc. Rev. 53 (2024) 2211–2247.

[175] W.F. Qiao, W.Q. Liu, D.M. Yin, N. Ding, S.L. Zhao, H.X. Xiu, C. Liu, Y. Wang, M. He, C.L. Wang, L.M. Wang, Y. Cheng, Comprehensive improvement of AB_2 hydrogen storage alloy: substitution of rare Earth elements for different A-side alloys, Chem. Eng. J. 495 (2024) 153489.

[176] X.J. Zhang, Z. Zhang, C.M. Xu, X.F. Xing, M.X. Wei, B.Y. Cao, T. Liu, Ti/Cr regulated and strategic Ce doped V-Ti-Cr-Mn-Fe high-entropy alloys with extraordinary reversible hydrogen storage properties at ambient temperature, Chem. Eng. J. 499 (2024) 156643.

[177] H.W. Shang, Y.Q. Li, Y.H. Zhang, Y. Qi, S.H. Guo, D.L. Zhao, Structure and hydrogenation performances of as-cast $Ti_{1.1-x}RE_xFe_{0.8}Mn_{0.2}$ (RE = Pr, Sm and Nd; x = 0, 0.01) alloys, Int. J. Hydrogen Energy 43 (2018) 19091–19101.

[178] Z.D. Yao, L.X. Liu, X.Z. Xiao, C.T. Wang, L.J. Jiang, L.X. Chen, Effect of rare Earth doping on the hydrogen storage performance of $Ti_{1.02}Cr_{1.1}Mn_{0.3}Fe_{0.6}$ alloy for hybrid hydrogen storage application, J. Alloys Compd. 731 (2018) 524–530.

[179] L. Zhou, W.X. Li, H.Z. Hu, H.F. Zeng, Q.J. Chen, Ce-doped TiZrCrMn alloys for enhanced hydrogen storage, Energy Fuel. 36 (2022) 3997–4005.

[180] D.C. Feng, D.S. Zhou, Z.Y. Zhao, T.T. Zhai, Z.M. Yuan, H. Sun, H.P. Ren, Y. H. Zhang, Progress of graphene and loaded transition metals on Mg-based hydrogen storage alloys, Int. J. Hydrogen Energy 46 (2021) 33468–33485.

[181] F. Marques, H.C. Pinto, S.J.A. Figueroa, F. Winkelmann, M. Felderhoff, W. J. Botta, G. Zepon, Mg-containing multi-principal element alloys for hydrogen storage: a study of the $MgTiNbCr_{0.5}Mn_{0.5}Ni_{0.5}$ and $Mg_{0.68}TiNbNi_{0.55}$ compositions, Int. J. Hydrogen Energy 45 (2020) 19539–19552.

[182] J. Montero, G. Ek, M. Sahlberg, C. Zlotea, Improving the hydrogen cycling properties by Mg addition in Ti-V-Zr-Nb refractory high entropy alloy, Scripta Mater. 194 (2021) 113699.

[183] Y.H. Deng, X. Chen, H.B. Qi, S. Feng, W.D. Wang, L. Xie, G.A. Sun, H.H. Shen, X. T. Zu, H.Y. Xiao, The design of Mg-Ti-V-Nb-Cr lightweight high entropy alloys for hydrogen storage, Int. J. Hydrogen Energy 87 (2024) 1327–1337.

[184] K.R. Cardoso, V. Roche, A.M. Jorge Jr., F.J. Antiqueira, G. Zepon, Y. Champion, Hydrogen storage in MgAlTiFeNi high entropy alloy, J. Alloys Compd. 858 (2021) 158357.

[185] J. Montero, G. Ek, L. Laversenne, V. Nassif, M. Sahlberg, C. Zlotea, How 10 at% Al addition in the Ti-V-Zr-Nb high-entropy alloy changes hydrogen sorption properties, Molecules 26 (2021) 2470.

[186] B.H. Silva, C. Zlotea, Y. Champion, W.J. Botta, Design of TiVNb-(Cr, Ni or Co) multicomponent alloys with the same valence electron concentration for hydrogen storage, J. Alloys Compd. 865 (2021) 158767.

[187] I. Kunce, M. Polanski, J. Bystrzycki, Microstructure and hydrogen storage properties of a TiZrNbMoV high entropy alloy synthesized using laser engineered net shaping (LENS), Int. J. Hydrogen Energy 39 (2014) 9904–9910.

[188] J. Montero, G. Ek, L. Laversenne, V. Nassif, G. Zepon, M. Sahlberg, C. Zlotea, Hydrogen storage properties of the refractory Ti-V-Zr-Nb-Ta multi-principal element alloy, J. Alloys Compd. 835 (2020) 155376.

[189] G. Ek, M.M. Nygård, A.F. Pavan, J. Montero, P.F. Henry, M.H. Sørby, M. Witman, V. Stavila, C. Zlotea, B.C. Hauback, M. Sahlberg, Elucidating the effects of the composition on hydrogen sorption in TiVZrNbHf-based high-entropy alloys, Inorg. Chem. 60 (2021) 1124–1132.

[190] M.Y. Piao, X.Z. Xiao, Z.M. Cao, P.P. Zhou, L.J. Zhan, J.C. Qi, Z.N. Li, L.J. Jiang, L. X. Chen, Low-cost vanadium-free Ti-Zr-Cr-Mn-Fe based alloys for metal hydride hydrogen compressor under mild conditions, Mater. Chem. Phys. 297 (2023) 127407.

[191] G. Andrade, G. Zepon, K. Edalati, A. Mohammadi, Z. Ma, H.W. Li, R. Floriano, Crystal structure and hydrogen storage properties of AB-type TiZrNbCrFeNi high-entropy alloy, Int. J. Hydrogen Energy 48 (2023) 13555–13565.

[192] I. Kunce, M. Polański, T. Czujko, Microstructures and hydrogen storage properties of La-Ni-Fe-V-Mn alloys, Int. J. Hydrogen Energy 42 (2017) 27154–27164.

[193] B. Cheng, L.J. Kong, H.M. Cai, Y.K. Li, Y.M. Zhao, D. Wan, Y.F. Xue, Pushing the boundaries of solid-state hydrogen storage: a refined study on TiVNbCrMo high-entropy alloys, Int. J. Hydrogen Energy 60 (2024) 282–292.

[194] Y.F. Liu, H.G. Pan, M.X. Gao, Q.D. Wang, Advanced hydrogen storage alloys for Ni/MH rechargeable batteries, J. Mater. Chem. 21 (2011) 4743–4755.

[195] L.Z. Ouyang, J.L. Huang, H. Wang, J.W. Liu, M. Zhu, Progress of hydrogen storage alloys for Ni-MH rechargeable power batteries in electric vehicles: a review, Mater. Chem. Phys. 200 (2017) 164–178.

[196] G.Z. Guo, C.C. Ji, J.D. Lin, T.L. Wu, Y.L. Luo, C.R. Sun, M.J. Li, H.Y. Mi, L.X. Sun, H.J. Seifert, Interfacial domino effect triggered by beta-alanine cations realized highly reversible zinc-metal anodes, Angew. Chem., Int. Ed. 63 (2024) e202407417.

[197] M.L. Jiao, Q. Zhang, C.L. Ye, Z.B. Liu, X.W. Zhong, J.X. Wang, C. Li, L.X. Dai, G. M. Zhou, H.M. Cheng, Recycling spent $LiNi_{1-x-y}Mn_xCo_yO_2$ cathodes to bifunctional NiMnCo catalysts for zinc-air batteries, Proc. Natl. Acad. Sci. USA 119 (2022) e2202202119.

[198] Z.J. Wu, S.N. He, C. Zheng, J.T. Gan, L.N. She, M.C. Zhang, Y. Gao, Y.X. Yang, H. G. Pan, Fabrication pressures and stack pressures in solid-state battery, eScience 4 (2024) 100247.

[199] H. Miao, M.X. Gao, Y.F. Liu, D. Zhu, H.G. Pan, An improvement on cycling stability of Ti-V-Fe-based hydrogen storage alloys with Co substitution for Ni, J. Power Sources 184 (2008) 627–632.

[200] K. Young, D.F. Wong, T. Ouchi, B. Huang, B. Reichman, Effects of La-addition to the structure, hydrogen storage, and electrochemical properties of C14 metal hydride alloys, Electrochim. Acta 174 (2015) 815–825.

[201] D.F. Wong, K. Young, J. Nei, L. Wang, K.Y.S. Ng, Effects of Nd-addition on the structural, hydrogen storage, and electrochemical properties of C14 metal hydride alloys, J. Alloys Compd. 647 (2015) 507–518.

[202] K. Young, B. Chao, B. Huang, J. Nei, Effects of Cu-substitution on $La_{0.62}Ce_{0.38}(NiCoMnAlSiZr)_{5.3}$ metal hydride alloy, J. Alloys Compd. 588 (2014) 235–241.

[203] B. Sarac, V. Zadorozhnyy, E. Berdonosova, Y.P. Ivanov, S. Klyamkin, S. Gumrukcu, A.S. Sarac, A. Korol, D. Semenov, M. Zadorozhnyy, A. Sharma, A. L. Greer, J. Eckert, Hydrogen storage performance of the multi-principal-component CoFeMnTiVZr alloy in electrochemical and gas-solid reactions, RSC Adv. 10 (2020) 24613–24623.

[204] T. Fukagawa, Y. Saito, A. Matsuyama, Effect of varying Ni content on hydrogen absorption-desorption and electrochemical properties of Zr-Ti-Ni-Cr-Mn high-entropy alloys, J. Alloys Compd. 896 (2022) 163118.

[205] S. Liu, Y. Wang, T.L. Jiang, S. Jin, M. Sajid, Z.D. Zhang, J.W. Xu, Y.P. Fan, X. Y. Wang, J.H. Chen, Z.C. Liu, X.H. Zheng, K. Zhang, Q.S. Nian, Z.X. Zhu, Q. Peng, T. Ahmad, K. Li, W. Chen, Non-noble metal high-entropy alloy-based catalytic electrode for long-life hydrogen gas batteries, ACS Nano 18 (2024) 4229–4240.

[206] P. Edalati, A. Mohammadi, Y. Li, H.W. Li, R. Floriano, M. Fuji, K. Edalati, High-entropy alloys as anode materials of nickel-metal hydride batteries, Scripta Mater. 209 (2022) 114387.

[207] M.X. Gao, H. Miao, Y. Zhao, Y.F. Liu, H.G. Pan, Effects of rare Earth elements substitution for Ti on the structure and electrochemical properties of a Fe-doped Ti-V-based hydrogen storage alloy, J. Alloys Compd. 484 (2009) 249–255.

[208] S.J. Qiu, J.L. Huang, H.L. Chu, Y.J. Zou, C.L. Xiang, H.Z. Zhang, F. Xu, L.X. Sun, H.Y. Zhou, Influence of boron introduction on structure and electrochemical hydrogen storage properties of Ti-V-based alloys, J. Alloys Compd. 648 (2015) 320–325.

[209] X.B. Zhang, D.Z. Sun, W.Y. Yin, Y.J. Chai, M.S. Zhao, Crystallographic and electrochemical characteristics of $La_{0.7}Mg_{0.3}Ni_{3.5-x}(Al_{0.5}Mo_{0.5})_x$ (x = 0-0.8) hydrogen storage alloys, J. Power Sources 154 (2006) 290–297.

[210] Y. Li, S.M. Han, J.H. Li, X.L. Zhu, L. Hu, The effect of Nd content on the electrochemical properties of low-Co La-Mg-Ni-based hydrogen storage alloys, J. Alloys Compd. 458 (2008) 357–362.

[211] S. Ma, M.X. Gao, R. Li, H.G. Pan, Y.Q. Lei, A study on the structural and electrochemical properties of $La_{0.7-x}Nd_xMg_{0.3}Ni_{2.45}Co_{0.75}Mn_{0.1}Al_{0.2}$ (x = 0.0-3.0) hydrogen storage alloys, J. Alloys Compd. 457 (2008) 457–464.

[212] W.Q. Jiang, C.S. Qin, R.R. Zhu, J. Guo, Annealing effect on hydrogen storage property of Co-free $La_{1.8}Ti_{0.2}MgNi_{8.7}Al_{0.3}$ alloy, J. Alloys Compd. 565 (2013) 37–43.

[213] Y.H. Zhang, Z.H. Hou, T. Yang, G.F. Zhang, X. Li, D.L. Zhao, Structure and electrochemical hydrogen storage characteristics of $La_{0.8-x}Pr_xMg_{0.2}Ni_{3.15}Co_{0.2}Al_{0.1}Si_{0.05}$ (x = 0-0.4) electrode alloys, J. Cent. South Univ. 20 (2013) 1142–1150.

[214] R.F. Li, R.H. Yu, X.F. Liu, J. Wan, F. Wang, Study on the phase structures and electrochemical performances of $La_{0.6}Gd_{0.2}Mg_{0.2}Ni_{3.15-x}Co_{0.25}Al_{0.1}Mn_x$ (x = 0-0.3) alloys as negative electrode material for nickel/metal hydride batteries, Electrochim Acta 158 (2015) 89–95.

[215] W. Li, B. Zhang, J.G. Yuan, Y.H. Yan, Y. Wu, Effect of Mo content on the microstructures and electrochemical performances of $La_{0.75}Mg_{0.25}Ni_{3.2-x}Co_{0.2}Al_{0.1}Mo_x$ (x = 0, 0.10, 0.15, 0.20) hydrogen storage alloys, J. Alloys Compd. 692 (2017) 817–824.

[216] H.Z. Yan, W. Xiong, L. Wang, B.Q. Li, J. Li, X. Zhao, Investigations on AB_3-, A_2B_7- and A_5B_{19}-type La-Y-Ni system hydrogen storage alloys, Int. J. Hydrogen Energy 42 (2017) 2257–2264.

[217] H. Lu, Y.N. Guo, Q. Wang, A.Y. Zhang, Y. Li, N. Xi, X.M. Zhu, S.M. Han, L. Zhang, Phase transformation and electrochemical feature of an AB_4-type $La_{0.60}Sm_{0.20}Mg_{0.20}Ni_{3.50}Al_{0.20}$ hydrogen storage alloy for Ni/MH batteries, J. Electrochem. Soc. 170 (2023) 080504.

[218] S.P. Wu, Y.P. Chen, W.L. Kang, X.L. Cai, L. Zhou, Hydrogen storage properties of MgTiVZrNb high-entropy alloy and its catalytic effect upon hydrogen storage in Mg, Int. J. Hydrogen Energy 50 (2024) 1113–1128.

[219] Y.F. Sun, S. Dai, High-entropy materials for catalysis: a new frontier, Sci. Adv. 7 (2021) eabg1600.

[220] H. Luo, L. Li, F.X. Lin, Q.H. Zhang, K. Wang, D.W. Wang, L. Gu, M.C. Luo, F. Lv, S. J. Guo, Sub-2 nm microstrained high-entropy-alloy nanoparticles boost hydrogen electrocatalysis, Adv. Mater. 36 (2024) 2403674.

[221] M.S. Salman, C. Pratthana, Q. Lai, T. Wang, N. Rambhujun, K. Srivastava, K.F. A. Zinsou, Catalysis in solid hydrogen storage: recent advances, challenges, and perspectives, Energy Technol. 10 (2022) 2200433.

[222] Y.X. Yang, X. Zhang, L.C. Zhang, W.X. Zhang, H.F. Liu, Z.G. Huang, L.M. Yang, C. D. Gu, W.P. Sun, M.X. Gao, Y.F. Liu, H.G. Pan, Recent advances in catalyst-modified Mg-based hydrogen storage materials, J. Mater. Sci. Technol. 163 (2023) 182–211.

[223] B. Peng, J. Liang, Z.L. Tao, J. Chen, Magnesium nanostructures for energy storage and conversion, J. Mater. Chem. A 19 (2009) 2877–2883.

[224] S. Wei, J.X. Liu, Y.P. Xia, H.Z. Zhang, R.G. Cheng, L.X. Sun, F. Xu, Y.T. Bu, Z. Y. Liu, P.R. Huang, K.X. Zhang, F. Rosei, A.A. Pimerzin, H.J. Seifert, Enhanced hydrogen storage properties of $LiAlH_4$ by excellent catalytic activity of $XTiO_3$@h-BN (X = Co, Ni), Adv. Funct. Mater. 32 (2021) 2110180.

[225] Y.X. Jia, B. Han, J.C. Wang, S.C. Yuan, L. Tang, Z.Y. Zhang, Y.J. Zou, L.X. Sun, Y. Du, L.X. Chen, X.Z. Xiao, Inducing one-step dehydrogenation of magnesium borohydride via confinement in robust dodecahedral nitrogen-doped porous carbon scaffold, Adv. Mater. 36 (2024) e2406152.

[226] H.Y. Wang, J. Li, X.L. Wei, Y. Zheng, S.L. Yang, Y.F. Lu, Z. Ding, Q. Luo, Q. Li, F. S. Pan, Thermodynamic and kinetic regulation for Mg-based hydrogen storage materials: challenges, strategies, and perspectives, Adv. Funct. Mater. 34 (2024) 2406639.

[227] B. Peng, L.L. Li, W.Q. Ji, F.Y. Cheng, J. Chen, A quantum chemical study on magnesium(Mg)/magnesium-hydrogen(Mg-H) nanowires, J. Alloys Compd. 484 (2009) 308–313.

[228] P. Meena, R. Singh, V.K. Sharma, I.P. Jain, Role of $NiMn_{9.3}Al_{4.0}Co_{14.1}Fe_{3.6}$ alloy on dehydrogenation kinetics of MgH_2, J. Magnesium Alloys 6 (2018) 318–325.

[229] J.X. Zhang, H. Liu, C.S. Zhou, P. Sun, X.Y. Guo, Z.Z. Fang, TiVNb-based high entropy alloys as catalysts for enhanced hydrogen storage in nanostructured MgH_2, J. Mater. Chem. A 11 (2023) 4789–4800.

[230] L. Wang, L.T. Zhang, X. Lu, F.Y. Wu, X. Sun, H. Zhao, Q. Li, Surprising cocktail effect in high entropy alloys on catalyzing magnesium hydride for solid-state hydrogen storage, Chem. Eng. J. 465 (2023) 142766.

[231] M.C. Song, F.Y. Wu, Y.Q. Jiang, X.Z. Wang, H. Zhao, L.X. Chen, L.T. Zhang, Optimizing FeCoNiCrTi high-entropy alloy with hydrogen pumping effect to boost de/hydrogenation performance of magnesium hydride, Rare Met. 43 (2024) 3273–3285.

[232] T. Zhong, H.Y. Zhang, M.C. Song, Y. Jiang, D.H. Shang, F.Y. Wu, L.T. Zhang, FeCoNiCrMo high entropy alloy nanosheets catalyzed magnesium hydride for solid-state hydrogen storage, Int. J. Min. Met. Mater. 30 (2023) 2270–2279.

[233] H.Y. Wan, X. Yang, S.M. Zhou, L. Ran, Y.F. Lu, Y.A. Chen, J.F. Wang, F.S. Pan, Enhancing hydrogen storage properties of MgH_2 using FeCoNiCrMn high entropy alloy catalysts, J. Mater. Sci. Technol. 149 (2023) 88–98.

[234] S.K. Verma, S.S. Mishra, N.K. Mukhopadhyay, T.P. Yadav, Superior catalytic action of high-entropy alloy on hydrogen sorption properties of MgH_2, Int. J. Hydrogen Energy 50 (2024) 749–762.

[235] F.H. Yin, Z.Z. Chen, T.Z. Si, D.M. Liu, Y.T. Li, H.W. Li, Q.A. Zhang, Structural-regulation of Laves phase high-entropy alloys to catalytically enhance hydrogen desorption from MgH_2, J. Alloys Compd. 997 (2024) 174822.

[236] Y.K. Yadav, M.A. Shaz, T.P. Yadav, Al-Cu-Fe-Ni-Ti high entropy alloy nanoparticles as new catalyst for hydrogen sorption in MgH_2, Int. J. Hydrogen Energy 137 (2024) 1137–1147.

[237] Y.K. Yadav, M.A. Shaz, T.P. Yadav, Notable catalytic activity of Al-Cu-Fe-Ni-Cr high entropy alloy nanoparticles for hydrogen sorption in MgH_2, Int. J. Hydrogen Energy 141 (2025) 935–945.

[238] S. Wang, S.Q. Qu, Z.H. Liu, Y.Y. Zhu, Z.L. Li, H.F. Liu, M.X. Gao, H.G. Pan, *In situ* coupling metallophilic Zn sites and interfacial LiCl stabilizer to achieve one-step reversible hydrogen storage in Li/Na dual-cation borohydride, Chem. Eng. J. 488 (2024) 150889.

[239] E.M. Dematteis, A. Santoru, M.G. Poletti, C. Pistidda, T. Klassen, M. Dornheim, M. Baricco, Phase stability and hydrogen desorption in a quinary equimolar mixture of light-metals borohydrides, Int. J. Hydrogen Energy 43 (2018) 16793–16803.

[240] J.H. Li, X.Y. Hong, Y.L. Wang, Y.M. Luo, P.R. Huang, B. Li, K.X. Zhang, Y.J. Zou, L.X. Sun, F. Xu, F. Rosei, S.P. Verevkin, A.A. Pimerzin, Encapsulated cobalt nanoparticles as a recoverable catalyst for the hydrolysis of sodium borohydride, Energy Storage Mater. 27 (2020) 187–197.

[241] J. Mu, Y.Q. Ye, J.L. Wang, Z.W. Zhu, Y.D. Wang, H.F. Zhang, Dislocation-driven high catalytic performance of FeCoNiCrMn high-entropy alloy for the hydrolysis of $NaBH_4$, Appl. Phys. Lett. 119 (2021) 121901.

[242] H.L. Chu, G.Y. Li, C. Liu, C.H. Cui, Y.T. Li, S.J. Qiu, Y.P. Xia, Y.J. Zou, F. Xu, L. X. Sun, Ruthenium-based high-entropy alloys expediting hydrogen evolution through catalytic hydrolysis of ammonia borane, ACS Appl. Energy Mater. 7 (2024) 9625–9633.

[243] S.Y. Jiang, Y.T. Xu, R.H. Wang, X.R. Chen, C.S. Guan, Y. Peng, F.Z. Liu, M. X. Wang, X. Liu, S.Y. Zhang, G.Q. Tian, S.B. Jin, H.Y. Wang, H. Toda, X.J. Jin, G. Liu, B. Gault, J. Sun, Structurally complex phase engineering enables hydrogen-tolerant Al alloys, Nature 641 (2025) 358–364.

[244] H.S. Bao, Z.H. Gong, Z.Z. Chen, G. Yang, Evolution of precipitates in Ni-Co-Cr-W-Mo superalloys with different tungsten contents, Rare Met. 39 (2020) 716–724.

[245] E.H. Yan, Y.C. Chen, K.X. Zhang, Y.J. Zou, H.L. Chu, L.X. Sun, Design of hydrogen separatinwg Nb-Ti-Fe membranes with high permeability and low cost, Sep. Purif. Technol. 257 (2021) 117945.

[246] E.H. Yan, Z.R. Zhou, R.J. Huang, K.X. Zhang, S. Zhang, Y. Wang, Y.C. Chen, Y. J. Zou, H.L. Chu, H.Z. Zhang, F. Xu, L.X. Sun, Microstructure and hydrogen transport behaviour of $Nb_5Ti_{58}Fe_{35}M_2$ alloy membranes, J. Alloys Compd. 958 (2023) 170520.

[247] N.A. Khan, B. Akhavan, C. Zhou, H. Zhou, L. Chang, Y. Wang, Y. Liu, M.M. Bilek, Z. Liu, High entropy nitride (HEN) thin films of $AlCoCrCu_{0.5}FeNi$ deposited by reactive magnetron sputtering, Surf. Coating. Technol. 402 (2020) 126327.

[248] H.X. Tang, K. Ishikawa, K. Aoki, Effect of elements addition on hydrogen permeability and ductility of $Nb_{40}Ti_{18}Zr_{12}Ni_{30}$ alloy, J. Alloys Compd. 461 (2008) 263–266.

[249] S.C. Marques, A.V. Castilho, D.S. Dos Santos, Effect of alloying elements on the hydrogen diffusion and trapping in high entropy alloys, Scripta Mater. 201 (2021) 113957.

[250] X.L. Ren, P.H. Shi, B.D. Yao, L. Wu, X.Y. Wu, Y.X. Wang, Hydrogen solution in high-entropy alloys, Phys. Chem. Chem. Phys. 23 (2021) 27185–27194.

[251] E. Kashkarov, D. Krotkevich, M. Koptsev, S. Ognev, L. Svyatkin, N. Travitzky, A. Lider, Microstructure and hydrogen permeability of Nb-Ni-Ti-Zr-Co high entropy alloys, Membranes 12 (2022) 1157.

[252] Y.P. Xu, Y.M. Lyu, H.D. Liu, X.D. Pan, T. Lu, T. Zhu, H.S. Zhou, X.C. Li, Q. Xu, X. L. Wang, F. Ding, Z.S. Yang, X.Z. Cao, G.N. Luo, Hydrogen isotope permeation and retention behavior in the CoCrFeMnNi high-entropy alloy, J. Nucl. Mater. 522 (2019) 41–44.

[253] W. Zhang, L. Wang, X.F. Luo, B.P. Gong, X.Y. Wang, J.J. Yang, Y.J. Feng, Deuterium permeability of a novel AlCrTaTiZr high entropy alloy coating, Mater. Res. Express 8 (2021) 056401.
[254] W. Li, B. Luo, H. Huang, Y. Liu, W. Wang, J. Luo, B. Fu, A comparative study of deuterium permeation behaviors of CoCrMnFeNi and AlCoCrFeNi high entropy alloys, Int. J. Hydrogen Energy 48 (2023) 19657–19665.
[255] C.Y. Yin, W.X. Li, X. Qiu, B. Luo, H.T. Huang, Characterization of the oxide film and deuterium permeation behavior of CoCrMnFeNi high entropy alloy oxidized at 550 °C for 24 h, Mater. Lett. 347 (2023) 134632.
[256] Z.H. Hong, L. Wang, W. Zhang, J. Yang, Y.J. Feng, J.J. Yang, H.X. Li, H.Q. Yin, L. Zhang, X.Y. Wang, Hydrogen isotope permeation behavior of AlCrFeTiNb, AlCrMoNbZr and AlCrFeMoTi high-entropy alloys coatings, Coatings 12 (2022) 171.
[257] Q.C. Zhao, H. Luo, Z.S. Yang, Z.M. Pan, Z.J. Wang, R.K. Islamgaliev, X.G. Li, Hydrogen induced cracking behavior of the dual-phase $Co_{30}Cr_{10}Fe_{10}Al_{18}Ni_{30}Mo_2$ eutectic high entropy alloy, Int. J. Hydrogen Energy 50 (2024) 134–147.
[258] D.C. Feng, W.J. Wang, Y.F. Liu, W.J. Zheng, D.J. Yan, C.A. Li, M. Huang, Y.M. He, S. B. Lai, J.G. Yang, Hydrogen-induced evolution associated with nano-scale precipitated phases in $AlCoCrFeNi_{2.1}$ high-entropy alloy, J. Alloys Compd. 944 (2023) 169116.
[259] E.B. Kashkarov, L.A. Svyatkin, K.S. Gusev, S.O. Ognev, M. Koptsev, D. V. Terenteva, Effect of high and low Nb content in multicomponent Nb-Ni-Ti-Zr-Co alloy on its structure, hardness and hydrogen permeability, Intermetallics 166 (2024) 108180.
[260] T.R. Yang, Y.X. Wang, Y.H. Li, S.J. Zhao, H.B. Zhou, F.Y. Tian, G.H. Lu, Exploring the inhibitory effect of WTaVCr high-entropy alloys on hydrogen retention: from dissolution, diffusion to desorption, J. Nuc, Mater 601 (2024) 155346.
[261] Y.J. Zou, Q.Y. Wang, D.D. Jiang, C.L. Xiang, H.L. Chu, S.J. Qiu, H.Z. Zhang, F. Xu, L.X. Sun, S.S. Liu, Pd-doped TiO_2@polypyrrole core-shell composites as hydrogen-sensing materials, Ceram. Int. 42 (2016) 8257–8262.
[262] K.F. Chen, D.P. Yuan, Y.Y. Zhao, Review of optical hydrogen sensors based on metal hydrides: recent developments and challenges, Opt. Laser Technol. 137 (2021) 106808.
[263] C. Wang, J.X. Yang, J.L. Li, C.L. Luo, X.W. Xu, F. Qian, Solid-state electrochemical hydrogen sensors: a review, Int. J. Hydrogen Energy 48 (2023) 31377–31391.
[264] Y.J. Zou, Q.Y. Wang, C.L. Xiang, C.Y. Tang, H.L. Chu, S.J. Qiu, E.H. Yan, F. Xu, L. X. Sun, Doping composite of polyaniline and reduced graphene oxide with palladium nanoparticles for room-temperature hydrogen-gas sensing, Int. J. Hydrogen Energy 41 (2016) 5396–5404.
[265] B. Sharma, S. Harini, A possibility of Pd based high entropy alloy for hydrogen gas sensing applications, Mater. Res. Express 6 (2019) 1165d1167.
[266] K. Zhu, X. Li, Y. Zhang, X. Zhao, Z. Liu, J. Guo, Tailoring the hydrogen transport properties of highly permeable $Nb_{51}W_5Ti_{23}Ni_{21}$ alloy membrane by Pd substitution, Int. J. Hydrogen Energy 47 (2022) 6734–6744.
[267] K.M.B. Urs, N.K. Katiyar, R. Kumar, K. Biswas, A.K. Singh, C.S. Tiwary, V. Kamble, Multi-component (Ag-Au-Cu-Pd-Pt) alloy nanoparticle-decorated p-type 2D-molybdenum disulfide (MoS_2) for enhanced hydrogen sensing, Nanoscale 12 (2020) 11830–11841.
[268] B. Mondal, X. Zhang, S. Kumar, F. Long, N.K. Katiyar, M. Kumar, S. Goel, K. Biswas, A resistance-driven H_2 gas sensor: High-entropy alloy nanoparticles decorated 2D MoS_2, Nanoscale 15 (2023) 17097–17104.